MODIFIED EXPANSION RATE OF THE UNIVERSE IN SCALAR-TENSOR THEORIES OF GRAVITY AND ITS PHYSICAL IMPLICATIONS

A Dissertation

by

ESTEBAN JIMENEZ MOYA

Submitted to the Office of Graduate and Professional Studies of
Texas A&M University
in partial fulfillment of the requirements for the degree of

DOCTOR OF PHILOSOPHY

Chair of Committee,	Bhaskar Dutta
Committee Members,	Stephen Fulling
	Dimitri Nanopoulos
	Teruki Kamon
Head of Department,	Grigory Rogachev

August 2018

Major Subject: Physics

ABSTRACT

We study the impact of a modified expansion rate on the dark matter relic abundance and leptogenesis in two types of scalar-tensor theories. The first scenario is motivated from string theory constructions, which have conformal as well as disformally coupled matter to the scalar. The second scenario is called disformal D-brane coupling, which stems from D-brane models of cosmology. In both scenarios, the conformal and disformal couplings modify the expansion rate of the universe prior to BBN. Furthermore, we investigate the effects of such couplings to the dark matter relic abundance for a wide range of initial conditions, masses, and cross-sections. It is found that the annihilation cross-section required to satisfy the dark matter content can differ from the thermal average cross-section in the standard cosmology, which can be tested in future experiments. In addition, we discuss how non-standard cosmologies can open new pathways for low scale leptogenesis. Within these scenarios direct tests of leptogenesis could also provide information on the very early Universe evolution, corresponding to temperatures in the TeV range.

DEDICATION

Este trabajo es dedicado a mi madre, Ana Isabel Moya, quien siempre ha estado a mi lado.

Gracias Ma, por todo el apoyo y amor incondicional que me has dado.

ACKNOWLEDGMENTS

First and foremost, I would like to thank my advisor, Bhaskar Dutta, for his invaluable support and guidance, for the numerous discussions we had and for sharing with me all the ideas that lead me to conclude this dissertation.

Also, I would like to express my gratitude to my collaborators Ivonne Zavala, Chee Sheng Fong, Enrico Nardi, Kuver Sinha and Francesco D'eramo, for all the work we have done together and for all their discussions, which have been instrumental in development as a researcher.

In addition, I would like to thank and acknowledge the Universidad de Costa Rica for the partial support provided during my graduate studies at Texas A&M University.

Finally, I would also like to thank my family and friends, who have always supported me and have been there for me throughout the past years.

CONTRIBUTORS AND FUNDING SOURCES

Contributors

This work was supported by a dissertation committee consisting of Professors Bhaskar Dutta (advisor), Dimitri Nanopoulos and Teruki Kamon of the Department of Physics and Professor Stephen Fulling of the Department of Mathematics.

Chapters 2 and 4 contains a reprint of sections extracted from an article entitled "Dark Matter Relics and the Expansion Rate in Scalar-Tensor Theories". This work was completed in collaboration with Bhaskar Dutta and Ivonne Zavala, and is reprinted with permission from the IOP Publishing.

Chapters 3 and 4 contains a reprint of sections extracted from an article entitled "D-brane Disformal Coupling and Thermal Dark Matter". This work was completed in collaboration with Bhaskar Dutta and Ivonne Zavala, and is reprinted with permission from the American Physical Society.

Chapter 5 contains a reprint of sections extracted from an article entitled "A Cosmological Pathway to Testable Leptogenesis". This work was completed in collaboration with Bhaskar Dutta, Chee Sheng Fong and Enrico Nardi, and has been submited to JCAP.

All other work conducted for the dissertation was completed by the student independently.

Funding Sources

Graduate study was supported in part by the Department of Energy Grants DE-FG02-13ER42020 and DE-SC0010813, and in part by the Scholarship for Graduate Studies for Faculty from the Universidad de Costa Rica.

NOMENCLATURE

CDM	Cold Dark Matter
SM	Standard Model of Particles
BBN	Big Bang Nucleosynthesis
DM	Dark Matter
GR	General Relativity
ST	Scalar-Tensor Theories of Gravity
VEV	Vacuum Expectation Value
CP	Charge-conjugation Parity
BE	Boltzmann Equation
MSSM	Minimal Supersymmetric Standard Model
FRW	Friedmann-Robertson-Walker
NEC	Null Energy Condition
DBI	Dirac-Born-Infeld
RH	Right-handed

TABLE OF CONTENTS

Page

LIST OF FIGURES

FIGURE Page

LIST OF TABLES

TABLE Page

1. INTRODUCTION

Recent cosmological data support the phenomenological Λ-Cold Dark Matter (ΛCDM) model of cosmology, which describes the energy density content of the universe in terms of a cosmological constant, Λ, cold dark matter and baryonic matter. The first two components together make up 95% of the universe's energy density budget, while the other 5% is made of baryonic standard model (SM) particles. This phenomenological model is complemented by the inflationary mechanism, which is the most successful framework to account for the origin of structure in the universe. After inflation, the universe reheated, providing the conditions for the hot big bang.

The predicted abundances of the light elements resulting from big bang nucleosynthesis (BBN) are in very good agreement with available observational data [1], which strongly supports the ΛCDM model and our understanding of the universe's evolution back to the first few seconds after the big bang.

However, the physics describing the universe's evolution from the end of inflation (reheating) to just before BBN ($t \lesssim 10$ s) remains relatively unconstrained. During this period, the universe could have gone through a "non-standard" period of expansion, and still be compatible with BBN predictions. If such modification happened at temperatures around few GeV, during the dark matter (DM) decoupling, the DM freeze-out may have been modified with measurable consequences for the relic DM abundances. Also, if this modification occured at a higher temperature, say few TeV, it may have had an impact on the scale of the leptogenesis mechanism that produces the baryon asymmetry of the universe. Indeed, one of our the main goals is to study the effect of a "non-standard" cosmological expansion on the thermal DM freeze-out picture and on the scale of leptogenesis.

Departures from the standard cosmology between reheating and BBN will mainly be a consequence of a modified expansion rate ($\tilde{H}$), which can be due to a modification of General Relativity (GR). Such modifications are well motivated by attempts to embed the ΛCDM and inflation models into a fundamental theory of gravity and particle physics, such as theories with extra-

dimensions, supergravity and string theory.

String theory approaches, to SM particle physics and inflation model building, generically predict the presence of several new ingredients, and in particular scalar fields with clear geometrical interpretations. For example, type II string theory models of particle physics introduce new ingredients such as D-branes, where matter (and DM) is to be localised[1]. In D-brane constructions, longitudinal string fluctuations are identified with the matter fields such as the SM and/or DM particles, while transverse fluctuations correspond to scalar fields, which may play a role during the cosmological evolution[2]. These scalar fields couple conformally and disformally to the matter living on the brane [3] and thus may change the cosmological expansion rate felt by matter. The gravitational theory arising from the coupling belongs to a class of theories of gravity called Scalar-Tensor (ST) theories.

In this work, we focus on ST theories where the gravitational interaction is mediated by both the metric and only one scalar field. In these type of theories, the cosmological evolution deviates from the standard expansion of the Universe at early times, but an attractor mechanism [4, 5] relaxes the theory towards GR prior to the onset of BBN. ST theories are often formulated in one of two frames of reference, namely, the Jordan or Einstein frames. As it is shown in [6], the most general transformation, physically consistent, between the metrics of these frames is given by [3]

$$\tilde{g}_{\mu\nu} = C(\phi) g_{\mu\nu} + D(\phi) \partial_\mu \phi \partial_\nu \phi \,. \tag{1.1}$$

where $\tilde{g}_{\mu\nu}$ is metric in the Jordan frame, $C(\phi)$ is the conformal coupling, $g_{\mu\nu}$ is the metric in the Einstein frame and $D(\phi)$ is the so-called disformal coupling.

The first term in (1.1) is the well-known conformal transformation which characterizes the Brans-Dicke class of scalar-tensor theories explored in [7, 8, 9, 10, 11, 12]. The second term is the disformal contribution, which is generic in extensions of general relativity. In particular, it

[1]For a review on D-brane models of particle physics see [2].

[2]For example, a coupled dark energy-dark matter D-brane scenario was proposed in[3].

[3]More generally, the functions, C and D can depend on $X = \frac{1}{2}(\partial\phi)^2$ as well. We do not consider this case in the present paper.

arises naturally in D-brane models, as discussed in [3], in a model of coupled dark matter and dark energy.

We will investigate two classes of ST theories in the two following chapters. In Chapter 2, we consider the general action consider in [7, 12] and take into account the disformal coupling, entering only through the metric. We revisit the conformal case, that is $D = 0$, and explore the expansion rate modification providing new interesting results with new boundary conditions. We further discuss the general modifications to the expansion rate due to a disformal coupling and present an explicit non-trivial example for the case in which the conformal term in (1.1) is a monomial. In such a case, the functions C and D are in principle independent functions, as long as they satisfy the causality constraints: $C(\phi) > 0$ and $C(\phi) + 2D(\phi)X > 0$ ($X = \frac{1}{2}(\partial\phi)^2$) [13].

In Chapter 3, we study in detail the effects on the expansion rate of the disformal coupling in (1.1), which arises in the case of matter localized on D-branes. In this case, the conformal and disformal terms are closely related and dictated by the underlying theory, such as type IIB flux compactifications in string theory. The picture we have in mind goes as follows. After string theory inflation, reheating took place, giving rise to a thermal universe. At this stage standard model particles and dark matter was produced. The SM would arise from stacks of D-branes at singularities or D-branes intersecting at suitable angles [2], while DM particles could arise from the same or a different stack of D-branes, which may be moving towards their final stable positions in the internal six-dimensional space before the onset of BBN. From the end of inflation to BBN, a nonstandard cosmological evolution can take place without spoiling the predictions of BBN, in particular, a change in the expansion rate felt by the matter particles due to the D-brane conformal and disformal couplings between the scalar field and matter fields. As we will see, due to the coupling the expansion rate will generically be enhanced[4]. Let us stress that a realistic string theory scenario would be more complicated and may include nonuniversal couplings to baryonic and dark matter. However, it is very interesting that scalar couplings present in string theory can give interesting modifications of the post-inflationary evolution after string inflation.

[4]It is interesting to notice that a phenomenological model with a faster-than-usual expansion at early times, driven by a new cosmological species, has recently been discussed in [14].

In this work, we show for the first time that the enhanced expansion rate can also happen due to a purely disformal contribution or a combination of conformal and disformal terms. The former case - a disformal enhancement - is particularly interesting as it can be interpreted in terms of an "unwarped" compactification, which is typical of a large-volume compactification of string theory, which is needed for perturbative control. When we identify the scale arising from the disformal coupling with the tension of a moving D3-brane, where matter is localized, this scale is determined by the string scale and the string coupling. Interestingly, the modification of the expansion rate can take place at different temperature scales, depending on the value of the string scale.

The enhancement of the expansion rate, due to conformal and disformal couplings, impact the early universe cosmology. In this thesis, we study DM phenomenology and a simple model of leptogenesis as well. In Chapter 4, we focus on the general thermal DM freeze-out picture as an example and study how it is modified due to the faster-than-usual expansion of the universe. We further investigate the correlation of the annihilation cross section with the dark matter content. In Chapter 5, we study a simple model of leptogenesis type-I seesaw and show that the enhanced expansion rate lowers the scale of leptogenesis to few TeV.

In an attractive scenario of the cosmic history, the universe is radiation dominated prior to BBN and dark matter is produced from the thermal bath, which was created at the end of inflation. In this thermal picture, the observed relic density is satisfied for DM species with weak-scale interaction rate $\langle \sigma v \rangle$, which is around $3.0 \times 10^{-26} \mathrm{cm}^3 \mathrm{s}^{-1}$ (or $\sigma \sim 1$ picobarn), corresponding to weak interactions. Despite such a small value, the Fermi-LAT and Planck experiments have been exploring upper bounds on $\langle \sigma v \rangle$ [15, 16]. In the future, HAWC [17] and CTA [18] will probe the annihilation rate for a wide range of dark matter masses. It is thus worth establishing whether an annihilation rate, larger or smaller than the standard thermal prediction, could still have a thermal origin due a modified cosmological evolution before BBN.

Modifications to the DM relic abundances in conformally coupled scalar-tensor theories (ST), such as generalizations of the Brans-Dicke theory, were first discussed in [7] by Catena et al. These authors showed a faster-than-usual expansion rate, $\tilde{H}$, which well before the onset of BBN,

rapidly drops back to the standard GR expansion rate, H_{GR}. Due to this rapid relaxation of $\tilde{H}$ towards H_{GR}, they found a DM reannihilation effect: after the initial particle decoupling, the dark matter species experienced a subsidiary period of annihilation as the expansion rate of the universe dropped below the interaction rate. Further studies on conformally coupled ST models have been performed in recent years in [8, 9, 10, 11, 12] (see also[19, 20, 21, 22, 23, 24, 25]).

On the other hand, one of the most popular mechanisms to explain the cosmological baryon asymmetry is leptogenesis [26], according to which an initial lepton asymmetry is generated and then partly converted to a baryon asymmetry by sphaleron processes [27, 28] (for reviews on the leptogenesis mechanism see [29, 30]). In standard leptogenesis, based on type-I seesaw mechanism, this initial lepton asymmetry is produced in the decay of the lightest RH neutrino, N_1. In order to produce enough CP asymmetry to account for the observed baryon asymmetry, the mass of N_1 cannot be smaller than $\sim 10^9$ GeV [31]. Therefore, this implies that direct tests of standard type-I seesaw leptogenesis are out of experimental reach.

This constraint is quite specific of the type-I seesaw leptogenesis and is often lost in other models. The most direct way to go around this bound is in models where the neutrinos only couple through a neutrinophilic Higgs which obtains a vacuum expectation value (VEV) much smaller than the electroweak breaking VEV, $v_\nu \ll 174$ GeV [32, 33]. Other examples and their references are mention in Chapter 5.

Most of the models that attempt to generate the baryon asymmetry from heavy particle decays are subject to an additional constraint. This constraint originates from a general relation between the strength of the washout scatterings, which tend to erase any lepton number asymmetry present in the thermal bath, and the charge conjugation parity (CP) asymmetries in the decays of the heavy states. In this thesis, we show how this constraint can be avoided in the context of ST theories and how the scale of leptogenesis can be as low as few TeV.

The dissertation is organized as follows:

- In Chapter 2, we introduce the ST theory conformally and disformally coupled to matter. Then, we examine the formulation of this theory in the Einstein and Jordan frames, com-

ment on their physical interpretation and derive the equations that describe the cosmological evolution of the Universe. Subsequently, we discuss the expansion rate modifications caused by the presence of the conformal and disformally coupled scalar field.

- In Chapter 3, we first briefly introduce the general D-brane-like setup. We then go directly to the cosmological equations and discuss how the expansion rate is modified in general. Then, we move on to the D-brane-like case, where the conformal and disformal functions are related. We start discussing the equations in the Jordan frame as well as the initial conditions and constraints that we use to numerically solve the full equations. We then discuss in detail the solutions for the unwarped case, that is, a purely disformal effect (or C =const.). Next, we discuss the warped case, using for concreteness the same conformal function used in Chapter 2. We also comment on the result of using other functions.

- In Chapter 4, we briefly introduce the DM thermal freeze-out picture and the Boltzmann equation (BE). Then, we investigate in detail the impact of the modified expansion rates, described in both Chapters 2 and 3, on the dark matter relic abundance and annihilation cross section.

- In Chapter 5 we start by motivating leptogenesis in a faster-than-usual universe, discuss some constraints on the leptogenesis scale and then add few more comments on boosted expansion rates. Later, we present a simple benchmark model which will be used for the leptogenesis analysis and discuss the network of BE for leptogenesis in the modified cosmology. In our last two sections, we present our leptogenesis results and comment on the enhancement scales in the extensions of the SM, e.g., Minimal Supersymmetric Standard Model (MSSM).

- In Chapter 6, we finally present our conclusions.

2. CONFORMALLY AND DISFORMALLY COUPLED SCALAR-TENSOR THEORY[1]

We are interested in scalar-tensor theories coupled to matter both conformally and disformally [13]. Our motivation comes from theories with extra dimensions and in particular string theory compactifications, where several additional scalar fields appear, from closed and open string theory sectors of the theory [3]. Our approach in this work nonetheless will be phenomenological and therefore our equations will be simplified. However, we present the more general set-up, which can accommodate a realization from concrete string theory compactifications in Appendix A.

As was mentioned in chapter 1, ST theories are often formulated in one of two frames of reference, namely, the Jordan or Einstein frames. The respective advantages of these two frames are that the scalar couplings enter through either the gravitational sector (Jordan frame) or the matter sector (Einstein frame), leaving the other sector unaffected. In the Jordan frame matter fields, Ψ, are coupled directly to the metric, $\tilde{g}_{\mu\nu}$, which means that the matter sector of the action can be written as $S_{Matter} = S_{Matter}(\tilde{g}_{\mu\nu}, \Psi)$. Thus, this frame is more convenient for particle physics considerations because the usual observables, e.g. a mass, have their standard interpretation. However, the scalar field couples to the gravitational sector producing rather cumbersome gravitational field equations.

On the other hand, in the Einstein frame, the matter piece of the action becomes $S_{Matter} = S_{Matter}(g_{\mu\nu}, \phi, \partial_\mu\phi, \Psi)$. This implies that physical quantities associated with particles (i.e. mass) measured in this frame have a spacetime dependency. However, the gravitational field equations take their standard form, where the Einstein tensor is proportional to the total energy-momentum tensor.

The most common strategy followed in the literature [7, 12] is to determine the cosmic evolution in the Einstein frame, where the cosmological equations take a more straightforward form, and then transform the results over to the Jordan frame. As was already hinted out before, the effect

[1]Reprinted with permission from "Dark matter relics and the expansion rate in scalar-tensor theories" by B. Dutta, E. Jimenez, I. Zavala, 2017. JCAP no.06, 032. Copyright SISSA Medialab Srl. All rights reserved.

of modified gravity will enter the computation of particle physics processes through the expansion rate, $\tilde{H}$, in the Jordan frame.

The action we want to consider is given by:

$$S_{EH} = \frac{1}{2\kappa^2}\int d^4x\sqrt{-g}\,R - \int d^4x\sqrt{-g}\left[\frac{1}{2}(\partial\phi)^2 + V(\phi)\right] + S_{Matter}\,. \tag{2.1}$$

where $S_{Matter} = -\int d^4x\sqrt{-\tilde{g}}\,\mathcal{L}_M(\tilde{g}_{\mu\nu}, \Psi)$, with $\mathcal{L}_M$ the lagrangian density of the matter sector.

Here the disformally coupled metric is given by

$$\tilde{g}_{\mu\nu} = C(\phi)g_{\mu\nu} + D(\phi)\partial_\mu\phi\partial_\nu\phi\,, \tag{2.2}$$

and the inverse by:

$$\tilde{g}^{\mu\nu} = \frac{1}{C}\left[g^{\mu\nu} - \frac{D\,\partial^\mu\phi\partial^\nu\phi}{C + D(\partial\phi)^2}\right]\,. \tag{2.3}$$

Moreover, $\kappa^2 = M_P^{-2} = 8\pi G$, but keep in mind that G is not in general equal to Newton's constant as measured by e.g. local experiments. Further, $C(\phi), D(\phi)$ are functions of ϕ, which can be identified as a conformal and disformal couplings of the scalar to the metric, respectively (note that the conformal coupling is dimensionless, whereas the disformal one has units of $mass^{-4}$).

The equations of motion obtained from (2.1) are:

$$R_{\mu\nu} - \frac{1}{2}g_{\mu\nu}R = \kappa^2\left(T^\phi_{\mu\nu} + T_{\mu\nu}\right)\,, \tag{2.4}$$

where, in the frame relative to $g_{\mu\nu}$, the energy-momentum tensors are defined as

$$T^\phi_{\mu\nu} = -\frac{2}{\sqrt{-g}}\frac{\delta S_\phi}{\delta g^{\mu\nu}}\,, \qquad T_{\mu\nu} = -\frac{2}{\sqrt{-g}}\frac{\delta\left(-\sqrt{-\tilde{g}}\,\mathcal{L}_M\right)}{\delta g^{\mu\nu}}\,, \tag{2.5}$$

and we model the energy-momentum tensor for matter and both dark components as perfect fluids, that is:

$$T^i_{\mu\nu} = P_i g_{\mu\nu} + (\rho_i + P_i)u_\mu u_\nu\,, \tag{2.6}$$

where ρ_i, P_i are the energy density and pressure for each fluid i with equation of state $P_i/\rho_i = \omega_i$. For the scalar field, the energy-momentum tensor takes the form:

$$T^{\phi}_{\mu\nu} = -g_{\mu\nu}\left[\frac{1}{2}(\partial\phi)^2 + V\right] + \partial_\mu\phi\,\partial_\nu\phi\,, \tag{2.7}$$

and one can define the energy density and pressure of the scalar field as:

$$\rho_\phi = -\frac{1}{2}(\partial\phi)^2 + V\,, \qquad P_\phi = -\frac{1}{2}(\partial\phi)^2 - V\,. \tag{2.8}$$

Finally the equation of motion for the scalar field dark energy becomes:

$$-\nabla_\mu\nabla^\mu\phi + V' - \frac{T^{\mu\nu}}{2}\left[\frac{C'}{C}g_{\mu\nu} + \frac{D'}{C}\partial_\mu\phi\partial_\nu\phi\right] + \nabla_\mu\left[\frac{D}{C}T^{\mu\nu}\partial_\nu\phi\right] = 0\,. \tag{2.9}$$

Due to the nontrivial coupling, the individual conservation equations for the two fluids are modified. However, the conservation equation for the full system is preserved and given in the usual way by

$$\nabla_\mu\left(T^{\mu\nu}_\phi + T^{\mu\nu}\right) = 0\,. \tag{2.10}$$

Thus using (2.7) and the equation of motion for the scalar field we can write

$$\nabla_\mu T^{\mu\nu}_\phi = Q\,\partial^\nu\phi = -\nabla_\mu T^{\mu\nu}\,, \tag{2.11}$$

where

$$Q \equiv \nabla_\mu\left[\frac{D}{C}\,T^{\mu\lambda}\,\partial_\lambda\phi\right] - \frac{T^{\mu\nu}}{2}\left[\frac{C'}{C}g_{\mu\nu} + \frac{D'}{C}\,\partial_\mu\phi\,\partial_\nu\phi\right]\,. \tag{2.12}$$

In the Jordan, as defined above, matter is conserved,

$$\tilde{\nabla}_\mu\tilde{T}^{\mu\nu} = 0\,, \tag{2.13}$$

where $\tilde{\nabla}_\mu$ is the covariant derivative computed with respect to the disformal metric (2.2) with the

Christoffel symbols given by

$$\tilde{\Gamma}^{\mu}_{\alpha\beta} = \Gamma^{\mu}_{\alpha\beta} + \frac{C'}{C}\,\delta^{\mu}_{(\alpha}\partial_{\beta)}\phi - \gamma^2\,\frac{C'}{2C}\,\partial^{\mu}\phi\,g_{\alpha\beta} + \frac{D}{C}\,\gamma^2\,\partial^{\mu}\phi\left[\nabla_{\alpha}\nabla_{\beta}\phi + \left(\frac{D'}{2D} - \frac{C'}{C}\right)\partial_{\alpha}\phi\partial_{\beta}\phi\right]\,, \tag{2.14}$$

and we have introduced the "Lorentz factor" γ defined as

$$\gamma = \frac{1}{\sqrt{1 + \frac{D}{C}(\partial\phi)^2}}\,. \tag{2.15}$$

In this frame, the energy-momentum tensor is defined as

$$\tilde{T}^{\mu\nu} = \frac{2}{\sqrt{-\tilde{g}}}\frac{\delta S_M}{\delta \tilde{g}_{\mu\nu}} \tag{2.16}$$

and the disformal energy-momentum tensor can be written as:

$$\tilde{T}^{\mu\nu} = (\tilde{\rho} + \tilde{P})\tilde{u}^{\mu}\tilde{u}^{\mu} + \tilde{P}\,\tilde{g}^{\mu\nu}\,, \tag{2.17}$$

where $\tilde{u}^{\mu} = C^{-1/2}\gamma\,u^{\mu}$. Using (2.16), we obtain a relation between the energy momentum tensor in both frames as:

$$\tilde{T}^{\mu\nu} = C^{-3}\gamma\,T^{\mu\nu}\,. \tag{2.18}$$

Further using (2.17) we arrive at a relation among the energy densities and pressures in both frames, given by

$$\tilde{\rho} = C^{-2}\gamma^{-1}\rho\,, \qquad \tilde{P} = C^{-2}\gamma\,P, \tag{2.19}$$

and therefore the equations of state in both frames are related by $\tilde{\omega} = \omega\,\gamma^2$. Note that in the pure conformal case, $D = 0$, $\gamma = 1$ and therefore $\tilde{\omega} = \omega$.

2.1 Cosmological equations

Consider an homogeneous and isotropic FRW metric $g_{\mu\nu}$,

$$ds^2 = -dt^2 + a(t)^2 dx_i dx^i \,, \tag{2.20}$$

where $a(t)$ is the scale factor. In this background, the Einstein and Klein-Gordon equations become, respectively

$$H^2 = \frac{\kappa^2}{3}\left[\rho_\phi + \rho\right] \,, \tag{2.21}$$

$$\dot{H} + H^2 = -\frac{\kappa^2}{6}\left[\rho_\phi + 3P_\phi + \rho + 3P\right] \,, \tag{2.22}$$

$$\ddot{\phi} + 3H\dot{\phi} + V_{,\phi} + Q_0 = 0 \,, \tag{2.23}$$

where, $H = \frac{\dot{a}}{a}$, dots are derivatives with respect to t and we have denoted $V_{,\phi} \equiv \frac{dV}{d\phi}$. Also the Lorentz factor becomes

$$\gamma = (1 - D\,\dot{\phi}^2/C)^{-1/2}.$$

The continuity equations for the scalar field and matter are given by

$$\dot{\rho}_\phi + 3H(\rho_\phi + P_\phi) = -Q_0\dot{\phi} \,, \tag{2.24}$$

$$\dot{\rho} + 3H(\rho + P) = Q_0\,\dot{\phi} \,, \tag{2.25}$$

where Q_0 is given by

$$Q_0 = \rho\left[\frac{D}{C}\,\ddot{\phi} + \frac{D}{C}\,\dot{\phi}\left(3H + \frac{\dot{\rho}}{\rho}\right) + \left(\frac{D_{,\phi}}{2C} - \frac{D}{C}\frac{C_{,\phi}}{C}\right)\dot{\phi}^2 + \frac{C_{,\phi}}{2\,C}(1 - 3\,\omega)\right] . \tag{2.26}$$

Using (2.25) we can rewrite this in a more compact and useful form as

$$Q_0 = \rho \left(\frac{\dot{\gamma}}{\dot{\phi}\,\gamma} + \frac{C_{,\phi}}{2C}(1 - 3\,\omega\,\gamma^2) - 3H\omega\,\frac{(\gamma^2 - 1)}{\dot{\phi}} \right) . \tag{2.27}$$

Plugging this into the (non-)conservation equation for dark matter (2.25), gives:

$$\dot{\rho} + 3H(\rho + P\,\gamma^2) = \rho \left[\frac{\dot{\gamma}}{\gamma} + \frac{C_{,\phi}}{2C}\,\dot{\phi}\,(1 - 3\,\omega\gamma^2) \right] . \tag{2.28}$$

Using the relations for the physical proper time and the scale factors in the two frames, given by

$$\tilde{a} = C^{1/2} a\,, \qquad\qquad d\tilde{\tau} = C^{1/2}\gamma^{-1} d\tau\,, \tag{2.29}$$

we can define the disformal-frame Hubble parameter $\tilde{H} \equiv \frac{d\ln\tilde{a}}{d\tilde{\tau}}$, as

$$\tilde{H} = \frac{\gamma}{C^{1/2}} \left[H + \frac{C_{,\phi}}{2C}\dot{\phi} \right] , \tag{2.30}$$

so that (2.13) takes the standard form in terms of $\tilde{H}$:

$$\frac{d\tilde{\rho}}{d\tilde{\tau}} + 3\tilde{H}(\tilde{\rho} + \tilde{P}) = 0\,. \tag{2.31}$$

Equations (2.30) and (2.31) give the background evolution equations for the modified expansion rate and matter's density evolution.

2.2 Master equations

In order to solve the cosmological equations, it is convenient to replace time derivatives with derivatives with respect to the number of e-folds N, defined as $N = \ln a/a_0$ and define $\lambda = \frac{V}{\rho}(=$

$\frac{\tilde{V}}{\tilde{\rho}}$). With these definitions, we can rewrite the Friedmann equation (2.21) and Q_0 as:

$$H^2 = \frac{\kappa^2\rho}{3}\frac{(1+\lambda)}{\left(1-\frac{\kappa^2\phi'^2}{6}\right)}\,, \tag{2.32}$$

$$\frac{Q_0}{\rho} = \frac{\gamma^2 H^2}{2}\left[\frac{2D}{C}\phi'' - \frac{2D}{C}\phi'\left(3\,\omega + \frac{\kappa^2\phi'^2}{2} + \frac{3(1+\omega)B}{2(1+\lambda)}\right) + \left(\frac{D}{C}\right)_{,\phi}\phi'^2 + \frac{C_{,\phi}}{H^2 C}(\gamma^{-2}-3\omega)\right], \tag{2.33}$$

where here we denote $' = d/dN$. Note also that (2.32) implies that $\kappa\,\phi' \leq \pm\sqrt{6}$.

Using these equations and further defining a dimensionless scalar field $\varphi = \kappa\,\phi$, we can rewrite (2.22) and (2.23) as:

$$H' = -H\left[\frac{3B}{2(1+\lambda)}(1+\omega) + \frac{\varphi'^2}{2}\right], \tag{2.34}$$

$$\begin{aligned}\varphi''\left[1+\frac{3H^2\gamma^2 B}{\kappa^2(1+\lambda)}\frac{D}{C}\right] + 3\,\varphi'\left[1-\omega\frac{3H^2\gamma^2 B}{\kappa^2(1+\lambda)}\frac{D}{C}\right] + \frac{H'}{H}\varphi'\left[1+\frac{3H^2\gamma^2 B}{\kappa^2(1+\lambda)}\frac{D}{C}\right] \\ +\frac{3B}{1+\lambda}\alpha(\varphi)(1-3\,\omega\gamma^2) + \frac{3B\lambda}{(1+\lambda)}\frac{V_{,\varphi}}{V} + \frac{3H^2\gamma^2 B}{\kappa^2(1+\lambda)}\frac{D}{C}\left[(\delta(\varphi)-\alpha(\varphi))\,\varphi'^2\right] = 0\,,\end{aligned} \tag{2.35}$$

where we defined:

$$B \equiv 1 - \frac{\varphi'^2}{6}, \tag{2.36}$$

$$\gamma^{-2} = 1 - \frac{H^2}{\kappa^2}\frac{D}{C}\varphi'^2\,, \tag{2.37}$$

$$\alpha(\varphi) = \frac{d\ln C^{1/2}}{d\varphi}, \tag{2.38}$$

$$\delta(\varphi) = \frac{d\ln D^{1/2}}{d\varphi}\,. \tag{2.39}$$

One can solve the system of coupled equations above for H and φ as functions of N. However, in some cases it is simpler to use (2.34) into (2.35) and solve the following disformal master

equation:

$$\frac{2(1+\lambda)}{3B}\,\varphi'' \;+\; (2\lambda+1-\omega)\,\varphi' + 2\lambda\,\frac{d\ln V}{d\varphi} + 2(1-3\,\omega\,\gamma^2)\,\alpha(\varphi) \\ +\; \frac{2\gamma^2(1+\lambda)}{3B}\frac{D\rho}{C}\left(\varphi'' - 3\,\varphi'\left[\omega+\frac{\varphi'^2}{6}+\frac{(1+\omega)B}{2(1+\lambda)}\right] + \frac{C}{2D}\left(\frac{D}{C}\right)_{,\varphi}\varphi'^2\right) = 0\,, \tag{2.40}$$

with γ given by:

$$\gamma^{-2} = 1 - \frac{(1+\lambda)}{3B}\frac{D\rho}{C}\varphi'^2\,. \tag{2.41}$$

From (2.40) we see that the conformal case is recovered for $D = 0$ when the second line vanishes. Moreover, the disformal piece appears always together with derivatives of the scalar field, as expected and also nontrivially coupled to the energy density. This complicates considerably the analysis of the disformal case, as we will see below.

2.3 Modified expansion rate

The effect of the expansion rate during the early time evolution due to the presence of a scalar field can be extracted from the Hubble parameter evolution in the Jordan frame defined as:

$$\tilde{H} = d(\log\tilde{a})/d\tilde{\tau},$$

which can be written using (2.29) as:

$$\tilde{H} = \frac{H\gamma}{C^{1/2}}\left(1+\alpha(\varphi)\varphi'\right)\,, \tag{2.42}$$

where remember that γ depends on H (or ρ) as seen from (2.37), while in the pure conformal case $D = 0$ and $\gamma = 1$. Note that in principle, the factor $(1+\alpha(\varphi)\varphi')$ can be positive or negative, indicating an expansion or contraction modified rate. We stick to positive definite values for this factor and therefore only modified expansion rates, though, in principle, one could have a brief

contraction period during the early universe evolution, before the onset of BBN[2]. Moreover, notice that while $\tilde{H}$ can grow during the cosmological evolution, the null energy condition (NEC) is not violated. This is because the Einstein frame expansion rate H is dictated by the energy density ρ and pressure p, which obey the NEC and therefore $\dot{H} < 0$ during the whole evolution, as it should (see for example [35]).

We further want to relate the modified expansion rate to the expected expansion rate in general relativity (GR), that is:

$$H_{GR}^2 = \frac{\kappa_{GR}^2}{3}\,\tilde{\rho}\,. \tag{2.43}$$

We can do this be using the Friedmann equation (2.32) and the relation between the energy densities (2.19) to write

$$\gamma^{-1} H^2 = \frac{\kappa^2}{\kappa_{GR}^2}\frac{C^2\,(1+\lambda)}{B}\,H_{GR}^2\,. \tag{2.44}$$

Using the definition of γ (see (2.37)) into this equation, one finds a cubic equation for H^2 in terms of all the other parameters. The real positive solution to that equation can then be replaced into (2.42) to find the modified expansion rate $\tilde{H}$, which will thus be a complicated function of H_{GR} as we now see. The cubic equation for H takes the form:

$$d_1 H^6 - H^4 + d_2^2 = 0\,, \tag{2.45}$$

where

$$d_1 = \frac{D}{C}\frac{\varphi'^2}{\kappa^2}\,, \qquad d_2 = \frac{\kappa^2}{\kappa_{GR}^2}\frac{C^2(1+\lambda)H_{GR}^2}{B}\,. \tag{2.46}$$

The solutions to (2.45) can be written as

$$H^2 = \frac{1}{3d_1}\left(1 + \left(\frac{2}{\Delta}\right)^{1/3} + \left(\frac{\Delta}{2}\right)^{1/3}\right)\,, \tag{2.47}$$

[2]See [34] for a review on scenarios with a possible contraction phase in the early universe.

with $\Delta = 2 - 27d_1^2d_2^2 + d_1d_2\sqrt{27(27d_1^2d_2^2-4)}$. The other two solutions can be obtained by replacing

$$\left(\frac{2}{\Delta}\right)^{1/3} \to e^{2\pi i/3}\left(\frac{2}{\Delta}\right)^{1/3} \qquad \text{and} \qquad \left(\frac{2}{\Delta}\right)^{1/3} \to e^{4\pi i/3}\left(\frac{2}{\Delta}\right)^{1/3}.$$

We are interested in real positive solutions for H^2. One possibility to get this is to have the imaginary part of $(\Delta/2)^{1/3}$ vanish by requiring that $\Delta > 0$, which is impossible. Therefore, the way to obtain real solutions for H is to have the imaginary parts of $(\Delta/2)^{1/3}$ and $(\Delta/2)^{-1/3}$ cancel each other, leaving a real positive solution.

For this, we need that $27d_1^2d_2^2 \leq 4$, which implies the following relation between the conformal and disformal functions:

$$\frac{3\sqrt{3}\,DC\,\varphi'^2(1+\lambda)}{B}\frac{H_{GR}^2}{\kappa_{GR}^2} \leq 2\,. \tag{2.48}$$

Under this condition, we can rewrite Δ as:

$$\Delta = 2 - 27d_1^2d_2^2 + id_1d_2\sqrt{27(4-27d_1^2d_2^2)}\,,$$

which allows us to define a complex number $Z \equiv \Delta/2$ and it is easy to check that $\bar{Z} = 2/\Delta$ and thus $|Z|^2 = 1$. Denoting further Z_i with $i = 1, 2, 3$ denoting the three solutions to H as explained above, the solutions for H, (2.47) takes the simple form:

$$H_i^2 = \frac{1}{3d_1}\left[1 + Z_i^{1/3} + \bar{Z}_i^{1/3}\right], \tag{2.49}$$

and remember that we are interested only in the real positive solution. We can now plug in (2.49), as well as the expression for γ in terms of H into the Jordan frame expansion rate (2.42), can be written as:

$$\tilde{H}^2 = \frac{\kappa^2}{\kappa_{GR}^2}\frac{\gamma^3\,C(1+\lambda)(1+\alpha(\varphi)\varphi')^2}{B}\,H_{GR}^2\,, \tag{2.50}$$

where there is a non-trivial dependence of H_{GR} encoded in

$$\gamma_i = \frac{1}{3d_1 d_2}\left[1 + Z_i^{1/3} + \bar{Z}_i^{1/3}\right] . \tag{2.51}$$

In the conformal case, $D = 0$, $\gamma = 1$ and therefore (2.50) is simply

$$\tilde{H}^2 = \frac{\kappa^2}{\kappa_{GR}^2}\frac{C(1+\lambda)(1+\alpha(\varphi)\varphi')^2}{B} H_{GR}^2 . \tag{2.52}$$

From this relation we define a speed-up parameter ξ, which will be useful below to measure the departures from the GR expansion rate result:

$$\xi \equiv \frac{\tilde{H}}{H_{GR}} . \tag{2.53}$$

We now revisit the conformal case, discussed originally in [7]. We first solve (numerically) the master equation for the scalar field (2.40) in order to compute the modified expansion rate $\tilde{H}$ and compare it with the standard expansion rate, H_{GR}.

Before solving the master equation (2.40), we would like to write it in terms of Jordan frame quantities $\tilde{\omega} = \omega\gamma^2$, $\tilde{\rho} = C^{-2}\gamma^{-1}\rho$. Moreover, the number of e-folds N can be expressed in terms of Jordan frame quantities as follows. In this frame, the entropy is conserved and is given by $\tilde{S} = \tilde{a}\,\tilde{s}$, where $\tilde{s} = \frac{2\pi}{45} g_s(\tilde{T})\tilde{T}^3$. So, the conservation of entropy and (2.29) show that N is a function of temperature and the scalar field as:

$$N \equiv \ln\frac{a}{a_0} = \ln\left[\frac{\tilde{T}_0}{\tilde{T}}\left(\frac{g_s(\tilde{T}_0)}{g_s(\tilde{T})}\right)^{1/3}\right] + \ln\left[\frac{C_0}{C}\right]^{1/2} . \tag{2.54}$$

Therefore, we can introduce the parameter, $\tilde{N}$, defined as

$$\tilde{N} \equiv \ln\left[\frac{\tilde{T}_0}{\tilde{T}}\left(\frac{g_s(\tilde{T}_0)}{g_s(\tilde{T})}\right)^{1/3}\right] , \tag{2.55}$$

and transform to derivatives w.r.t. $\tilde{N}$ (assuming well behaved functions):

$$\varphi' = \frac{1}{\left(1-\alpha(\varphi)\frac{d\varphi}{d\tilde{N}}\right)}\frac{d\varphi}{d\tilde{N}}\,, \qquad \varphi'' = \frac{1}{\left(1-\alpha(\varphi)\frac{d\varphi}{d\tilde{N}}\right)^3}\left(\frac{d^2\varphi}{d\tilde{N}^2}+\frac{d\alpha}{d\varphi}\left(\frac{d\varphi}{d\tilde{N}}\right)^3\right). \tag{2.56}$$

In a slight abuse of notation and to keep expressions neat, in what follows we denote derivatives w.r.t. $\tilde{N}$ with a prime $'$.

2.4 Pure conformal case

We start with the pure conformal case. That is, we take $D(\phi) = 0$ in (2.40) and therefore $\gamma = 1$ (and $\tilde{\omega} = \omega$). Moreover, during the radiation and matter dominated eras, of interest for us, the potential energy of the scalar field is subdominant and thus, we take $\lambda \sim 0$. Therefore the master equation (2.40) simplifies to:

$$\frac{2}{3(1-\varphi'^2/6)}\,\varphi'' \quad + \quad (1-\tilde{\omega})\,\varphi' + 2(1-3\,\tilde{\omega})\,\alpha(\varphi) = 0, \tag{2.57}$$

which in terms of derivatives wrt $\tilde{N}$ takes the form:

$$\frac{1}{3B\left[1-\alpha(\varphi)\varphi'\right]^3}\left(\varphi'' + \frac{d\alpha}{d\varphi}\left(\varphi'\right)^3\right) + \frac{(1-\tilde{\omega})}{\left[1-\alpha(\varphi)\varphi'\right]}\,\varphi' + (1-3\,\tilde{\omega})\,\alpha(\varphi) = 0\,, \tag{2.58}$$

where $B = 1 - \frac{(\varphi')^2}{6(1-\alpha(\varphi)\varphi')^2}$. Using the relation between $\tilde{H}$ and H_{GR} defined in (2.52), we can write the speed-up parameter as

$$\xi = \frac{\tilde{H}}{H_{GR}} = \frac{C^{1/2}(\varphi)}{C^{1/2}(\varphi_0)}\frac{1}{(1-\alpha(\varphi)\varphi')\sqrt{B}}\frac{1}{\sqrt{1+\alpha^2(\varphi_0)}}\,, \tag{2.59}$$

where we have used the relation between the bare gravitational constant and that measured by local experiments for conformally coupled theories [36]:

$$\kappa_{GR}^2 = \kappa^2 C(\varphi_0)[1 + \alpha^2(\varphi_0)]\,, \tag{2.60}$$

where φ_0 is the value of the scalar field at present time.

2.4.1 Expansion rate modification

The scalar equation in the conformal case (2.57), as function of N (for $\lambda = 0$) contains a term which can be interpreted as an effective potential, dictated by $V_{eff} = \ln C^{1/2}$. For a strictly radiation dominated era, $\tilde{\omega} = 1/3$, the effective potential term vanishes and we are left with an equation that can be solved analytically [37], giving $\varphi' \propto e^{-N}$. That is, any initial velocity will rapidly go to zero (remember that from the Friedmann equation (2.32), φ' is constrained to be $|\varphi'| \lesssim \sqrt{6}$). Therefore we explore the effects of having a non-zero initial velocity in our analysis below. Since the scalar field is expressed in Planck units, we focus on order one or smaller field variations $\Delta\varphi$. One can check, using the analytic solution to (2.57) deep in the radiation era, that for initial velocities $\varphi_0' \ll \pm\sqrt{6}$, the total field displacement is of order $\Delta\varphi \sim \varphi_0'$ [37]. However, given that we don't know much about the theory before BBN, we explore different initial values for (φ_0, φ_0') and study their consequences. In particular we explore initial values φ_0 and $\varphi_0' \in (-1.0, 1.0)$.

We now concentrate on an explicit conformal factor. We use the same conformal factor as that studied in [7], which is given by:

$$C(\varphi) = (1 + b\, e^{-\beta\,\varphi})^2\,, \tag{2.61}$$

with the values $b = 0.1$, $\beta = 8$, which have been shown to satisfy the constraints imposed by tests of gravity, for the parameters α, β, ξ. As we will see, the requirement of reaching the GR expansion rate value by the time of the onset of BBN drives these parameters to very small values,

which are thus consistent with the constraints from gravity for their values today.

As we discussed above, in the equation of motion for φ, with $\tilde{\omega} \neq 1/3$, the conformal factor acts as an effective potential on which the scalar field moves, damped by the Hubble friction (see (2.23)). Since any initial velocity φ' goes rapidly to zero deep in the radiation era, in the subsequent evolution of φ, the term $(\varphi')^2$ in the master equation will be negligible. In this regime, the equation is that of a particle moving in an effective potential with a damping term. Therefore, one can understand the evolution of φ from the form of the effective potential ($V_{eff} = \ln C^{1/2}$) and the initial conditions used. For the conformal function we are considering (2.61), one sees that there is a set of initial conditions that will give rise to an interesting behavior in φ, and therefore an interesting modified expansion rate in the Jordan frame $\tilde{H}$ (2.52), as we now explain.

In general, both the initial position and velocity of the scalar field can take any value, positive and negative. In the runaway effective potential dictated by $\ln C^{1/2}$ for the conformal factor (2.61) we consider here, we have the following possibilities. i) The scalar field starting somewhere up in the runaway effective potential with zero initial velocity. In this case, the scalar field will roll-down the potential, eventually stopping due to Hubble friction, at some constant value of φ, which depends on its initial value. So long as $(1 + \alpha(\varphi)\,\varphi')$ stays positive (see (2.42)), C will evolve rapidly towards 1. More generally, the initial velocity can be different from zero. If the initial velocity is positive, the behavior will be similar to the previous case. The field will roll-down the effective potential towards its final terminal value.

ii) A more interesting possibility arises when one allows for negative initial velocities. In this case, the field will start rolling-up the effective potential towards smaller values of the field, eventually turning back down and moving towards its terminal value. It is easy to see that an interesting effect happens when the field starts at an initial positive value. Given a sufficient initial negative velocity the field will move towards negative values until its velocity becomes zero and then positive again, as it rolls back down the effective potential. This change in sing for the scalar evolution will produce a pick in the conformal function that will give rise to a non-trivial modification of Jordan's frame expansion rate $\tilde{H}$, as we are looking for. As mentioned before, we

are interested in (sub-)Planckian initial values (φ_0, φ_0'), such that $\tilde{H} > 0$. With these requirements, one can see that given an initial negative velocity, there is a suitable initial value of the scalar field such that the behavior just described holds and the expansion rate $\tilde{H}$ has an interesting evolution before the onset of BBN. At late times the conformal function goes to one and the GR expansion is recovered. We show this behaviour explicitly in Figures 2.1 and 2.2 where we plot the numerical solution for the evolution of φ and $C(\varphi)$ as functions of the temperature. In these plots we find $\varphi = \varphi(\tilde{T})$ by first solving (2.58) numerically with initial conditions $(\varphi_0, \varphi_0') = (0.2, -0.99)$ and then use (2.55) to express $\varphi(\tilde{N})$ as function of $\tilde{T}$. As we can see, the conformal factor starts growing towards a maximum value as φ moves to negative values, to rapidly drop down towards its GR value at $C \to 1$ as φ moves down the effective potential towards positive values. This non-trivial effect will give rise to the possibility of re-annihilation, as we discuss below.

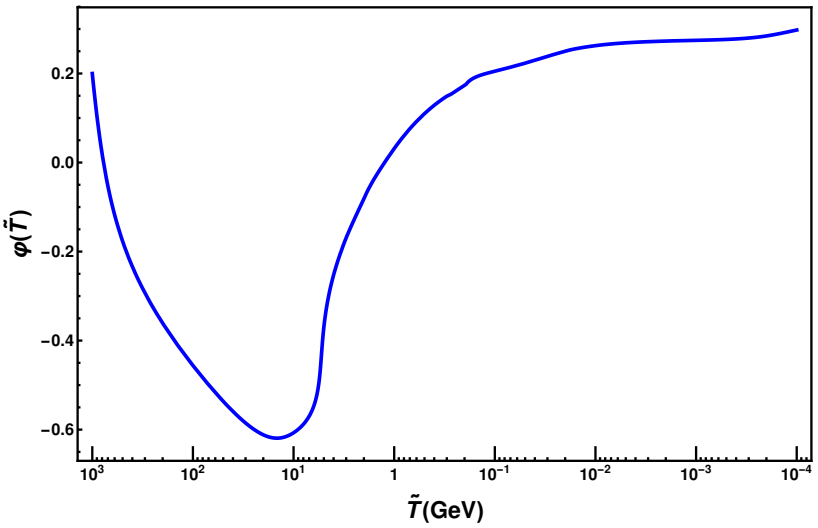

Figure 2.1: Typical evolution of the scalar field as temperature decreases. The initial values are $(\varphi, d\,\varphi/d\,\tilde{N}) = (0.2, -0.994)$. Reprinted with permission from "Dark matter relics and the expansion rate in scalar-tensor theories" by B. Dutta, E. Jimenez, I. Zavala, 2017. JCAP no.06, 032, Figure 1, p. 12. Copyright SISSA Medialab Srl. All rights reserved.

Based on the discussion above, we have solved the master equation (2.58), to find the scalar field as a function of $\tilde{N}$ for various initial conditions, where we see the interesting behavior ex-

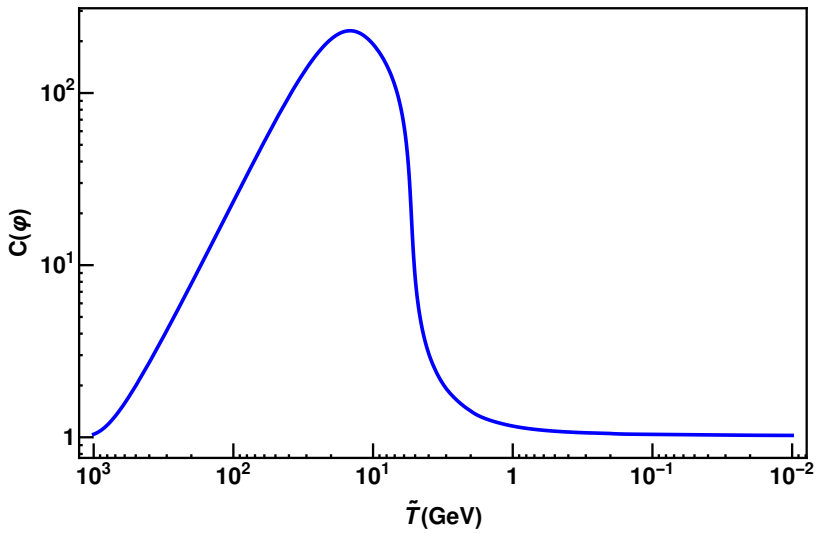

Figure 2.2: Behaviour of the conformal factor, $C(\varphi)$ as a function of the temperature for the same initial values as in Figure 2.1. Reprinted with permission from "Dark matter relics and the expansion rate in scalar-tensor theories" by B. Dutta, E. Jimenez, I. Zavala, 2017. JCAP no.06, 032, Figure 2, p. 13. Copyright SISSA Medialab Srl. All rights reserved.

plained above. The resulting modified expansion rate and its comparison with the standard case are shown in Figure 2.3 for the same initial conditions as in Figures 2.1 and 2.2. In our numerical exploration, we choose initial conditions for which the notch in the expansion rate (see Fig. 2.3) occurs closer to the BBN time. This has interesting consequences for the dark matter annihilation, as we discuss in chapter 4.

2.4.2 The equation of state parameter, $\tilde{\omega}$

When solving the master equation (2.58), we have taken into account an important effect that occurs during the radiation dominated era. Deep in this epoch, the equation of state is given by $\tilde{\omega} = 1/3$. When a particle species in the cosmic soup becomes non-relativistic, $\tilde{\omega}$ differs slightly from $1/3$. When the temperature of the universe drops below the rest mass of each of the particle types, there are non-zero contributions to $1 - 3\tilde{\omega}$. This activates the effective potential, which can be seen in the last term of (2.58), and displaces, or "kicks" the field along V_{eff}.

To examine this effect in more detail, we start by writing $1 - 3\,\tilde{\omega}$ during the early stages of the

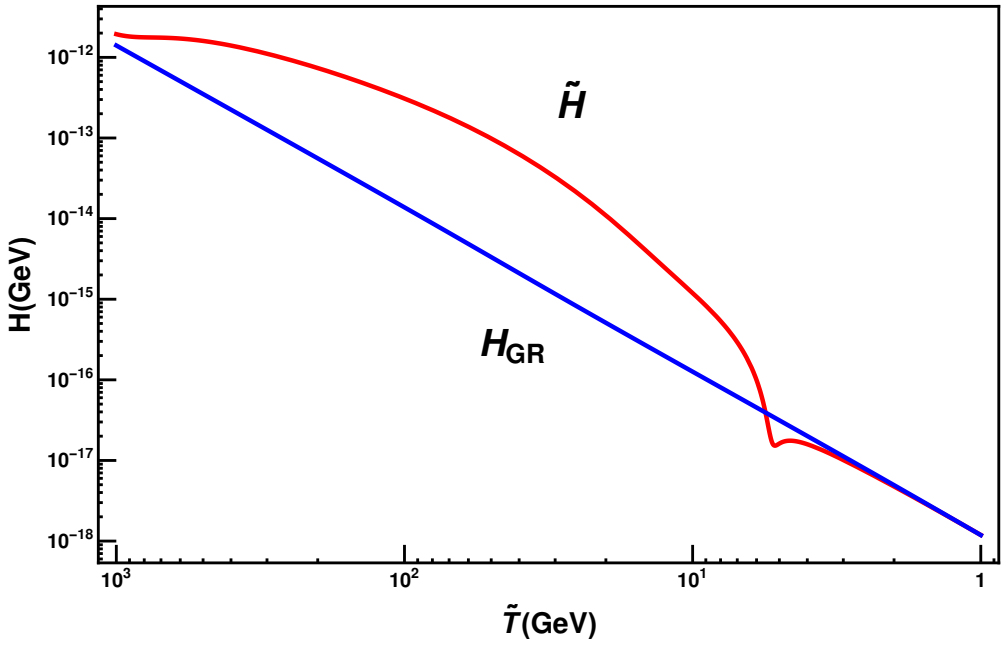

Figure 2.3: Comparing the Hubble expansion rate $\tilde{H}$ in the Jordan Frame with the standard Hubble expansion rate H_{GR}. The presence of the scalar field enhances and decreases the expansion rate during the radiation dominated era. This plot corresponds to initial conditions given by $(\varphi_0, \varphi_0') = (0.2, -0.994)$. Reprinted with permission from "Dark matter relics and the expansion rate in scalar-tensor theories" by B. Dutta, E. Jimenez, I. Zavala, 2017. JCAP no.06, 032, Figure 3, p. 13. Copyright SISSA Medialab Srl. All rights reserved.

universe as in [7] and [12]

$$1 - 3\,\tilde{\omega} = \frac{\tilde{\rho} - 3\,\tilde{p}}{\tilde{\rho}} = \sum_A \frac{\tilde{\rho}_A - 3\tilde{p}_A}{\tilde{\rho}} + \frac{\tilde{\rho}_m}{\tilde{\rho}}\,, \tag{2.62}$$

where the sum runs over all particles in thermal equilibrium during the radiation dominated era and $\tilde{\rho}_m$ is the contribution from the non-relativistic decoupled and pressureless matter. The summation over all the particle is responsible for the kicking effect discussed above. Then, a kick function is defined as

$$\Sigma(\tilde{T}) \equiv \sum_A \frac{\tilde{\rho}_A - 3\tilde{p}_A}{\tilde{\rho}}\,, \tag{2.63}$$

where the energy density $\tilde{\rho}_A$ and pressure $\tilde{p}_A$ of each type A of particle are given by

$$\tilde{\rho}_A(\tilde{T}) = \frac{g_A}{2\pi^2}\int_{m_A}^{\infty}\frac{(E^2-m_A^2)^{1/2}}{\exp(E/\tilde{T})\pm 1}E^2dE\,, \tag{2.64}$$

$$\tilde{p}_A(\tilde{T}) = \frac{g_A}{6\pi^2}\int_{m_A}^{\infty}\frac{(E^2-m_A^2)^{3/2}}{\exp(E/\tilde{T})\pm 1}E^2dE\,, \tag{2.65}$$

with g_A being the number of internal degrees of freedom of species of type A and the plus (minus) sign in the integral corresponds to fermions (bosons).

After using $\tilde{\rho} \simeq \pi^2 g_{eff}(\tilde{T})\tilde{T}^4/30$, (2.64) and (2.65) Σ becomes

$$\Sigma(\tilde{T}) = \sum_A \frac{15}{\pi^4}\frac{g_A}{g_{eff}(\tilde{T})}\,y_A^2\int_{y_A}^{\infty}dx\frac{\sqrt{x^2-y_A^2}}{e^x\pm 1}\,, \tag{2.66}$$

where $g_{eff}(\tilde{T})$ is the total number of relativistic degrees of freedom[3] and $y_A = m_A/\tilde{T}$.

To compute (2.66), we consider the Standard Model particle spectrum. In particular, we take into account the top quark, the Higgs boson, Z boson, W bosons, bottom quark, tau lepton, charm quark, charged pions, neutral pion, muon lepton and the electron (See Table 2.1 for details on the masses and internal degrees of freedom per species). As we show in Figure 2.4, Σ is mostly zero, except when the kicks happen. Then, during the radiation dominated era, we compute the equation of state parameter from (2.62) as $\tilde{\omega} = (1-\Sigma(\tilde{T}))/3$[4].

In Figure 2.5 we show the evolution of $\tilde{\omega}$ between 10 TeV and 10 eV. This figure shows four troughs, which are the "kicks" mentioned above. Each kick corresponds to the transition of one or more particles to the non-relativistic regime. For example, the trough at around 0.5 MeV is due to the electron, while the one at around 100 GeV is due to the heavy particles (t, H, Z and W).

Towards the end of the radiation era, approaching the transition to the matter dominated era,

[3]To calculate g_{eff} we follow the numerical procedure described in Appendix A of [38].
[4]$\tilde{\rho}$ is dominated by radiation, thus $\tilde{\rho}_m/\tilde{\rho}$ is negligible.

Particle	Mass (GeV)	g_A
t	173.2	12
H	125.1	1
Z	91.19	3
$W^{\pm}$	80.39	6
b	4.18	12
τ	1.78	4
c	1.27	12
π^0	0.140	12
$\pi^{\pm}$	0.135	2
μ	0.106	4
e	0.000511	4

Table 2.1: Spectrum of particles used to calculate the kick function (2.66). For each particle, we show its mass and number of internal degrees of freedom, g_A.

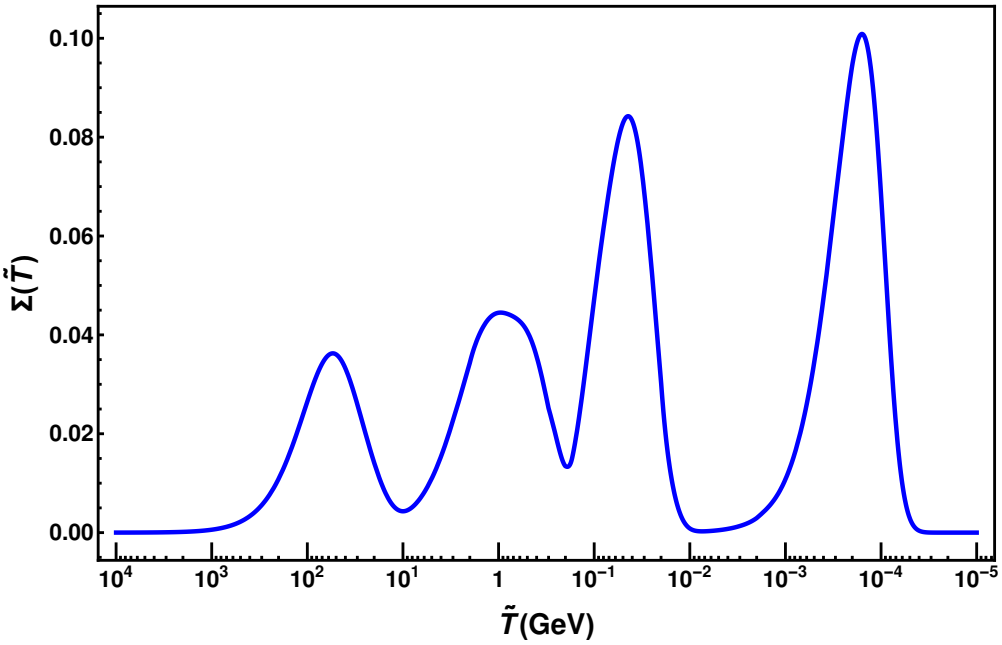

Figure 2.4: Thermal evolution of the kick function during the radiation dominated era. Outside the interval of temperatures shown, Σ vanishes. Reprinted with permission from "Dark matter relics and the expansion rate in scalar-tensor theories" by B. Dutta, E. Jimenez, I. Zavala, 2017. JCAP no.06, 032, Figure 10, p. 22. Copyright SISSA Medialab Srl. All rights reserved.

(2.62) takes the approximate form:

$$1 - 3\,\tilde{\omega} \simeq \frac{\tilde{\rho}_m}{\tilde{\rho}_m + \tilde{\rho}_r} \simeq \frac{1}{1 + \tilde{T}/\tilde{T}_{eq}}\,, \tag{2.67}$$

where $\tilde{T}_{eq} \sim \mathcal{O}(10^{-9})$GeV is the temperature at matter-radiation equality, that is, $\tilde{\rho}_m(\tilde{T}_{eq}) = \tilde{\rho}_r(\tilde{T}_{eq})$. We can now combine (2.63) and (2.67) to compute the thermal evolution of (2.62) in the radiation dominated and matter dominated eras and use it in the master equation.

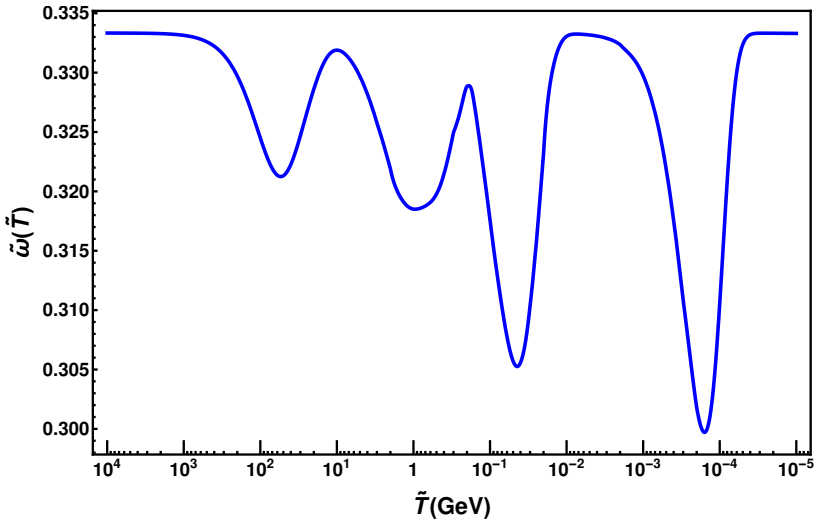

Figure 2.5: Evolution of $\tilde{\omega}$ in (2.62) as function of temperature during the radiation dominated era. Reprinted with permission from "Dark matter relics and the expansion rate in scalar-tensor theories" by B. Dutta, E. Jimenez, I. Zavala, 2017. JCAP no.06, 032, Figure 4, p. 15. Copyright SISSA Medialab Srl. All rights reserved.

2.4.3 Parameter Constraints

In scalar-tensor theories of gravity, there are some constraints on the parameters that need to be taken into account. Deviations from GR can be parametrised in terms of the post-Newtonian parameters γ_{PN} and β_{PN}, which are given in terms of $\alpha(\varphi_0)$ defined in (2.38) and its derivative

$\alpha_0' = d\alpha/d\varphi|_{\varphi_0}$ as [39, 40]:

$$\gamma_{PN} - 1 = -\frac{2\alpha_0^2}{1+\alpha_0^2}\,, \qquad \beta_{PN} - 1 = \frac{1}{2}\frac{\alpha_0'\alpha_0^2}{(1+\alpha_0^2)^2}\,. \tag{2.68}$$

Solar system tests of gravity, including the perihelion shift of Mercury, Lunar Laser Ranging experiments, and the measurements of the Shapiro time delay by the Cassini spacecraft [41, 42, 43] indicate that α_0 should be very small, with values $\alpha_0^2 \lesssim 10^{-5}$, while binary pulsar observations impose that $\alpha_0' \gtrsim -4.5$. The last constraint applies to the speed-up factor ξ, which has to be of order 1 before the onset of BBN. In our examples we have $\alpha_0^2 \simeq 2\times 10^{-5}$, $\alpha_0' > 0$ and $\xi \approx 1.05$.

2.5 Conformal case plus a simple disformal coupling

We now discuss briefly the effect of the disformal factor in the metric (2.2) to the expansion rate of the universe, $\tilde{H}$, and compare it to the conformal modification to $\tilde{H}$[5]. Hence, we explore $D(\phi) \neq 0$ for the same conformal factor studied before, that is, $C(\varphi) = (1 + b\, e^{-\beta\,\varphi})^2$ for $b = 0.1$, $\beta = 8$. To investigate these modifications, we first need to look at the scalar field evolution with temperature.

In the pure conformal case studied above, we found the thermal evolution of the scalar field by solving the master equation (2.58) numerically, which is (2.40) for $D(\phi) = 0$. However, to study the effects of the disformal factor on the scalar field, it is more convenient to solve the system of two coupled equations (2.34) and (2.35). Using these equations we find solutions for the dimensionless scalar field φ, and for the expansion rate in the Einstein frame H.

Notice that solving the system of coupled equations or solving the master equation to find the thermal evolution of the scalar field are equivalent methods (as we have explicitly checked), because (2.40) it is nothing but a combination (2.34) and (2.35). However, while in the pure conformal case the master equation can be made independent of H (or ρ), this is not the case for the more general disformal case, as we can see in (2.40).

In the same way, as for the conformal case, we are interested mainly in the radiation and matter

[5] We leave a detailed exploration for a future publication.

eras and therefore we can neglect the potential energy of the scalar field. Thus, we consider $V \sim 0$ and $\lambda = 0$. Also, while solving the coupled equations we have to express ω in the Jordan frame by using $\tilde{\omega} = \omega\gamma^2$ and transform all derivatives w.r.t. N to derivatives w.r.t. $\tilde{N}$ by using (2.56).

With this information, we solve the system of coupled equations numerically to find the dimensionless scalar field φ and the Hubble parameter H, as functions of the number of e-folds $\tilde{N}$ (and the temperature). We choose the same initial conditions for the scalar field and its derivative as in the conformal case and to obtain the initial condition for H, we use (2.49).

Once we have the solutions for φ and H as functions of temperature, we can go back to (2.42) and (2.37) to obtain the expansion rate for the disformal model. As an example, in Figure 2.6 we show the effects of a disformal factor given by $D(\varphi) = D_0\,\varphi^2$ with $D_0 = -4.9 \times 10^{-14}$. In this plot, we illustrate the effect of the disformal contribution on the expansion rate ($\tilde{H}_{Disformal}$) and compare it to the modified expansion rate for the conformal case ($\tilde{H}_{Conformal}$) and the standard case (H_{GR}). We use the same initial conditions as in Figures 2.1 and 2.2 for the scalar field and its derivative.

Also, it is important to mention that for the case shown the parameter constraints described in section 2.4.3 are satisfied. In particular we find $\alpha_0^2 \simeq 2 \times 10^{-5}$, $\alpha_0' > 0$ and $\xi \approx 1.02$.

From our example, with C and D as indicated above, we can clearly see the differences from the disformally modified expansion rate $\tilde{H}_{Disformal}$ compared to the conformally modified and standard case, H_{GR}. The evolution of $\tilde{H}_{Disformal}$ is similar to that of $\tilde{H}_{Conformal}$, having an enhancement and a decrement compared to the standard expansion rate H_{GR}. Moreover, the main differences with respect to the conformal modification are the position of the notch and its shape. The notch is moved to higher temperatures and it becomes a little bit sharper.

These differences between the expansion rates can be understood from (2.35). First, in this equation, we see that the factor $\frac{3H^2\gamma^2 BD}{\kappa^2(1+\lambda)C}$ in the coefficients of φ'', φ' and φ'^2 vanishes when $D = 0$. For the disformal example shown in Figure 2.6, this factor is a very small correction to the equation, which is reflected in the slight shape modification of $\tilde{H}_{Disformal}$ compared to $\tilde{H}_{Conformal}$. Second, the term proportional to $\delta(\varphi)$ plays a more important role, being responsible for the shifting of the

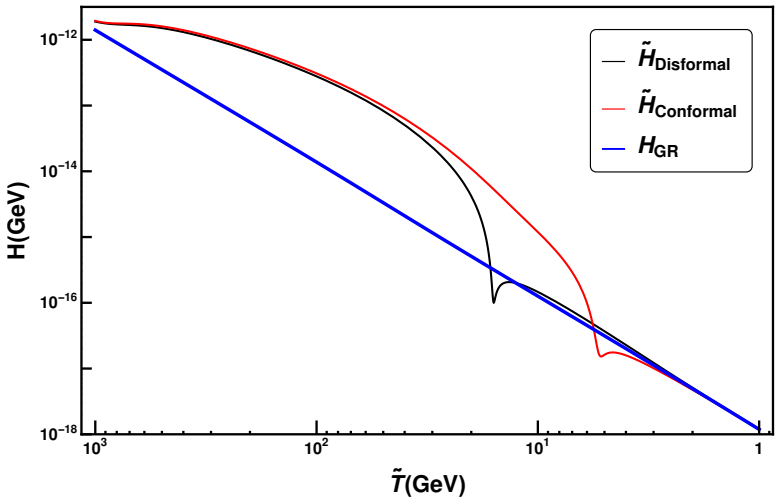

Figure 2.6: Comparing the modified expansion rate of the universe in the disformal and conformal scenarios for the same initial conditions as in Fig. 2.3. Reprinted with permission from "Dark matter relics and the expansion rate in scalar-tensor theories" by B. Dutta, E. Jimenez, I. Zavala, 2017. JCAP no.06, 032, Figure 9, p. 19. Copyright SISSA Medialab Srl. All rights reserved.

notch.

3. DISFORMAL D-BRANE COUPLING SCENARIO[1]

In this chapter, we introduce the second class of ST theories, which is Disformal D-Brane Coupling scenario. This scenario, as was pointed out in the introduction, can arise from a post-string inflationary scenario. At this stage, the universe is already four-dimensional and moduli associated to the compactification have been properly stabilised[2]. However, the relevant parameters in the model will depend on the string theory quantities such as the string scale, string coupling and compactification volume as we will argue.

One of the main differences between this scenario and the one studied in the previous chapter is that the disformal coupling enters not only enter through the metric (as in the previous scenario) but also through the action. We can see this clearly by comparing the action of the conformally coupled ST theory, given by (2.1), and the action we consider for the disformal D-brane coupling scenario, given below by (3.1).

The starting action we consider is given by

$$S = S_{EH} + S_{brane}\,, \tag{3.1}$$

where:

$$S_{EH} = \frac{1}{2\kappa^2}\int d^4x\sqrt{-g}\,R, \tag{3.2}$$

$$S_{brane} = -\int d^4x\sqrt{-g}\left[M^4C^2(\phi)\sqrt{1+\frac{D(\phi)}{C(\phi)}(\partial\phi)^2}+V(\phi)\right] - \int d^4x\sqrt{-\tilde{g}}\,\mathcal{L}_M(\tilde{g}_{\mu\nu})\,, \tag{3.3}$$

where in a string setup, $\kappa^2 = M_P^{-2} = 8\pi G$ is related to the string coupling, scale and overall compactification volume by $M_P^2 = \frac{2\mathcal{V}_6}{2\pi g_s^2\alpha'}$, where $M_s^{-2} = \ell_s^2 = \alpha'(2\pi)^2$ is the string scale, $\mathcal{V}_6$ is

[1] Reprinted with permission from "D-brane disformal coupling and thermal dark matter" by B. Dutta, E. Jimenez, I. Zavala, 2017. PhysRevD.96.103506. Copyright American Physical Society.

[2] Though these fields might be displaced from their minima, giving rise to a matter dominated regime, with interesting consequences (see e.g. [44]).

the dimensionless six-dimensional (6D) volume in string units and g_s is the string coupling. Note also that G is not in general equal to Newton's constant as measured by e.g. local experiments.

In (3.3) we describe the brane dynamics (of transverse and longitudinal fluctuations associated to the scalar and matter respectively) given by the Dirac-Born-Infeld (DBI) and Chern-Simons actions for a single D3-brane. The DBI part gives rise to the noncanonically normalized scalar field ϕ, associated to the single overall position, $r^2 = \sum_i^6 y_i^2$, of the brane in the internal 6D space[3] with coordinates y_i. In this case, the scale M is dictated by the tension of a D3-brane as $M^4 = T_3 = (g_s \alpha'^2 (2\pi)^3)^{-1} = M_s^4 (2\pi) g_s^{-1} = \frac{g_s^3}{8\pi \mathcal{V}_6^2} M_P^4$ and thus by the string scale and coupling. In reality, one would most likely have a stack of branes moving in the internal space. However, to study the cosmological evolution after inflation, it is enough to model all matter living on the moving brane as in (3.3) (see also [3, 45]) via the disformally coupled matter Lagrangian $\mathcal{L}_M$.

In (3.3), the disformally coupled metric $\tilde{g}_{\mu\nu}$ is given by the induced metric on the brane, which for a brane moving along a single internal direction can be written as

$$\tilde{g}_{\mu\nu} = C(\phi) g_{\mu\nu} + D(\phi) \partial_\mu \phi \partial_\nu \phi \,. \tag{3.4}$$

where the scalar field is related to the D-brane position by[4] $\phi = \sqrt{T_3}\, r$, and while $C(\phi)$ is dimensionless, $D(\phi)$ has units of mass^{-4}. These functions are specified by the ten-dimensional (10D) compactification and therefore in general will be related to each other as we see below (see also [3]).

3.1 The equations of motion

Einstein's equations obtained from (3.1) are given by

$$R_{\mu\nu} - \frac{1}{2} g_{\mu\nu} R = \kappa^2 \left(T^\phi_{\mu\nu} + T_{\mu\nu} \right) \,, \tag{3.5}$$

[3] In general, a D3-brane can move in all six of the internal dimensions.

[4] For the D3-brane case, one can also consider different dimensionalities, which will add extra factors due to the internal volumes wrapped by the brane in that case.

where the energy-momentum tensors are defined with respect to the Einstein-frame metric $g_{\mu\nu}$ and are given by

$$T_{\mu\nu} = P g_{\mu\nu} + (\rho + P) u_\mu u_\nu \,, \tag{3.6}$$

for matter, where ρ, P are the energy density and pressure for matter with equation of state $P/\rho = \omega$. For the scalar field, the energy-momentum tensor takes the form:

$$T^{\phi}_{\mu\nu} = -g_{\mu\nu}\left[M^4 C^2 \gamma^{-1} + V\right] + M^4 C D\, \gamma \partial_\mu\phi\, \partial_\nu\phi \tag{3.7}$$

where the energy density and pressure for the scalar field are identified as:

$$\rho_\phi = M^4 C^2 \gamma + V \,, \qquad P_\phi = -M^4 C^2 \gamma^{-1} - V \,, \tag{3.8}$$

and the "Lorentz factor" γ introduced above is defined by

$$\gamma \equiv \left(1 + \frac{D}{C}\,(\partial\phi)^2\right)^{-1/2} \,. \tag{3.9}$$

It will be convenient to rewrite (3.8) by introducing $\mathcal{V} \equiv V + C^2 M^4$, as

$$\rho_\phi = -\frac{M^4 C D \gamma^2}{\gamma + 1}(\partial\phi)^2 + \mathcal{V} \,, \qquad P_\phi = -\frac{M^4 C D\, \gamma}{\gamma + 1}(\partial\phi)^2 - \mathcal{V} \,. \tag{3.10}$$

The equation of motion for the scalar field is:

$$\begin{aligned} -\nabla_\mu\left[M^4 D C \gamma\ \partial^\mu\phi\right] + \frac{\gamma^{-1} M^4 C^2}{2}\left[\frac{D_{,\phi}}{D} + 3\frac{C_{,\phi}}{C}\right] + \frac{\gamma\, M^4 C^2}{2}\left[\frac{C_{,\phi}}{C} - \frac{D_{,\phi}}{D}\right] + V_\phi \\ - \frac{T^{\mu\nu}}{2}\left[\frac{C_{,\phi}}{C} g_{\mu\nu} + \frac{D_{,\phi}}{C}\partial_\mu\phi\partial_\nu\phi\right] + \nabla_\mu\left[\frac{D}{C} T^{\mu\nu}\partial_\nu\phi\right] = 0 \,, \end{aligned} \tag{3.11}$$

where $C_{,\phi}$ denotes derivative of C with respect to ϕ, and similarly for D, V. Finally, the energy-momentum conservation equation, $\nabla_\mu T^{\mu\nu}_{tot} = \nabla_\mu\left(T^{\mu\nu}_{\phi} + T^{\mu\nu}\right) = 0$, combined with the equation

of motion for the scalar field allows us to define Q as

$$Q \equiv \nabla_\mu \left[\frac{D}{C}\, T^{\mu\lambda}\, \partial_\lambda \phi \right] - \frac{T^{\mu\nu}}{2} \left[\frac{C_{,\phi}}{C} g_{\mu\nu} + \frac{D_{,\phi}}{C}\, \partial_\mu \phi\, \partial_\nu \phi \right] , \tag{3.12}$$

so that, $\nabla_\mu T^{\mu\nu}_\phi = -\nabla_\mu T^{\mu\nu} = Q \partial^\nu \phi$.

3.2 Cosmological equations

Let us now look at the cosmological evolution. We start with a FRW background metric:

$$ds^2 = -dt^2 + a^2(t) dx_i dx^i \,, \tag{3.13}$$

where $a(t)$ is the scale factor in the Einstein frame. With this metric, the equations of motion become

$$H^2 = \frac{\kappa^2}{3} \left[\rho_\phi + \rho \right] , \tag{3.14}$$

$$\dot{H} + H^2 = -\frac{\kappa^2}{6} \left[\rho_\phi + 3P_\phi + \rho + 3P \right] , \tag{3.15}$$

$$\ddot{\phi} + 3H\dot{\phi}\,\gamma^{-2} + \frac{C}{2D} \left(\frac{D_{,\phi}}{D} - \frac{C_{,\phi}}{C} + \gamma^{-2} \left[\frac{5C_{,\phi}}{C} - \frac{D_{,\phi}}{D} \right] - 4\gamma^{-3} \frac{C_{,\phi}}{C} \right) + \frac{1}{M^4 C D \gamma^3} \left(\mathcal{V}_{,\phi} + Q_0 \right) = 0 \,, \tag{3.16}$$

where, $H = \frac{\dot{a}}{a}$, dots are derivatives with respect to t,

$$\gamma = (1 - D\,\dot{\phi}^2/C)^{-1/2},$$

and

$$Q_0 = \rho \left[\frac{D}{C}\, \ddot{\phi} + \frac{D}{C}\, \dot{\phi} \left(3H + \frac{\dot{\rho}}{\rho} \right) + \left(\frac{D_{,\phi}}{2C} - \frac{D}{C} \frac{C_{,\phi}}{C} \right) \dot{\phi}^2 + \frac{C_{,\phi}}{2\,C} (1 - 3\,\omega) \right] , \tag{3.17}$$

where we have used the equation of state for matter $P = \omega\rho$. The continuity equations for the scalar field and matter are given by

$$\dot{\rho}_\phi + 3H(\rho_\phi + P_\phi) = -Q_0\dot{\phi}\,, \tag{3.18}$$

$$\dot{\rho} + 3H(\rho + P) = Q_0\,\dot{\phi}\,. \tag{3.19}$$

Using (3.19), we can rewrite this as

$$Q_0 = \rho\left(\frac{\dot{\gamma}}{\dot{\phi}\,\gamma} + \frac{C_{,\phi}}{2C}(1 - 3\,\omega\,\gamma^2) - 3H\omega\,\frac{(\gamma-1)}{\dot{\phi}}\right)\,. \tag{3.20}$$

Plugging this into the (non)conservation equation for matter (3.19) gives

$$\dot{\rho} + 3H(\rho + P\,\gamma^2) = \rho\left[\frac{\dot{\gamma}}{\gamma} + \frac{C_{,\phi}}{2C}\,\dot{\phi}\,(1 - 3\,\omega\gamma^2)\right]\,. \tag{3.21}$$

3.3 Modified and standard expansion rates

The modified expansion rate felt by matter $\tilde{H}$ (which will enter into the Boltzmann equation) is the Jordan-frame expansion rate, given in terms of Jordan (or disformal) frame quantities, and defined with respect to the disformal metric $\tilde{g}_{\mu\nu}$. In this frame, the Hubble parameter is given by:

$$\tilde{H} \equiv \frac{d\ln\tilde{a}}{d\tilde{\tau}} = \frac{\gamma}{C^{1/2}}\left[H + \frac{C_{,\phi}}{2C}\dot{\phi}\right]\,. \tag{3.22}$$

and it is thus a function of the Einstein-frame rate H, the scalar field and its derivatives. The proper time and the scale factors in the Jordan and Einstein frames are related by

$$\tilde{a} = C^{1/2}a\,, \qquad\qquad d\tilde{\tau} = C^{1/2}\gamma^{-1}d\tau\,. \tag{3.23}$$

Furthermore, the energy densities and pressures in the two frames are related by

$$\tilde{\rho} = C^{-2}\gamma^{-1}\rho\,, \qquad \tilde{P} = C^{-2}\gamma P\,, \tag{3.24}$$

while the equation of state is given by

$$\tilde{\omega} = \omega\gamma^2\,. \tag{3.25}$$

One can check that in the Jordan frame, the continuity equation for matter takes the standard form:

$$\frac{d\tilde{\rho}}{d\tilde{\tau}} + 3\tilde{H}(\tilde{\rho} + \tilde{P}) = 0\,. \tag{3.26}$$

To proceed further, we next swap time derivatives with derivatives with respect to the number of efolds, $N = \ln a/a_0$, so $dN = Hdt$. We also define a dimensionless scalar field $\varphi = \kappa\phi$. In this case, (3.22) becomes:

$$\tilde{H} = \frac{H\gamma}{C^{1/2}}\left[1 + \alpha(\varphi)\varphi'\right]\,, \tag{3.27}$$

where a prime denotes a derivatives with respect to N and we have defined

$$\alpha(\varphi) = \frac{d\ln C^{1/2}}{d\varphi}\,. \tag{3.28}$$

Note also that in terms of φ and N derivatives, the Lorentz factor is now given by

$$\gamma^{-2} = 1 - \frac{H^2}{\kappa^2}\frac{D}{C}\varphi'^2\,. \tag{3.29}$$

We want to compare the Jordan-frame expansion rate with that expected in GR, which is given by

$$H_{GR}^2 = \frac{\kappa_{GR}^2}{3}\tilde{\rho}\,. \tag{3.30}$$

We can write this in terms of H, φ and its derivatives as follows. We first write (3.14) as (see [7]):

$$H^2 = \frac{\kappa^2}{3}\frac{(1+\lambda)}{B}\rho = \frac{\kappa^2}{3}\frac{C^2\gamma(1+\lambda)}{B}\tilde{\rho}\,, \tag{3.31}$$

where $\lambda = \mathcal{V}/\rho\,(= \tilde{\mathcal{V}}/\tilde{\rho})$,

$$B = 1 - \frac{M^4 C D \gamma^2}{3(\gamma+1)}\varphi'^2\,, \tag{3.32}$$

and we have used (3.24) in the second equality of (3.31). By inserting (3.31) into (3.30), we can write H_{GR} entirely as a function of H, φ, φ' as:

$$H_{GR}^2 = \frac{\kappa_{GR}^2}{\kappa^2}\frac{C^{-2}B\,\gamma^{-1}H^2}{(1+\lambda)}\,. \tag{3.33}$$

Therefore, once we find a solution for H and φ, we can compare the expansion rates $\tilde{H}$ with H_{GR} using (3.27) and (3.33). To measure the departure from the standard expansion, we recall the speed-up factor parameter defined in (2.53):

$$\xi = \frac{\tilde{H}}{H_{GR}}\,.$$

Notice that ξ can be larger or smaller than one, indicating an enhancement or reduction of $\tilde{H}$ with respect to H_{GR}. This means that $\tilde{H}$ can grow during the cosmological evolution. However notice that this does not imply a violation of the the NEC. This is because the Einstein-frame expansion rate H is dictated by the energy density ρ and pressure p, which obey the NEC and therefore $\dot{H} < 0$ during the whole evolution, as it should (see [35]).

In the following section, we describe the procedure to solve the system of coupled equations for H and φ derived from (3.15) and (3.16).

3.3.1 Coupled equations for φ and H

The field equations (3.15) and (3.16) can be written as

$$H' = -H\left[\frac{3B}{2(1+\lambda)}(1+\omega) + \frac{\varphi'^2 M^4 C D \gamma}{2}\right], \tag{3.34}$$

$$\begin{aligned}
&\varphi''\left[1+\frac{3H^2\gamma^{-1}B}{M^4CD\kappa^2(1+\lambda)}\frac{D}{C}\right] + 3\,\varphi'\left[\gamma^{-2} - \frac{3H^2\gamma^{-1}B\omega}{M^4CD\kappa^2(1+\lambda)}\frac{D}{C}\right] \\
&+\frac{H'}{H}\varphi'\left[1+\frac{3H^2\gamma^{-1}B}{M^4CD\kappa^2(1+\lambda)}\frac{D}{C}\right] + \frac{3B\gamma^{-3}}{M^4CD(1+\lambda)}\alpha(\varphi)(1-3\,\omega\gamma^2) \\
&+\frac{3B\lambda\gamma^{-3}}{M^4CD(1+\lambda)}\frac{\mathcal{V}_{,\varphi}}{\mathcal{V}} + \frac{3H^2\gamma^{-1}B}{M^4CD\kappa^2(1+\lambda)}\frac{D}{C}\left[(\delta(\varphi)-\alpha(\varphi))\,\varphi'^2\right] \\
&+\frac{\kappa^2}{H^2}\frac{C}{D}\left[\gamma^{-2}\left(5\alpha(\varphi)-\delta(\varphi)\right) + \delta(\varphi) - \alpha(\varphi)\left(1+4\gamma^{-3}\right)\right] = 0\,,
\end{aligned} \tag{3.35}$$

where

$$\delta(\varphi) = \frac{d\ln D^{1/2}}{d\varphi}\,. \tag{3.36}$$

We notice here that, contrary to the pure conformal case discussed in chapter 2, we can not eliminate the equation for H, and we do not end up with a single master equation for the scalar field. Due to the disformal term, we need to consider the coupled equations for φ and H.

The cubic equation for H

Below we solve the equations numerically, for which we need the initial conditions for H_i and (φ_i, φ_i'). Therefore, we need to find an expression for H in terms of all other quantities and in particular $\tilde{\rho}$. We can obtain this from the Friedmann equation written in terms of $\tilde{\rho}$ in (3.31).

Recalling that γ depends nontrivially on H (3.29), one obtains a cubic equation for H^2 given by[5] :

$$A_1 H^6 + A_2 H^4 + A_3 H^2 + A_4 = 0 \tag{3.37}$$

where

$$A_1 = \frac{D\varphi'^2}{C\kappa^2}\,, \tag{3.38}$$

$$A_2 = \frac{2M^4 CD\varphi'^2}{3} - 1\,, \tag{3.39}$$

$$A_3 = \frac{M^4 C^2\kappa^2}{3}\left(\frac{M^4 CD\varphi'^2}{3} - 2\right)\,, \tag{3.40}$$

$$A_4 = \left(\frac{M^4\kappa^2 C^2}{3}\right)^2 \frac{(1+\lambda)\,\tilde{\rho}}{M^4}\left(\frac{(1+\lambda)\,\tilde{\rho}}{M^4} + 2\right)\,. \tag{3.41}$$

One of the solutions to (3.37) can be written as

$$H^2 = \frac{1}{3A_1}\left(-A_2 + \left(A_2^2 - 3A_1A_3\right)\left(\frac{2}{\Delta}\right)^{1/3} + \left(\frac{\Delta}{2}\right)^{1/3}\right)\,, \tag{3.42}$$

with

$$\begin{aligned}\Delta &= -27A_1^2A_4 + 9A_1A_2A_3 - 2A_2^3 + \sqrt{\left(-27A_1^2A_4 + 9A_1A_2A_3 - 2A_2^3\right)^2 - 4\left(A_2^2 - 3A_1A_3\right)^3} \\ &\equiv L + \sqrt{L^2 - 4\ell^3}.\end{aligned} \tag{3.43}$$

The other two solutions can be obtained by replacing

$$\left(\frac{2}{\Delta}\right)^{1/3} \to e^{2\pi i/3}\left(\frac{2}{\Delta}\right)^{1/3} \qquad \text{and} \qquad \left(\frac{2}{\Delta}\right)^{1/3} \to e^{4\pi i/3}\left(\frac{2}{\Delta}\right)^{1/3}\,.$$

We are interested in real positive solutions for H^2. These can be identified by considering a complex Δ, that is, $4\ell^3 > L^2$, which implies a condition on $\tilde{\rho},\ \varphi'$, and C. For this choice, the imaginary

[5] A similar equation was found in chapter 2, see (2.45), for the phenomenological disformal case. In that case, $A_2 = -1$ and $A_3 = 0$.

parts of $(\Delta/2)^{1/3}$ and $\ell(\Delta/2)^{-1/3}$ cancel each other[6]. We will use the real positive solutions in our numerical implementations to find the initial condition for H.

3.4 D-brane Disformal Solutions

As we discussed at the beginning of the chapter, when considering a probe D3-brane moving in a warped 10D space, which is a solution to the 10D equations of motion, C and D are related and given in terms of the warp factor of the geometry [3]. In particular, in the normalization where ϕ becomes canonically normalized once the DBI action is expanded, $M^4CD = 1$, (see Appendix B). Other normalizations are possible; however, the results will be equivalent. Thus in this section, we study solutions for the D-brane conformally and disformally coupled matter with the choice above, which implies $\delta(\varphi) = -\alpha(\varphi)$. We start by presenting the equations of motion for this case, followed by a discussion on the constraints and initial conditions we use in our numerical analysis. We first discuss in detail the numerical solutions for the $C =$ const or a pure disformal case, followed by the $C \neq$ const case.

3.4.1 Equations of motion and Jordan frame

We are interested in the radiation and matter dominated eras during which the potential energy of the scalar field is subdominant. Therefore in what follows we consider $\lambda \sim 0$. Also, to solve the equations (3.34) and (3.35), we need to write them in terms of Jordan-frame quantities $\tilde{\omega} = \omega\gamma^2$ and $\tilde{\rho} = C^{-2}\gamma^{-1}\rho$. After doing this, the coupled equations above become

[6]In this case, we can write $Z = \frac{\Delta}{2} = \frac{L+i\sqrt{4\ell^3-L^2}}{2}$, then $Z\bar{Z} = \ell^3$ and $\frac{2}{\Delta} = \frac{\bar{Z}}{\ell^3}$ and thus the imaginary parts in (3.42) cancel out.

$$H' = -H\left[\frac{3B}{2}(1+\tilde{\omega}\gamma^{-2}) + \frac{\varphi'^2}{2}\gamma\right], \tag{3.44}$$

$$\varphi''\left[1+\frac{3H^2\gamma^{-1}B}{M^4C^2\kappa^2}\right] + 3\,\varphi'\gamma^{-2}\left[1-\frac{3H^2\gamma^{-1}B}{M^4C^2\kappa^2}\tilde{\omega}\right] + \frac{H'}{H}\varphi'\left[1+\frac{3H^2\gamma^{-1}B}{M^4C^2\kappa^2}\right]$$

$$-\frac{6H^2\gamma^{-1}B}{M^4C^2\kappa^2}\,\alpha(\varphi)\varphi'^2 + 3B\gamma^{-3}\alpha(\varphi)(1-3\,\tilde{\omega}) - \frac{2M^4C^2\kappa^2}{H^2}\left[2\gamma^{-3}-3\gamma^{-2}+1\right]\alpha(\varphi) = 0\,. \tag{3.45}$$

Furthermore, we also convert derivatives with respect to N to derivatives with respect to $\tilde{N}$, the number of e-folds in the Jordan frame by following the procedure described at the end of section 2.3. Therefore, derivatives w.r.t. N transform to derivatives w.r.t. $\tilde{N}$ (assuming well behaved functions) according to (2.56) as:

$$\varphi' = \frac{1}{\left(1-\alpha(\varphi)\frac{d\varphi}{d\tilde{N}}\right)}\frac{d\varphi}{d\tilde{N}}\,, \qquad \varphi'' = \frac{1}{\left(1-\alpha(\varphi)\frac{d\varphi}{d\tilde{N}}\right)^3}\left(\frac{d^2\varphi}{d\tilde{N}^2} + \frac{d\alpha}{d\varphi}\left(\frac{d\varphi}{d\tilde{N}}\right)^3\right).$$

To avoid clutter we write down expressions with derivatives with respect to N, but it should be understood that all our numerical calculations are made using derivatives with respect to $\tilde{N}$.

Let us start by discussing (3.45) to understand the behavior of the solutions. Similarly to the conformal case discussed in section 2.4, the derivative of $C(\varphi)$ acts as an effective potential, given by[7]

$$V_{eff} \sim 3(1-3\,\tilde{\omega})\ln C\,. \tag{3.46}$$

Deep in the radiation-dominated era, the equation of state is given by $\tilde{\omega} = 1/3$ and the effective potential vanishes. As the temperature of the universe decreases, particle species in the cosmic

[7]Notice that the last term in (3.45) proportional to α is not part of an effective potential, as it vanishes when taking the velocity terms, φ' to zero (so $B = 1$ and $\gamma = 1$).

soup become nonrelativistic. When the temperature of the universe drops below the rest mass of each of the particle types, nonzero contributions to $1 - 3\tilde{\omega}$ arise, activating the effective potential. On the other hand, during the matter-dominated era, $\tilde{\omega} = 0$, and the effective potential is active through it. In section 2.4.2 we showed how to calculate $\tilde{\omega}$ during the radiation-dominated era, and plotted $\tilde{\omega}$, for the SM particle spectrum, during that era in Figure 2.5.

3.4.2 Initial conditions and parameter constraints

Before we move on to solving the coupled equations (3.44) and (3.45) to find the modified expansion rate, $\tilde{H}$, and compare it with the standard one, H_{GR}, we stop here to describe the constraints and initial conditions we use in our numerical analysis.

Parameter Constraints

As was discussed in section 2.4.3, in ST theories, deviations from GR can be parametrized in terms of the post-Newtonian parameters, γ_{PN} and β_{PN}. In the standard conformal case, these parameters are given in terms of $\alpha(\varphi_0)$ and its derivative, $\alpha_0' = d\alpha/d\varphi|_{\varphi_0}$ as in (2.68). Also, Solar System tests of gravity constrain α_0 to very small values of order $\alpha_0^2 \lesssim 10^{-5}$, while binary pulsar observations impose that $\alpha_0' \gtrsim -4.5$. Further, the relation between the bare gravitational constant and that measured by local experiments, for conformally coupled theories, is given by (2.60), $\kappa_{GR}^2 = \kappa^2 C(\varphi_0)[1 + \alpha^2(\varphi_0)]$. The strongest constraint applies to the speed-up factor ξ, which has to be of order 1 before the onset of BBN [37].

For the phenomenological disformal case, Solar System constraints and the ratio κ_{GR}/κ have been studied for constant D in Ref. [46]. In particular, they found $\kappa_{GR}^2 = \kappa^2(1 + 3\Upsilon/2)$, where $\Upsilon \propto \varphi_0'^2$. As we will see, all solutions we found have $\varphi' \approx 0$ at the onset of BBN. Therefore, for the constant disformal case, $\kappa_{GR}^2 = \kappa^2$. For the $C \neq$ const case, on the other hand, we will use the constraints on α above requiring that the standard expansion rate is recovered well before the onset of BBN. This is what we need to ensure that the predictions of the standard cosmological model are not modified.

Initial conditions and the scale M

To find the numerical solutions, we need to fix the initial conditions for H, φ, φ'. Since φ is given in Planck units, we take $\varphi_i, \varphi_i' \lesssim 1$. To find the initial value for H, based on the initial variables φ_i, φ_i' and $\tilde{\rho}_i$, we need a real positive solution to (3.37), which can be found from (3.42) for the case $CDM^4 = 1$. In this case the coefficients A_i simplify greatly.

Writing (3.43) as

$$\Delta = L + i\sqrt{\mathbb{L}}\,,$$

where now we have

$$L = 2 + 2\varphi'^2 - \frac{7}{3}\varphi'^4 + \frac{2}{27}\varphi'^6 - 3\varphi'^4 R\,, \tag{3.47}$$

$$\mathbb{L} = 4\ell^3 - L^2 = -\frac{\varphi'^4}{9}(1+R)\left[81\varphi'^4 R - (3+4\varphi'^2)(\varphi'^2-6)^2\right]\,, \tag{3.48}$$

$$\ell = \left(1 + \frac{\varphi'^2}{3}\right)^2\,, \tag{3.49}$$

$$R = \frac{\tilde{\rho}}{M^4}\left(\frac{\tilde{\rho}}{M^4} + 2\right)\,. \tag{3.50}$$

From here it is not hard to see that L can be either positive or negative and we require that $\mathbb{L} > 0$ for Δ to be complex, as required to find real positive solutions. In terms of the initial values for φ_i'[8], this requirement implies

$$R \leq \frac{(3+4\varphi_i'^2)(\varphi_i'^2-6)^2}{81\varphi_i'^4}\,. \tag{3.51}$$

Recalling that during the radiation-dominated era the energy density is given by $\tilde{\rho}(\tilde{T}) = \frac{\pi}{30} g_{eff}(\tilde{T})\tilde{T}^4$, once we fix φ_i' and the initial temperature T_i, the value of M is bound via (3.51). Indeed, (3.51), is satisfied for $\tilde{\rho}_i/M^4$ in the interval $\left(0, -1 + \frac{2}{9\varphi_i'^2}\sqrt{(3+\varphi_i'^2)^3}\right)$. Or, in terms of T_i and φ_i', the value of M lies in the interval:

$$\left[\left(\frac{3\,\pi\, g_{eff}(\tilde{T}_i)\,\varphi_i'^2}{-90\,\varphi_i'^2 + 20\sqrt{(3+\varphi_i'^2)^3}}\right)^{1/4}\tilde{T}_i\,, +\infty\right]\,. \tag{3.52}$$

[8]Recall that in our numerical solutions we take derivatives w.r.t. $\tilde{N}$, so φ_i' should be read as $\frac{\varphi_i'}{1-\alpha(\varphi_i)}$.

As an example, we show the lower bound for M as a function of $(\varphi_i')^2$ in Figure 3.1 for the initial temperature of 1.0 TeV. For simplicity, we take $C = 1$, so that derivatives with respect to N and $\tilde{N}$ are the same. As can be seen from (3.52) and Figure 3.1, for a given initial condition T_i, the closer φ_i' goes to $\sqrt{6}$, the larger the values of M, and vice versa. Also, the larger the value of T_i, the larger also the lower bound of M. In the D-brane-like scenario, as was described at the beginning of the chapter, the scale M is related to the string coupling and scale (or the six-dimensional volume) as $M = M_s(2\pi g_s^{-1})^{1/4}$. Therefore, we see that the scale decreases for small string scales (large compactification volumes) and small string couplings, which are needed for the string perturbative description to be valid. We will come back to this point below.

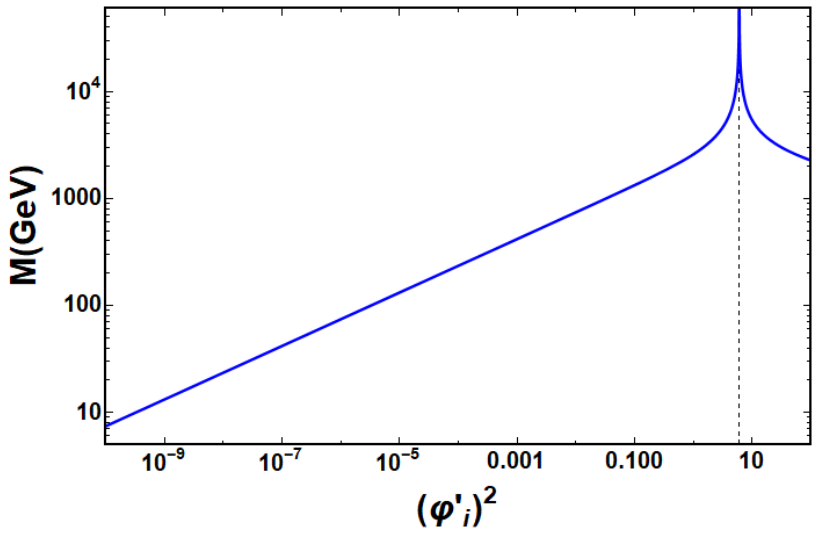

Figure 3.1: Lower bound for M (see (3.52)) as a function of $(\varphi_i')^2$ for $C = 1$. Reprinted with permission from "D-brane disformal coupling and thermal dark matter" by B. Dutta, E. Jimenez, I. Zavala, 2017. PhysRevD.96.103506, Figure 2, p. 9. Copyright American Physical Society.

3.4.3 Pure disformal case, $C =$ const.

We are now ready to discuss in detail the numerical solutions for H and φ and use them to compute the modified expansion rate. We start with the case $C(\varphi) =$ const which can be understood as a pure disformal case, which is presented here for the first time. Indeed, notice that in this

case $\gamma \neq 1$, which precisely carries the disformal (or derivative) effect, while $\alpha = 0$ (which carries the conformal effect)

Without loss of generality we can take $C(\varphi) = 1$ and therefore $D(\varphi) = \frac{1}{M^4}$. Comparing with the phenomenological case studied in chapter 2, one could think that an arbitrary choice of the function D there (with $C = 1$) would give different results. However, we expect that the effects of an arbitrary function, in that case, can be encoded in the choice of the scale M here, and therefore will give similar results to those presented here.

For $C = 1$, the system of coupled equations reduces to the following form,

$$H' = -H\left[\frac{3}{2}(1+\tilde{\omega}\gamma^{-2})B + \frac{\varphi'^2}{2}\gamma\right], \tag{3.53}$$

$$\varphi''\left[1+\frac{3H^2\gamma^{-1}B}{M^4\kappa^2}\right] + 3\,\varphi'\gamma^{-2}\left[1-\frac{3H^2\gamma^{-1}B}{M^4\kappa^2}\tilde{\omega}\right] + \frac{H'}{H}\varphi'\left[1+\frac{3H^2\gamma^{-1}B}{M^4\kappa^2}\right] = 0\,. \tag{3.54}$$

As expected, the effective potential is flat, since $\alpha = 0$ (see discussion above). We solve these equations numerically to find the dimensionless scalar field φ and the Hubble parameter H, as functions of $\tilde{N}$. We have explored a wide range of initial conditions for φ and φ' and values of the scale M. To find the initial condition for H (H_i), we use the appropriate real positive solution of (3.37), as was pointed out earlier. We find that at most two of the solutions (3.37) for H_i, are real and positive. For these two H_i's, the corresponding initial value of γ (γ_i) is obtained using (3.29) (setting $M^4CD = 1$). We find that one of these γ_i's is usually of order one while the other is 1 or 2 orders of magnitude larger (sometimes even larger). We find that the solutions to (3.53) and (3.54) that obey the necessary constraints are those with $\gamma_i \sim 1$. Once we have found the solutions for φ and H, we go back to (3.27) to obtain the expansion rate in the Jordan frame.

Before looking into the full numerical solutions, let us take a closer look at the ratio between the modified expansion rate and the standard rate, ξ. For $C =$ const this becomes

$$\xi = \frac{\gamma^{3/2}}{B^{1/2}}\,. \tag{3.55}$$

Since $\gamma, B \geq 1$, it is clear that $\xi \geq 1$, that is, $\tilde{H} \geq H_{GR}$. In other words, in this case, the expansion rate is always enhanced with respect to the standard evolution. Moreover, this enhancement is driven by γ and B. As soon as $\gamma > 1$, there will be a nontrivial disformal enhancement.

In Figure 3.2 we show the resulting modified expansion rate for different values of φ' and the mass scale M. In these plots, we use $\varphi_i = 0.2$, but any value in the interval $(0, 1)$ and appropriate choices of φ_i' and the mass scale M, will give similar results. As we can see in Figure 3.2, $\tilde{H}$ (colored lines) is always enhanced with respect to the standard expansion rate (black line), H_{GR}, as discussed above. From (3.55) and Figure 3.3, it is clear that the ratio ξ is always greater than or equal to 1. Moreover, as the temperature decreases, the ratio ξ grows from a value close to 1 (recall that $\gamma_i \sim 1$), reaches a maximum where γ is maximal and eventually decreases towards one before BBN. The maximum value of the ratio increases and moves to lower temperatures as the mass scale M becomes smaller.

We can understand this behavior by looking at the evolution of the factor $f = \frac{3H^2\gamma^{-1}B}{M^4\kappa^2}$, inside the square brackets of (3.54). We have seen numerically that this factor evolves as $f(\tilde{T}) \backsimeq \frac{3g_{eff}(\tilde{T})}{10}\left(\frac{\tilde{T}}{M}\right)^4$ as temperature decreases (see Figure 3.6). For the scale M and temperatures plotted in Figure 3.2, $f(\tilde{T})$ starts much bigger than one (up to $f(\tilde{T}_i) \backsimeq 10^9$) and decreases as the temperature decreases. The bigger the scale M, the earlier $f(\tilde{T})$ becomes of order 1. While $f(\tilde{T})$ is bigger than 1, ξ increases, the velocity of the scalar field φ' increases slowly, and thus the scalar field increases very slowly too (see Figure 3.3 and 3.4). As $f(\tilde{T})$ approaches 1, ξ reaches a maximum and the scalar field starts increasing faster. Then, as the temperature decreases further, $f(\tilde{T})$ becomes smaller than 1. Meanwhile, $\tilde{H}$ starts converging towards H_{GR} (that is, ξ starts decreasing) while the scalar field keeps increasing. Finally, when $\tilde{H}$ becomes of order H_{GR}, $f(\tilde{T})$ is much smaller than 1 and the scalar field starts moving towards a final constant value.

We see the behavior described above in Figures 3.3 and 3.4. For instance, for the plot corresponding to $M = 106$GeV, $f(\tilde{T})$ is approximately $\frac{3g_{eff}(\tilde{T})}{10}\left(\frac{\tilde{T}}{106\,\text{GeV}}\right)^4$, which becomes 1 at around $\tilde{T} = 50\,\text{GeV}$. Between 1000 GeV and 50 GeV, $\tilde{H}$ differs from H_{GR} and in this range the scalar field increases very slowly, looking almost constant. For lower temperatures, between 50 GeV

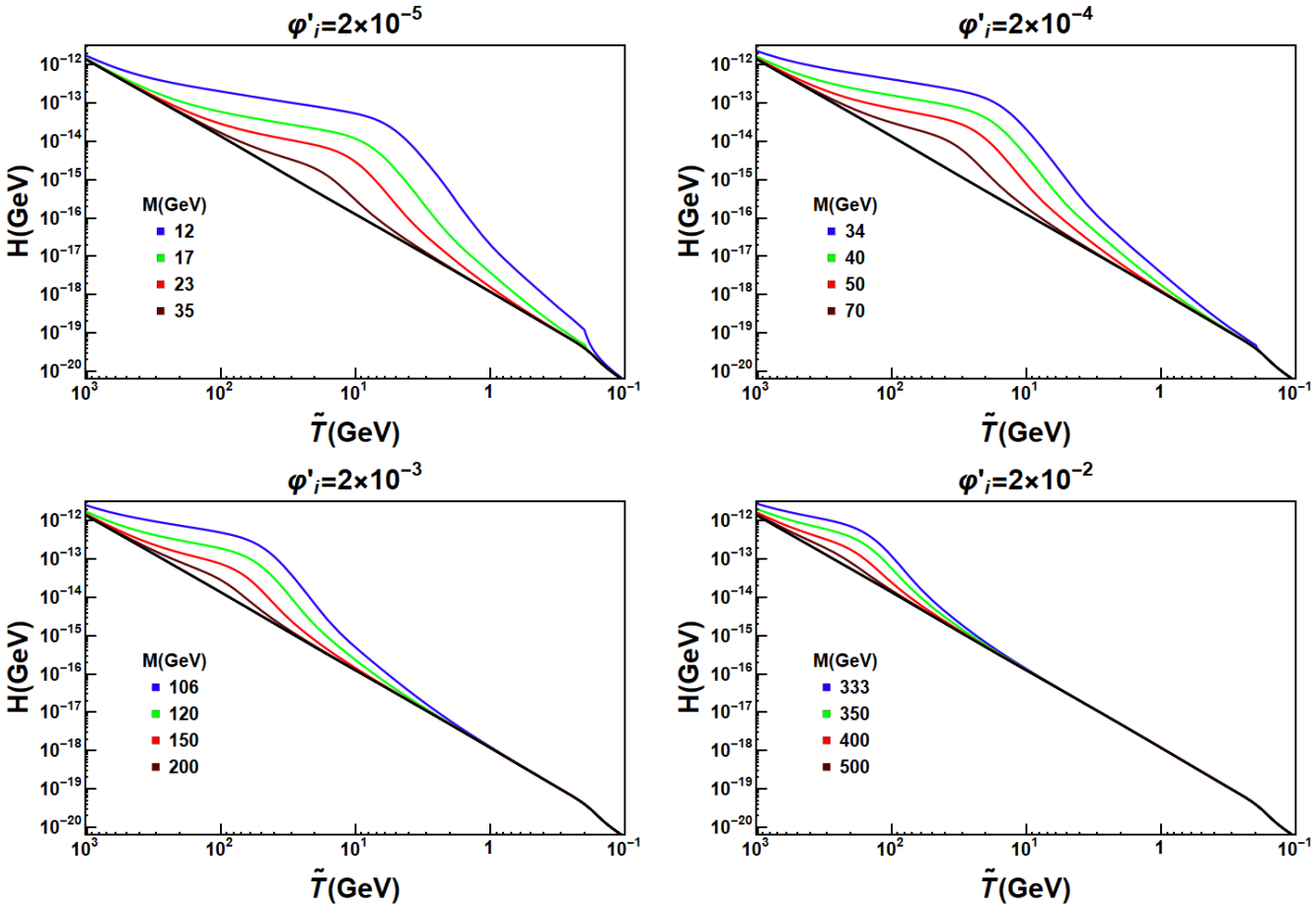

Figure 3.2: Modified expansion rate for the pure disformal case, $C = 1$. We show different boundary conditions and values of the scale parameter. The initial value of the scalar field for all the curves is $\varphi_i = 0.2$. The black lines in all plots represent the standard expansion rate H_{GR}. Reprinted with permission from "D-brane disformal coupling and thermal dark matter" by B. Dutta, E. Jimenez, I. Zavala, 2017. PhysRevD.96.103506, Figure 3, p. 10. Copyright American Physical Society.

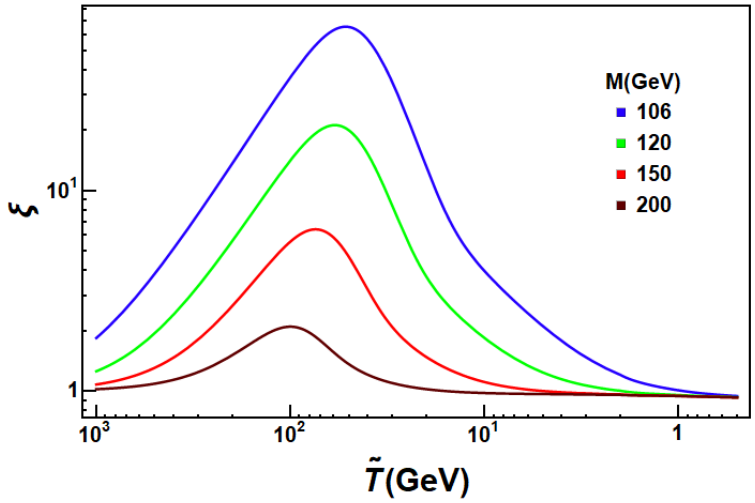

Figure 3.3: Speed-up factor, $\xi = \tilde{H}/H_{GR}$, as function of temperature for the expansion rates shown in the bottom left plot in Figure 3.2. The initial conditions chosen are $\varphi_i = 0.2$ and $\varphi_i' = 0.002$. Reprinted with permission from "D-brane disformal coupling and thermal dark matter" by B. Dutta, E. Jimenez, I. Zavala, 2017. PhysRevD.96.103506, Figure 4, p. 10. Copyright American Physical Society.

and 1 GeV, $\tilde{H}$ converges towards H_{GR} and the scalar field increases faster while for temperatures smaller than 1 GeV, $\tilde{H} \sim H_{GR}$ and the scalar field reaches its final value.

All the cases shown in Figure 3.2 satisfy the constraints discussed in section 3.4.2. In particular, $\varphi'_{BBN} = 0$ (so $\Upsilon = 0$) and the speed-up factor ξ is equal to 1 prior to BBN as shown in Figure 3.3. For scales M smaller than 10 GeV the last condition is not satisfied, that is $\xi > 1$ by the onset of BBN. Therefore, scales M smaller than 10 GeV are discarded.

As we have mentioned, if we consider larger values of M than the ones presented in Figure 3.2, the enhancement of the expansion rate will occur earlier, at higher temperatures, as long as M is smaller than $\tilde{T}_i$. We illustrate this in Figure 3.5. Here we show a series of plots were the mass scale takes values up to order EeV. This figure shows that the speed-up factor ξ, has the same behavior as long as the ratio $\tilde{T}_i/M$ does not change. For instance, see all the green lines $\tilde{T}_i/M$=58.8.

3.4.4 Conformal and disformal case $C \neq$ const

We now move to the case where the conformal coupling is not constant, so both conformal and disformal effects are turned on. For concreteness we consider the same conformal coupling as that

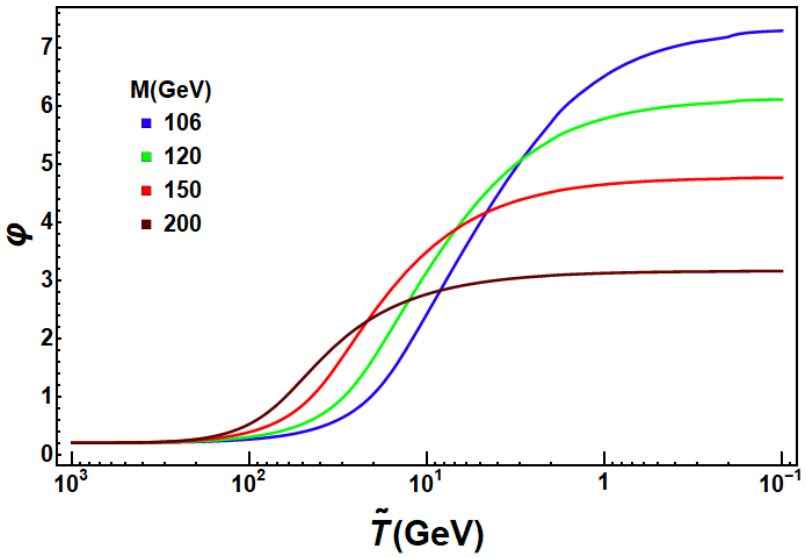

Figure 3.4: Scalar field as a function of temperature. The initial conditions chosen are $\varphi_i = 0.2$ and $\varphi_i' = 0.002$. These solutions of Eqs. (3.53) and (3.54) correspond to the expansion rates shown in the bottom left plot in Figure 3.2. Reprinted with permission from "D-brane disformal coupling and thermal dark matter" by B. Dutta, E. Jimenez, I. Zavala, 2017. PhysRevD.96.103506, Figure 5, p. 10. Copyright American Physical Society.

studied in chapter 2, which is given by (2.61) as

$$C(\varphi) = (1 + b\, e^{-\beta\,\varphi})^2\,, \tag{3.56}$$

with the values $b = 0.1$, $\beta = 8$. We have also analysed other functions such as $C = (b\,\varphi^2 + c)^2$ with $b = 4, 8, 15$, $c = 1$. However it is harder to find numerical solutions for this and other functions, which satisfy the phenomenological constraints. In those cases, the effect on the expansion rate $\tilde{H}$ was smaller with respect to the case where C is given by (3.56).

As mentioned in section 3.4.1, the conformal term acts as an effective potential, or force, in (3.45), given by Eq. (3.46). This effective force can be neglected when the factor $f_C = \frac{3H^2\gamma^{-1}B}{M^4C^2\kappa^2}$ is much larger than 1, as can be seen from (3.45). In this regime, the evolution of the scalar field is given by a flat effective potential, and the scalar field stays approximately constant. When f_C is becomes of order 1 or smaller and $\tilde{\omega} \neq 1/3$, the evolution of the scalar field is driven by the effective potential (3.46) and by the Hubble friction term.

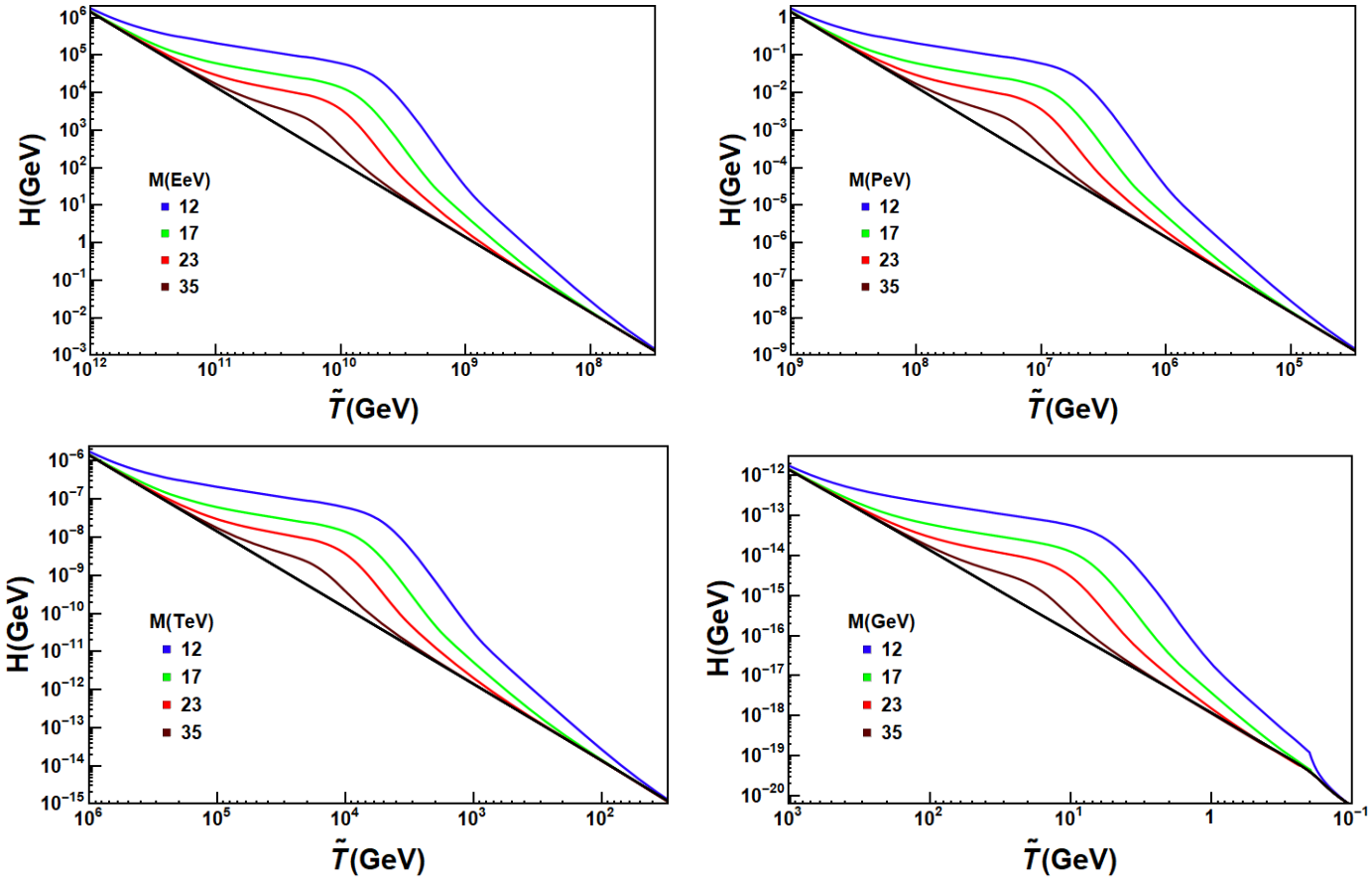

Figure 3.5: Modified expansion rate for the pure disformal case, $C = 1$, for larger values of M as compared to Fig. 3.2. For these plots, $\varphi_i = 0.2$ and $\varphi_i' = 2 \times 10^{-5}$. Reprinted with permission from "D-brane disformal coupling and thermal dark matter" by B. Dutta, E. Jimenez, I. Zavala, 2017. PhysRevD.96.103506, Figure 6, p. 11. Copyright American Physical Society.

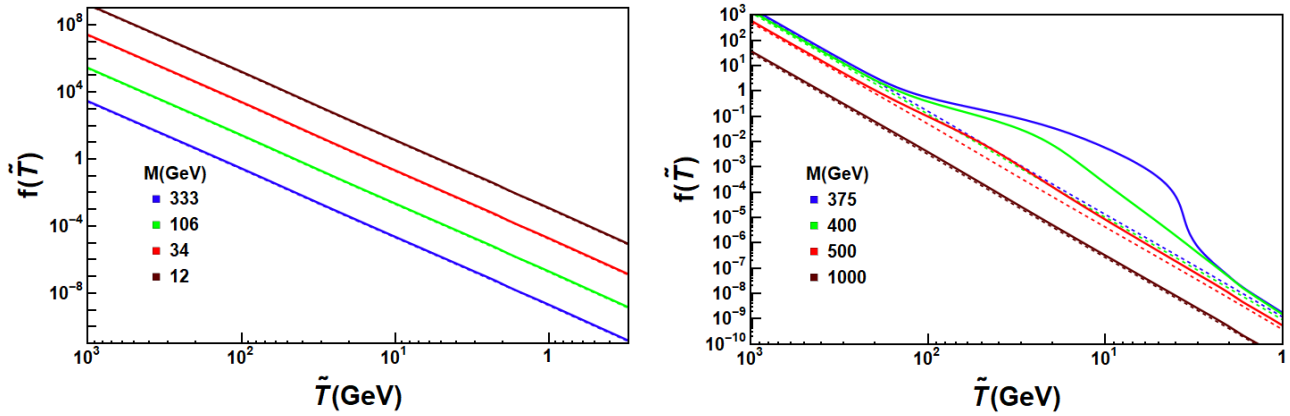

Figure 3.6: Evolution of the factor f as a function of temperature for $C = \text{const}$ case (left) and $C \neq \text{const.}$ (f_C, right). The initial conditions chosen in the left plot are shown in Figure 3.2, while in the right plot $\varphi_i = 0.2$ and $\varphi_i' = -0.004$. Reprinted with permission from "D-brane disformal coupling and thermal dark matter" by B. Dutta, E. Jimenez, I. Zavala, 2017. PhysRevD.96.103506, Figure 7, p. 12. Copyright American Physical Society.

For the conformal coupling (3.56), the effective potential allows for an interesting behavior, according to the choice of initial conditions chosen 2.4.1. That is, for negative initial velocities, $\varphi_i' < 0$, the scalar field will start rolling up the effective potential towards smaller values. After reaching a maximum point, it will turn back down the effective potential, eventually reaching its final value. This behavior in the scalar field sources a nontrivial behavior in C and (importantly) its derivative α, and therefore in the modified expansion rate $\tilde{H}$. Indeed, when $C \neq \text{const.}$, the speed-up factor, ξ, becomes

$$\xi = \frac{\kappa}{\kappa_{GR}} \frac{C^{1/2}\gamma^{3/2}}{B^{1/2}} \left[1 + \alpha(\varphi)\varphi'\right] . \tag{3.57}$$

It is not hard to see that for the initial conditions above, due to the factor inside the parentheses, ξ can become less than one during the evolution. Recalling that $\xi = \tilde{H}/H_{GR}$, $\xi < 1$ implies that $\tilde{H} < H_{GR}$, as shown in the explicit solutions below.

Let us now take a closer look at the evolution of f_C with temperature. Numerically, we found that when $f_C \gtrsim 1$ it behaves as $f_C(\tilde{T}) \backsimeq \frac{3g_{eff}(\tilde{T})}{10}\left(\frac{\tilde{T}}{M}\right)^4$. But when $f_C < 1$ then it evolves as $f_C(\tilde{T}) \backsimeq h(\tilde{T})\frac{3g_{eff}(\tilde{T})}{10}\left(\frac{\tilde{T}}{M}\right)^4$, where $h(\tilde{T})$ is a function that measures the enhancement of $\tilde{H}$,

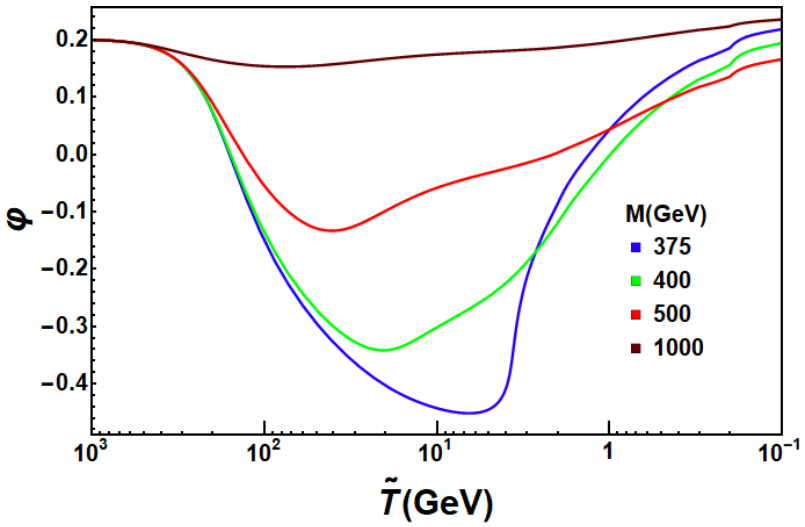

Figure 3.7: Scalar field as a function of temperature for different values of M. The conformal coupling is $(1 + 0.1\, e^{-8\varphi})^2$ and the initial conditions chosen are $\varphi_i = 0.2$ and $\varphi_i' = -0.004$. These solutions of Eqs. (3.44) and (3.45) correspond to the expansion rates shown in the right plot of Figure 3.8. Reprinted with permission from "D-brane disformal coupling and thermal dark matter" by B. Dutta, E. Jimenez, I. Zavala, 2017. PhysRevD.96.103506, Figure 8, p. 12. Copyright American Physical Society.

which is larger than 1 and depends on the scale M (see right plot in Figure 3.6). When $f_C \gg 1$, the effective force is negligible and the scalar field stays roughly constant. As f_C decreases and approaches and/or becomes smaller than 1, the effective force takes over the evolution of the scalar field. The velocity of the scalar field starts decreasing (we use small negative velocities), and for suitable values, the scalar field goes up the effective potential and comes back down again as described above.

In Figure 3.7 we plot the full numerical solution for the scalar field for $\varphi_i = 0.2$ and an initial velocity $\varphi' = -0.004$. The red, green and blue curves (scale masses smaller than $\tilde{T}_i = 1000$ GeV) show the scalar field going up the effective potential toward smaller values of the field, and then rolling down its terminal value., while for the brown curve (M =1000 GeV), the scalar field stays almost constant because for this value of M its initial velocity is not negative enough to move the field up the effective potential.

The effect of the scalar field on the modified expansion rate is shown in Figure 3.8 (the black

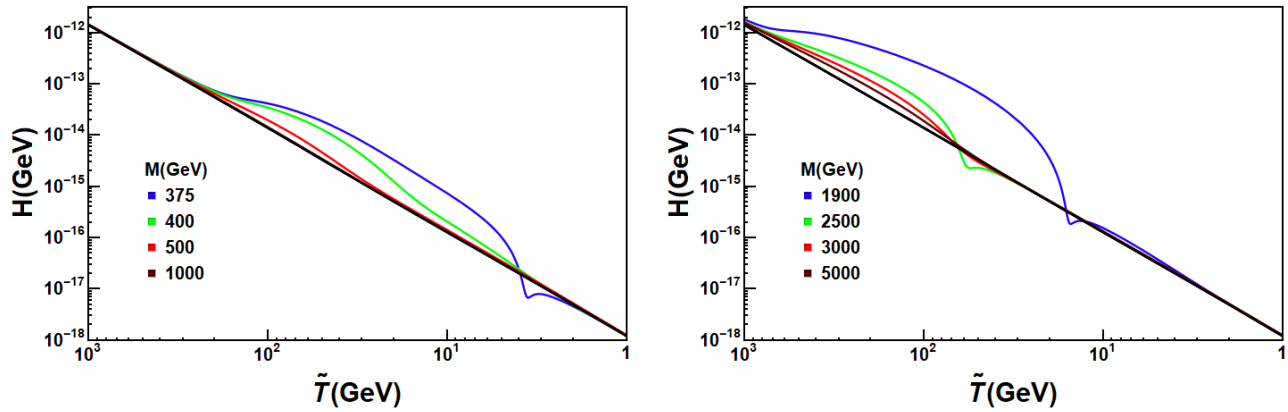

Figure 3.8: Modified expansion rate for the case $C = 1 + 0.1e^{-8\varphi}$. The initial value of the scalar field for all the curves is $\varphi_i = 0.2$. Also, $\varphi_i' = -0.004$ for the plot on the left and $\varphi_i' = -0.4$ for the plot on the right. Reprinted with permission from "D-brane disformal coupling and thermal dark matter" by B. Dutta, E. Jimenez, I. Zavala, 2017. PhysRevD.96.103506, Figure 9, p. 13. Copyright American Physical Society.

straight line is H_{GR}). The left plot shows $\tilde{H}$ corresponding to the scalar field solutions in Figure 3.7. For these solutions, the factor f_C is initially much bigger than 1 and as the temperature decreases it passes one (around 200 GeV) and keeps decreasing to very small values. For some values of M, the scalar field goes up and down the effective potential, producing the enhancement and the little notch in $\tilde{H}$ (blue), where $\xi < 1$ as explained above. On the other hand, in the right plots, f_C is initially of order 1 and then decreases to negligible values. The initial velocity used ($\varphi' = -0.4$) is sufficiently negative to produce the enhancement and notch in $\tilde{H}$ for some of the M values (green and blue).

Let us mention another point about the right plot in Figure 3.8. For the brown curve corresponding to $M = 5000\,\text{GeV}$, the enhancement is very small, and since the factor f_C decreases as the mass scale M increases, choosing larger values of M would give a similar result, for the same choice of initial conditions. Indeed, as $M \to \infty$, $f_C = \frac{3H^2\gamma^{-1}B}{M^4C^2\kappa^2} \to 0$ and we recover the pure conformal case in (3.45). Notice that the last term in this equation vanishes when M increases, since $\gamma \to 1$ as M increases. So, by dropping all terms proportional to f_C and the last term in (3.45) ones recovers the master conformal case equation, (2.57), studied in section 2.4. Thus, for

a very large value of M, we will recover the results of section 2.4, by suitably changing the initial conditions for φ_i and φ_i'.

Let us finally comment on the differences between the present case (conformal plus disformal) and the pure disformal and pure conformal cases, where there is no derivative interaction. We saw in the previous subsection that in the pure disformal case the enhancement in the expansion rate can be produced at any temperature (see Figure 3.5), by suitably changing the value of the scale M. However, in the present $C \neq 1$ case, this does not happen at any scale since $\omega \neq 1/3$ is needed and we get $\omega \neq 1/3$ when SM particles become nonrelativistic. This is due to the last term in (3.45), which makes the evolution of φ' go to zero very fast, effectively making $\gamma \sim 1$ throughout the evolution and thus an ineffective disformal enhancement. However, new physics at a higher scale causing a change in $\tilde{\omega}$ can introduce an enhancement at that scale. This will be similar to the case with the additional M scale associated with the D-brane models. The conformal enhancement is effective so long as the effective potential (3.46) is active, that is, whenever $\omega \neq 1/3$ (see Figure 2.5).

3.5 Post-inflationary string cosmology

The period after the end of inflation, from reheating up to the onset of BBN remains largely unconstrained. Let us now connect our results with a post-inflationary toy model of string cosmology and discuss the implications in terms of the parameters of the theory.

As described in the introduction of this chapter, we imagine a toy model where matter is coupled conformally and disformally to a scalar field, associated to an overall position of a (stack of) D-brane(s) in the internal six-dimensional compact space in a warped type IIB string compactification. In this case, we can relate the scale M to the tension of a D3-brane T_3 (for example), and thus to the string coupling g_s and the string scale M_s (or the six-dimensional volume $\mathcal{V}_6$) as $M = T_3^{1/4} = M_s(2\pi g_s^{-1})^{1/4}$. The pure disformal case $C = 1$ is very interesting and would correspond to a large-volume compactification, where the warping due to the presence of fluxes can be ignored [47, 48]. In this case, the lowest value we used for M that is relevant for the DM relic abundance (as we will see in the next chapter) was ~ 10 GeV and the largest (with a large effect)

was $M \sim 300$ GeV. For string couplings of order $g_s \sim 10^{-4}$, these give string scales $\sim 1 - 20$ GeV and thus exponentially large volumes $\mathcal{V}_6 \sim 10^{25} - 10^{27}$, that is, a very low string scale and very weakly coupled compactification. On the other hand, for larger values of M, or larger values of the string scale, the enhancement on the expansion rate will occur earlier in the universe's evolution (see Fig. 3.5). For example, the largest value we used, $M \sim 10^{10}$ GeV, for $g_s \sim 10^{-4}$ would give $M_s \sim 10^9$ GeV, volumes of order $\mathcal{V}_6 \sim 10^{10}$ and the expansion enhancement occurs at around $\tilde{T} \sim 10^{10}$ GeV. Therefore, depending on the string scale, coupling and compactification, we may expect the early pre-BBN cosmology to be affected at different epochs with interesting consequences for the post-inflationary string cosmological evolution. This will also be connected to string inflation, which usually requires large string scales (see Ref. [49] for a review).

Of course a more realistic model may involve, for example, other parameters of the theory in the scale M (due for example to higher-dimensional D-branes wrapping the internal space), nonuniversal couplings among the scalar (or scalars) to SM matter and DM as briefly discussed in Ref. [12] for the pure conformal case, etc. However, we find it very interesting that scalar couplings present in string theory can give important predictions for the post-inflationary evolution after string inflation.

Let us finally stress that the cosmological implications of conformal and disformal couplings in scalar-tensor theories are in any case very interesting from a more phenomenological point of view. Here we have taken a further step in making progress to address these implications and have presented the disformal effects for the first time.

4. DARK MATTER RELIC ABUNDANCES IN SCALAR-TENSOR THEORIES[1]

A popular framework to understand the origin of DM is the thermal relic scenario. In this scenario, at very early times when the universe was at a very high temperature, thermal equilibrium was obtained and the number density of DM particles χ was roughly equal to the number density of photons. During equilibrium, the dark matter number density decayed exponentially as $n_\chi^{eq} \sim e^{-m_\chi/T}$ for a non-relativistic DM candidate, where m_χ is the mass of the DM particle χ. As the universe cooled down as it expanded, DM interactions became less frequent and eventually, the DM interaction rate dropped below the expansion rate ($\Gamma_\chi < H$). At this point, the density number froze-out, and the universe was left with a "relic" of DM particles.

Therefore, the dependence of the number density at the time of freeze-out is crucial to determine the DM relic abundance. The longer the DM particles remain in equilibrium, the lower its density will be at freeze-out and vice-versa. In the standard ΛCDM scenario, particle freeze-out happens during the radiation era and DM species with weak scale interaction cross-section freeze-out with an abundance that matches the current observed value. The weakness of the interactions is reflected in the predicted thermally-averaged annihilation cross section, $\langle \sigma v \rangle$, which is around $3.0 \times 10^{-26} cm^3 s^{-1}$. Despite such a small value, the Fermi-LAT and Planck experiments have been exploring upper bounds on $\langle \sigma v \rangle$ (see [15, 16]). From observations, it appears that the annihilation cross-section can be smaller than the thermal average value for lower dark matter masses (≤ 100 GeV), whereas an annihilation cross-section larger than the thermal average value can still be allowed for larger DM mass.

If, from future measurements, $\langle \sigma v \rangle \neq 3.0 \times 10^{-26} cm^3 s^{-1}$ is established, what can we say about the origin of the dark matter? Can it still be the thermal dark matter or do we need non-thermal origin of dark matter? In the case of non-thermal origin, the DM can arise from the decay of a

[1]Sections 4.1 and 4.2 of this chapter are reprinted with permission from "Dark matter relics and the expansion rate in scalar-tensor theories" by B. Dutta, E. Jimenez, I. Zavala, 2017. JCAP no.06, 032. Copyright SISSA Medialab Srl. All rights reserved. Section 4.3 of this chapter is reprinted with permission from "D-brane disformal coupling and thermal dark matter" by B. Dutta, E. Jimenez, I. Zavala, 2017. PhysRevD.96.103506, Copyright American Physical Society.

heavy particle, e.g., moduli, and can satisfy the DM content with any value of $\langle\sigma v\rangle$. The primary motivation of this chapter is to show that the DM content can still have a thermal origin with larger or smaller $\langle\sigma v\rangle$ by utilizing non-standard cosmology.

4.1 Impact of the modified expansion rate on relic abundances

After presenting the ST models in chapters 2 and 3, and how the presence of the scalar field changes the cosmic evolution of the universe, we are ready to discuss the impact of the modified expansion rates on the relic abundance of dark matter species. For a dark matter species χ with mass m_χ and annihilation cross-section $\langle\sigma v\rangle$, where v is the relative velocity, the dark matter number density n_χ evolves according to the Boltzmann equation

$$\frac{dn_\chi}{dt} = -3\tilde{H}n_\chi - \langle\sigma v\rangle\left(n_\chi^2 - (n_\chi^{eq})^2\right) , \tag{4.1}$$

where, as we have discussed above, the relevant expansion rate is the Jordan frame one, which can give interesting effects due to the presence of the scalar field. Further n_χ^{eq} is the equilibrium number density. We can rewrite this equation in terms of $x = m_\chi/\tilde{T}$

$$\frac{dY}{dx} = -\frac{\tilde{s}\langle\sigma v\rangle}{x\tilde{H}}\left(Y^2 - Y_{eq}^2\right) , \tag{4.2}$$

where, $Y = \frac{n_\chi}{\tilde{s}}$, $\tilde{s} = \frac{2\pi}{45}g_s(\tilde{T})\tilde{T}^3$.

4.2 Dark Matter relics in the pure conformal scenario

In this section, we discuss the modifications to the DM relic abundances due a faster-than-usual expansion rate, which is caused by the presence of a scalar field coupled conformal and disformally to matter. In particular, we study the effect of the expansion rate, $\tilde{H}_{Conformal}$, discussed in chapter 2, which is shown in Figure 2.6. Also, at the end of this section, we comment the effect of $\tilde{H}_{Disformal}$ presented in the same figure.

Numerical solutions to (4.2), with the expansion rate $\tilde{H}_{Conformal}$ shown in Figure 2.6, were found for dark matter particles with masses ranging from 5 GeV to 1000 GeV. For instance, we

Mass (GeV)	$\langle\sigma v\rangle_{Conformal}(\times 10^{-26}\mathrm{cm}^3/\mathrm{s})$	$\langle\sigma v\rangle_{Standard}(\times 10^{-26}\mathrm{cm}^3/\mathrm{s})$
1000	9.57	2.23
130	1.68	2.04

Table 4.1: Annihilation cross-section for masses of 1000 GeV and 130 GeV in the conformal and standard scenarios.

show solutions in Figures 4.1 and 4.2 for two different masses. As we can see from (4.2), the annihilation cross-section influences the evolution of the abundance Y. The current value of Y determines the present dark matter content of the universe. This can be seen clearly by recalling the current value of the energy density parameter $\Omega_0 = \frac{\rho_0}{\rho_{c,0}} = \frac{m\, Y_0\, s_0}{\rho_{c,0}}$, where $\rho_{c,0}$ and s_0 are the well-known current values of the critical energy density and the entropy density of the universe, respectively. So, for every single mass, the thermally-averaged annihilation cross section, $\langle\sigma v\rangle$, was chosen such as the current DM content of the universe is 27 %, so $\Omega_0 = 0.27$.

In Figure 4.3 we show the annihilation cross-section, $\langle\sigma v\rangle_{Conformal}$, found for all masses and compare it to the annihilation cross sections for the standard cosmology model, $\langle\sigma v\rangle_{Standard}$. As it is shown, for large masses, $\langle\sigma v\rangle_{Conformal}$ is larger than $\langle\sigma v\rangle_{Standard}$, up to a factor of four. As the mass decreases $\langle\sigma v\rangle_{Conformal}$ decreases up to the point where it is smaller than $\langle\sigma v\rangle_{Standard}$. Then, for masses smaller than 100 GeV, $\langle\sigma v\rangle_{Conformal} \approx \langle\sigma v\rangle_{Standard}$. Thus, we have found that the annihilation cross-sections can be larger or smaller than the thermal average cross-section. Just to give an example of larger and smaller cross-section, in Table 4.1 we compare the numerical values of $\langle\sigma v\rangle_{Conformal}$ and $\langle\sigma v\rangle_{Standard}$ for two dark matter masses, 1000 GeV and 130 GeV.

Figures 4.1 and 4.2 show the evolution of the abundance $\tilde{Y}(x)$ for DM particles with masses 130 GeV and 1000 GeV, respectively. These figures also include the abundance $Y_{GR}(x)$ calculated in the standard cosmology model and the equilibrium abundance $Y_{Eq}(x)$.

The temperature evolution of the abundance for a 130 GeV mass is not noticeably affected by the presence of the scalar field ϕ. In this case, $\tilde{Y}$ and Y_{GR} are almost indistinguishable from one another. On the other hand, the scalar field ϕ has a prominent effect on the temperature

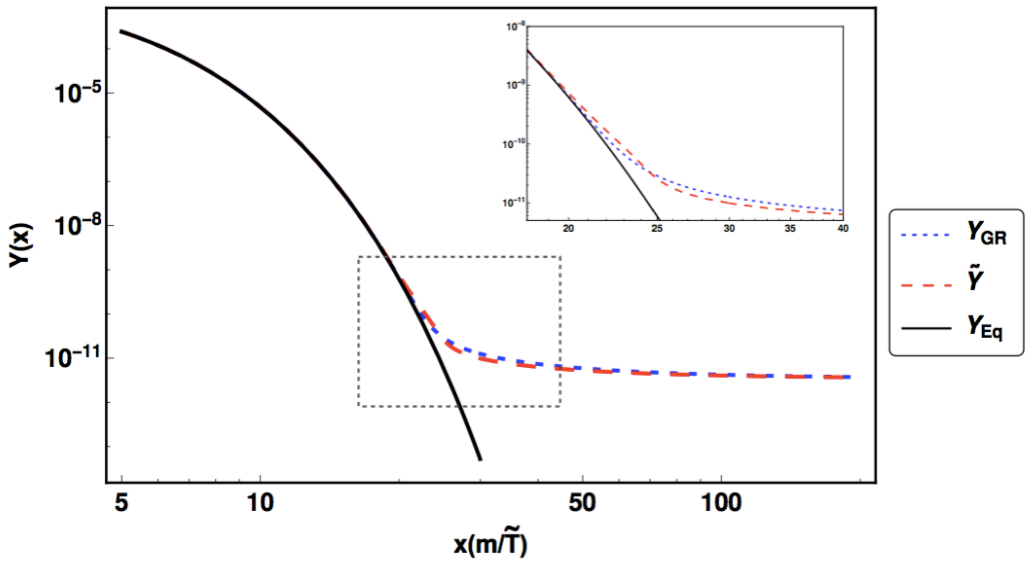

Figure 4.1: Evolution of the abundance as temperature changes for a DM particle of mass 130 GeV. Reprinted with permission from "Dark matter relics and the expansion rate in scalar-tensor theories" by B. Dutta, E. Jimenez, I. Zavala, 2017. JCAP no.06, 032, Figure 5, p. 16. Copyright SISSA Medialab Srl. All rights reserved.

evolution of the abundance for a 1000 GeV DM particle. First of all, the freeze-out happens earlier than expected due to the enhancement of the expansion rate, $\tilde{H}$. Then, an unusual effect appears. As the temperature decreases, $\tilde{H}$ becomes smaller than the interaction rate[2] $\tilde{\Gamma}$ and a short period of annihilation starts again called "re-annihilation". The re-annihilation process reduces the abundance of dark matter until a second and final freeze-out happens. After this final freeze-out, the abundance remains constant.

The re-annihilation phase can be described better by discussing the relation between the expansion rate $\tilde{H}$ and the interaction rate $\tilde{\Gamma}$. The first freeze-out happens when $\tilde{\Gamma}$ becomes smaller than $\tilde{H}$ which can be seen in Figure 4.4 to happen around a temperature of 50 GeV for a 1000 GeV particle. Then, near to 7 GeV, $\tilde{H}$ drops below $\tilde{\Gamma}$, and so the re-annihilation process starts and goes on until the second freeze-out occurs. Around 2 GeV $\tilde{H}$ becomes much larger than $\tilde{\Gamma}$ and so the abundance becomes almost constant. Our analysis shows that, as found in [7], re-annihilation

[2]The interaction rate is defined as $\tilde{\Gamma} \equiv \langle \sigma v \rangle_{Conformal}\, \tilde{s}\, \tilde{Y}$.

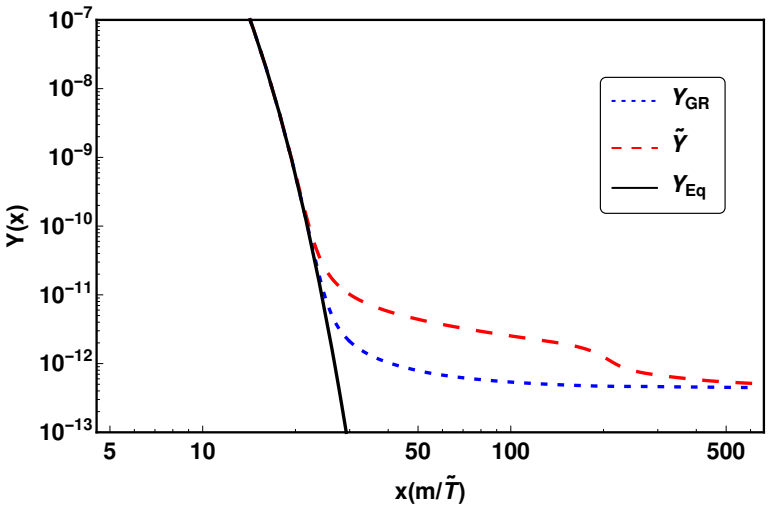

Figure 4.2: Abundance for a mass of 1000 GeV. Reprinted with permission from "Dark matter relics and the expansion rate in scalar-tensor theories" by B. Dutta, E. Jimenez, I. Zavala, 2017. JCAP no.06, 032, Figure 6, p. 17. Copyright SISSA Medialab Srl. All rights reserved.

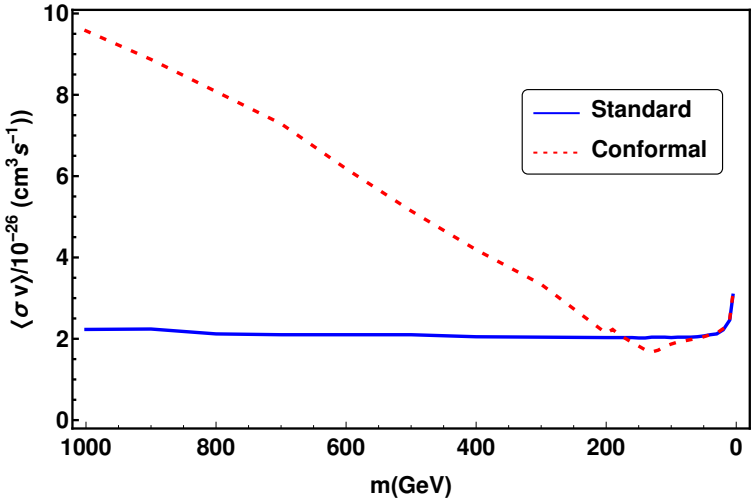

Figure 4.3: Annihilation cross section as function of mass. The presence of the scalar field enhances the $\langle\sigma v\rangle$ for large masses, and diminishes $\langle\sigma v\rangle$ for masses around 130 GeV, while small mass the effect is almost negligible. Reprinted with permission from "Dark matter relics and the expansion rate in scalar-tensor theories" by B. Dutta, E. Jimenez, I. Zavala, 2017. JCAP no.06, 032, Figure 7, p. 17. Copyright SISSA Medialab Srl. All rights reserved.

occurs for this particular choice of the conformal factor. However, we found that when fully integrating the master equation, the re-annihilation occurs only for very large masses of the dark matter

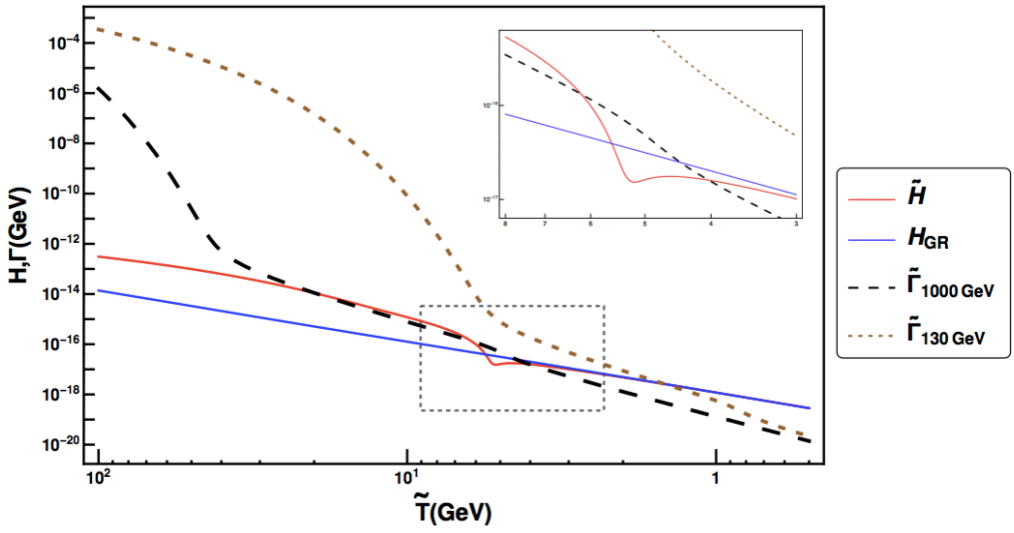

Figure 4.4: Expansion rate (as in Figure 2.3) and interaction rate as function of temperature. The interaction rate, $\tilde{\Gamma}$, is given by $\langle\sigma v\rangle_{Conformal}\,\tilde{s}\,\tilde{Y}$. We use $\tilde{Y}$ from Figures 4.1 and 4.2 and the values of $\langle\sigma v\rangle_{Conformal}$ presented previously for 130 GeV and 1000 GeV masses. Reprinted with permission from "Dark matter relics and the expansion rate in scalar-tensor theories" by B. Dutta, E. Jimenez, I. Zavala, 2017. JCAP no.06, 032, Figure 8, p. 18. Copyright SISSA Medialab Srl. All rights reserved.

particles (in [7] it was found for $m = 50$GeV). On the other hand, in [12], no re-annihilation was found[3], which was probably due to the initial conditions used and the values of the DM masses explored.

We have seen that the enhancement of $\tilde{H}$ allows bigger values of $\langle\sigma v\rangle$ for particles with masses within a certain range, and also, the notch of $\tilde{H}$ implies smaller $\langle\sigma v\rangle$ for particles with masses within a small interval (see Figure 4.3). Thus, the location and shape of the notch determine for which masses the annihilation cross section is smaller. In the disformal scenario (see $\tilde{H}_{Disformal}$ in Figure 2.6), the notch has been moved to higher temperatures, which allows particles with higher masses to have smaller and larger annihilation cross sections for the observed DM content.

[3]Although [12] used a different conformal factor to [7], we expect the re-annihilation effect to be present also in that case.

4.3 Dark Matter relics in the disformal D-brane coupling scenario

Since we computed the modified expansion rate in the disformal D-brane coupling scenario in Chapter 3, we can now move on to discuss its impact and implications on the dark matter relic abundance and cross section. In this section, we focus on the case $C = \text{const.}$ since the $C \neq \text{const.}$ case gives similar results to those studied in the previous section, as we discuss below.

As a concrete example, we solve (4.2) numerically, for the expansion rate corresponding to $M = 12$ GeV shown in the top left plot of Figure 3.2 and for dark matter particles with masses ranging from 10 GeV to 5000 GeV. Other choices of M would give similar results. In Figure 4.5 we show the solution for a DM particle of mass $m_\chi = 100$ GeV. In this plot, we also include the abundance $Y_{GR}(x)$ calculated in the standard cosmology model and the abundance when dark matter particles are in thermal equilibrium, $Y_{Eq}(x)$.

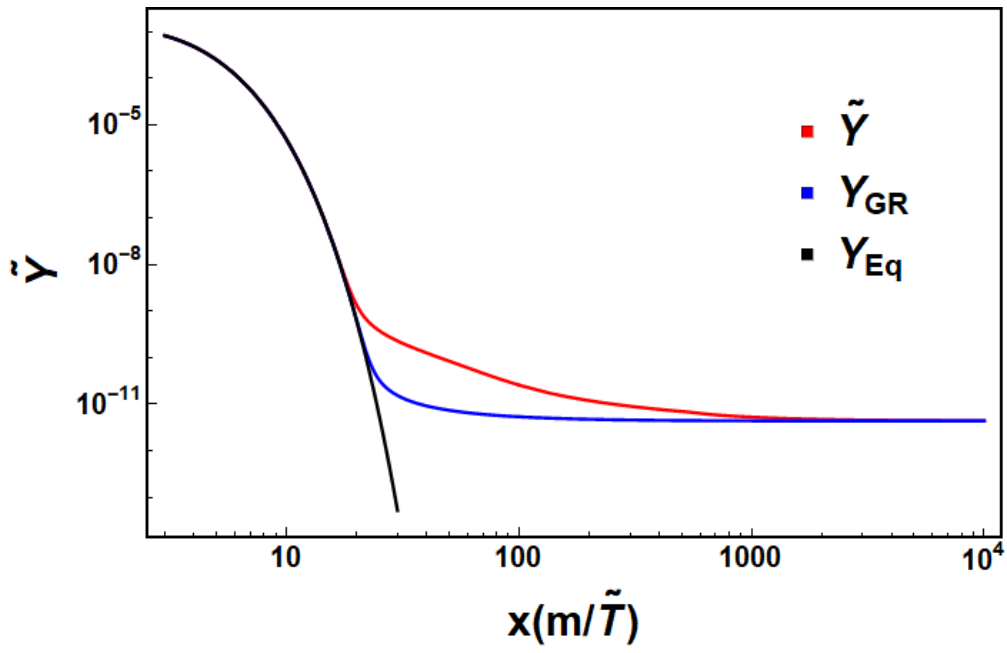

Figure 4.5: Abundance $\tilde{Y}$ for a dark matter particle with a mass of 100 GeV. Reprinted with permission from "D-brane disformal coupling and thermal dark matter" by B. Dutta, E. Jimenez, I. Zavala, 2017. PhysRevD.96.103506, Figure 10, p. 14. Copyright American Physical Society.

In the plot, we can see how the modification of the expansion rate gives rise to an earlier than standard freeze-out (see Figure 4.5 around $x = 20$). This is due to the enhancement of the expansion rate $\tilde{H}$. As the temperature decreases (x increases), $\tilde{H}$ becomes comparable to the interaction rate[4] $\tilde{\Gamma}$ and for a small period, between $x = 20$ and $x = 1000$, the abundance decreases slowly until it becomes constant. It is interesting to notice that a similar behavior was found in [14], where an extra scalar species drives a faster than usual expansion rate, giving rise to a similar behavior in the relic abundance. The comparison between $\tilde{H}$ (brown) and $\tilde{\Gamma}$ (purple) can be seen in Figure 4.6. Between around 5 GeV ($x = 20$) and 0.1 GeV ($x = 1000$), $\tilde{H}$ and $\tilde{\Gamma}$ are close to each other as temperature decreases.

In Figure 4.6, we also show the interaction rate for two other DM particle masses, 600 GeV (green) and 2500 GeV (red). Notice that for the three masses shown, once the interaction rate becomes smaller than the expansion rate $\tilde{H}$ (brown), it always stays smaller than it. Therefore, there is no reannihilation effect. However, reannihilation can occur for the $C \neq$ const. case, where after the first freeze-out $\tilde{\Gamma}$ can overcome $\tilde{H}$ due to $\xi < 1$, and later become smaller again.

Let us now turn our attention to the dark matter annihilation cross sections that we have used when solving the Boltzmann equation (4.2). To determine $\langle \sigma v \rangle$ numerically, we required that the observed dark matter density today be $\Omega_0 = 0.27$. The present dark matter content of the universe is determined by the current value of the relic abundance. This can be obtained from the current value of the energy density parameter $\Omega_0 = \frac{\rho_0}{\rho_{c,0}} = \frac{m\, Y_0\, s_0}{\rho_{c,0}}$. Here $\rho_{c,0}$ and s_0 are the well-known current values of the critical energy density and the entropy density of the universe, respectively.

The resulting annihilation cross sections, found in this way, are shown in Figure 4.7 for dark matter masses between 10 GeV and 5000 GeV. In this figure, we also show the effect that different values of M have on $\langle \sigma v \rangle$. The values of M chosen correspond to the expansion rates $\tilde{H}$ shown in Figure 3.2. We compare this to the annihilation cross sections $\langle \sigma v \rangle_{GR}$ predicted by the standard cosmology model (black line), which is around $2.1 \times 10^{-26} cm^3/s$.

The behavior of the cross section $\langle \sigma v \rangle$ in Figure 4.7 shows an enhancement with respect to the

[4]The interaction rate is defined as $\tilde{\Gamma} \equiv \langle \sigma v \rangle\, \tilde{s}\, \tilde{Y}$.

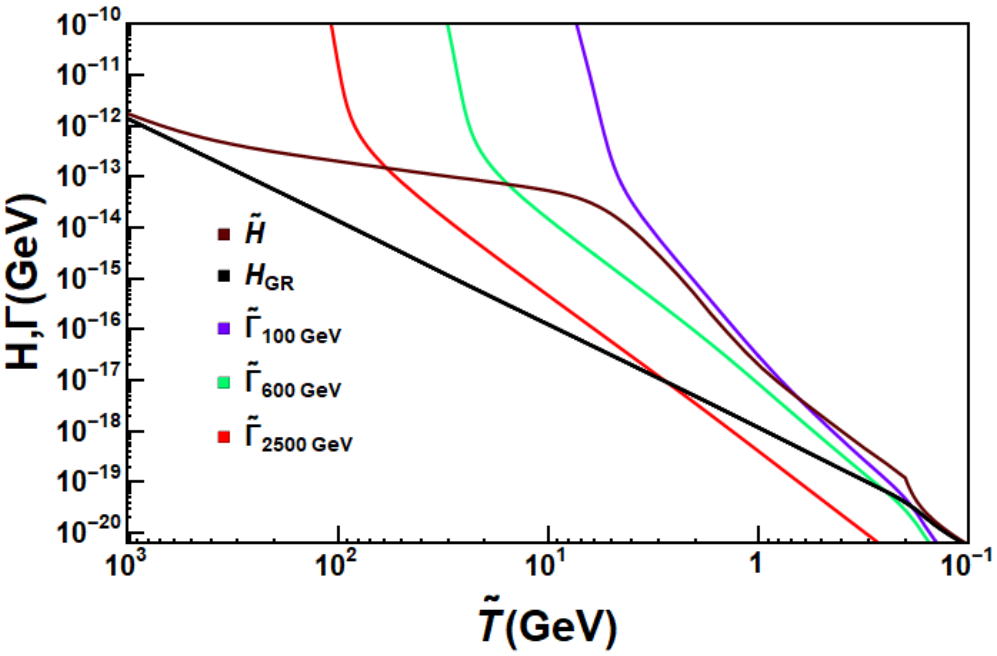

Figure 4.6: Expansion rate corresponding to $M = 12$ GeV shown in the top left plot of Figure 3.2, and interaction rates of 100 GeV (purple), 600 GeV (green) and 2500 GeV (red) GeV DM particle masses as a function of temperature. The interaction rate $\tilde{\Gamma}$ is given by $\langle\sigma v\rangle\tilde{s}\tilde{Y}$. Reprinted with permission from "D-brane disformal coupling and thermal dark matter" by B. Dutta, E. Jimenez, I. Zavala, 2017. PhysRevD.96.103506, Figure 11, p. 14. Copyright American Physical Society.

standard case, with a maximum that moves towards larger DM masses as the scale M increases. Therefore, the smaller the scale M the larger the annihilation cross section $\langle\sigma v\rangle$ for the DM masses shown in the figure.

As was discussed, a modification to the expansion rate of the universe prior to BBN has tremendous consequences on the abundance, $\tilde{Y}$, of DM particles. This modification implies that the thermally-averaged annihilation cross section, $\langle\sigma v\rangle$, differs significantly from the one predicted by the standard cosmological model, which is approximately $3.0 \times 10^{-26}\mathrm{cm}^3/\mathrm{s}$.

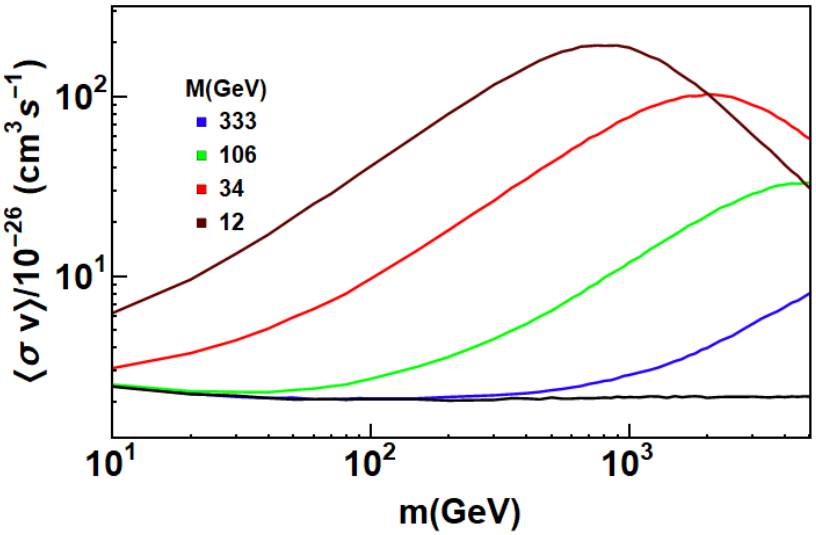

Figure 4.7: $\langle\sigma v\rangle$ as function of dark matter particle mass. $\langle\sigma v\rangle_{GR}$ predicted by the standard cosmology model correspond to the black line, while the colored lines correspond to $\langle\sigma v\rangle$ predicted by using the expansion rates (shown in Figure 3.2), representing mass scales of $M = 12$ (brown), 34 (red), 106 (green) and 333 GeV (blue). Reprinted with permission from "D-brane disformal coupling and thermal dark matter" by B. Dutta, E. Jimenez, I. Zavala, 2017. PhysRevD.96.103506, Figure 12, p. 14. Copyright American Physical Society.

5. LEPTOGENESIS IN A FASTER-THAN-USUAL UNIVERSE[1]

The cosmological baryon asymmetry is very elegantly explained via the leptogenesis mechanism [26] according to which an initial asymmetry is generated in lepton number and then partly converted in a baryon number asymmetry by $B + L$ violating sphaleron processes [27, 28] which, above the temperature of the electroweak (EW) phase transition, proceed with in-equilibrium rates (for reviews on the leptogenesis mechanism see [29, 30]). A very attractive feature of the standard leptogenesis realization based on the type-I seesaw [50, 51, 52, 53] is that it provides a semi-quantitative relation connecting the out-of-equilibrium condition [54] for the decays of the heavy right-handed (RH) neutrinos with the light neutrino mass scale. RH neutrino decays can be sufficiently out of equilibrium if $m_\nu \sim 10^{-2\pm1}$ eV, which is in beautiful agreement with neutrino oscillation data. On the other hand, type-I seesaw leptogenesis has also an unpleasant facet. A lepton asymmetry is preferably generated in the decay of the lightest RH neutrino N_1 since they generally occur at temperatures when the dynamics of the heavier $N_{2,3}$ neutrino is no more efficient. However, the CP asymmetry in N_1 decays is bounded by the following relation [31]:

$$|\epsilon_1| \leq \frac{3}{16\pi}\frac{M_1}{v^2}\frac{\Delta m^2_\oplus}{m_1 + m_3}\,, \tag{5.1}$$

where M_1 is the N_1 mass, $v \sim 174\,\text{GeV}$ is the SM electroweak (EW) breaking vacuum expectation value (VEV), $\Delta m^2_\oplus \sim 2.4 \times 10^{-3}\,\text{eV}^2$ is the atmospheric neutrino mass square difference, and $m_{1,3}$ are the lightest and heaviest light neutrino masses, which are bounded by cosmological data to lie not much above $\sim 10^{-1}$ eV. Since a minimum CP asymmetry $|\epsilon_1| \gtrsim \text{few} \times 10^{-7}$ is required to account quantitatively for the observed baryon asymmetry, the N_1 mass cannot lie much below 10^9 GeV.[2] The conclusion that the CP asymmetry is too small to explain the baryon asymmetry if

[1]The contents of this chapter appear in "A cosmological pathway to testable leptogenesis" by Bhaskar Dutta, Chee Sheng Fong, Esteban Jimenez and Enrico Nardi. arXiv: 1804.07676. This article was submitted to JCAP.

[2]The bound (5.1) can be somewhat weakened if the RH neutrinos masses are not sufficiently hierarchical [55], if $N_{2,3}$ decays also contribute to the generation of a lepton asymmetry [56], or if flavor effects [57, 58, 59] play a relevant role [60, 61]. However, the main conclusion regarding non-testability of the type-I seesaw leptogenesis model does not change.

the leptogenesis scale is too low, implies that direct tests of the standard type-I seesaw leptogenesis are out of experimental reach. Since the argument does not involve any cosmological input, it holds regardless of the assumed cosmological model.

In more generic realization of leptogenesis (5.1) does not necessarily hold: the simple relation between the CP asymmetries and the light neutrino masses is in fact quite specific of the type-I seesaw and is often lost in other models. The most direct way to relax this bound is to rescale v in (5.1) and this can be realized in a model where neutrinos only couple through a neutrinophilic Higgs which obtains a VEV $v_\nu \ll v$ [32, 33]. Other examples are the inert scalar doublet model [62] complemented with heavy Majorana neutrinos [63], as well as many other models, see [64, 65, 61, 66, 67, 68, 69] for a sample list. Still, the vast majority of models that attempt to generate the baryon asymmetry from heavy particle decays are subject to an additional constraint which, although less tight than the one implied by (5.1), is much more general. This constraint stems from a general relation between the strength of the washout scatterings which tend to erase any lepton number asymmetry present in the thermal bath, and the CP asymmetries in the decays of the heavy states. To our knowledge, in standard cosmologies only models which invoke a resonant enhancement of the CP asymmetries [70, 71, 72, 68, 73] can evade the corresponding bound and bring leptogenesis from heavy particle decays down to a testable scale [74].

In this chapter we point out that this conclusion can be avoided if, in the very early stages, the cosmological history of the Universe is described by an ST theory [75, 76, 77] rather than by GR. As we have seen, the cosmic expansion rate is boosted in both the pure conformal case and the disformal D-brane coupling scenario. The magnitude of the enhancement depends on boundary conditions and it can be a few orders of magnitude larger compared to the standard GR expansion. We will make use of this enhancement in the expansion rate in our study of leptogenesis.

Differently, from the case of DM, for which the typical decoupling temperature falls in the few GeV range, the generation of a baryon asymmetry via leptogenesis must occur above the EW scale before the EW sphaleron processes get out of equilibrium. Since a leptogenesis scale up to a couple of TeV might still be within the reach of collider tests, we are interested in modifications of

the standard cosmology at temperatures in the range $100\,\mathrm{GeV} - \text{few}\,\mathrm{TeV}$. Indeed, due to the larger scale in the game, we find that in the framework of conformally coupled ST theories the modified expansion does allow to lower the scale for successful leptogenesis down to $M_1 \lesssim 1\,\mathrm{TeV}$. Hence, in our analysis, we will mainly focus on conformally coupled ST theories since this conclusion holds also for ST theories with disformal couplings.

5.1 Constraints on the leptogenesis scale

The quantum field theory conditions required in order that loop diagrams can generate a lepton (L) number (or any other global quantum number) violating CP asymmetry in the decays of an heavy state X are: (i) complex couplings between X and the particles running in the loop (say Y and Z); (ii) a CP even phase from the loop factors, which only arises if the Y, Z propagators inside the loops can go on-shell; (iii) L violation inside the loop. Condition (ii) then implies that Y and Z can also participate as external asymptotic states in scattering processes, and condition (iii) implies that these scatterings are necessarily L violating. This means that decay CP asymmetries unavoidably imply L violating washout scatterings [63, 65]. Since the same couplings enter both in the expression for the CP asymmetries and for the washout scattering rates, it is not surprising that a quantitative relation between CP asymmetries and scattering rates can be worked out. A general expression for this relation has been obtained in [65] and reads:

$$\Gamma(YZ \leftrightarrow \bar{Y}\bar{Z}) \approx \frac{64}{\pi}\, T \left(\frac{T}{M_X}\right)^n \epsilon_X^2\,, \tag{5.2}$$

where Γ is the rate of the $\Delta L = 2$ washout scatterings, ϵ_X is the CP asymmetry in X decays, and $n = 0$ for a scalar X decaying into two scalars Y, Z; $n = 2$ for a fermion X decaying into a fermion and scalar pair, and $n = 4$ for a scalar X decaying into two fermions. Note that (5.2) relates scattering washout rates to CP asymmetries without any reference to the cosmological model. In relation to successful leptogenesis, cosmology enters through the requirement that at the

relevant temperature $T \sim M_X$ the washout rates do not attain thermal equilibrium:

$$\Gamma(YZ \leftrightarrow \bar{Y}\bar{Z}) \lesssim \tilde{H}(T)\big|_{T\sim M_X} , \tag{5.3}$$

where we parametrize the deviations of the expansion in terms of a temperature dependent function $\xi(T)$ multiplying the canonical GR expansion rate $H(T) = 1.66\sqrt{g_*}\,T^2/M_P$ (with $g_\star$ the relativistic degrees of freedom and $M_P = 1.22 \times 10^{19}$ GeV), namely $\tilde{H}(T) = \xi(T)H(T)$ (two examples of $\xi(T)$ are given in Figure 5.1) .

In the relevant temperature range $T \sim M_X$ the out-of-equilibrium condition (5.3) yields:

$$M_X \gtrsim 1.2 M_P \frac{\epsilon_X^2}{\xi(M_X)} . \tag{5.4}$$

Assuming as a benchmark value $\epsilon_X \gtrsim 10^{-7}$ as the lowest possible CP asymmetry able to explain $n_b/n_\gamma \sim 10^{-10}$, we see that standard cosmology with $\xi(T) = 1$ yields the (conservative) limit $M_X \gtrsim 1.4 \cdot 10^5$ GeV, so that in any generic model of leptogenesis from heavy particle decays the relevant scale lies well above experimental reach. As an example, we see from the left plot of Figure 5.1 that in modified ST cosmologies the function $\xi(T)$ can remain of order 10^2 in an interval centered at $T \sim$ TeV and spanning about two orders of magnitude in $z = \mathrm{TeV}/T$. Because of the boosted expansion, in the relevant temperature range, the dynamical processes that govern leptogenesis, in particular, the $\Delta L = 2$ washout processes discussed above, can more easily go out of equilibrium, rendering viable scales as low as $M_X \lesssim$ TeV for which direct tests can be foreseen.

5.2 A few comments on the modified expansion rate and the general Boltzman equation for RH neutrinos

In Section 2.4 we described the pure conformal scenario in ST theories and mentioned that the modified expansion rate depends on the initial conditions of the scalar field and initial temperature, the effective potential, and the particle content of the cosmic plasma (through the equation of state parameter $\tilde{\omega}$).

In general, both the initial position and velocity of the scalar field can take any positive or negative values. The most interesting result arises when considering negative velocities. In this case, the field will start rolling-up the effective potential towards smaller values of the field, eventually turning back down and moving towards its final value. So, if the field starts at a positive value, and given a sufficiently negative initial velocity, it will move towards negative values until its velocity becomes zero and then positive again, as it rolls back down the effective potential. This change in sign for the scalar field will produce a peak in the conformal coupling, which will give rise to a non-trivial modification of the expansion rate $\xi \neq 1$ (see (2.53)). This particular behavior is shown again, for a new set of initial conditions, in Figure 5.1.

The equation of state parameter $\tilde{\omega}$ plays an important role in locating the temperature at which the speedup factor, ξ, drops back to 1. Slight variations from the radiation dominated value, $\tilde{\omega} = 1/3$, appear when particles become non-relativistic. So, to calculate $\tilde{\omega}$, as discussed in Section (2.4.2), one has to take into account all the SM particles and, depending on the specific SM extensions one is dealing with, one would add RH neutrinos, supersymmetric partners or other types of heavy species.

Another interesting scenario yielding modified Hubble parameters is the disformal D-brane coupling scenario, which was studied extensively in Chapter 3. In Figure 5.1 we also present the speedup factor ξ in this scenario (thin red lines). Recall, M plays the most important role in the location and shape of ξ. The maximum ξ happens close to a temperature equal to M. It is interesting to notice that by rescaling M, ξ moves to a higher (or lower) temperature without changing shape.

Due to the fact that, as in GR, also in ST cosmologies the total entropy is conserved, adapting the BE for leptogenesis to ST cosmologies is rather straightforward. Considering just the BE for the evolution of the RH neutrinos density n_N including only decays and inverse decays will suffice to illustrate this. Denoting with a the scale factor, the BE reads:

$$a^{-3}\frac{d(n_N a^3)}{dt} = \langle \Gamma_N \rangle (n_N^{\rm eq} - n_N)\,, \tag{5.5}$$

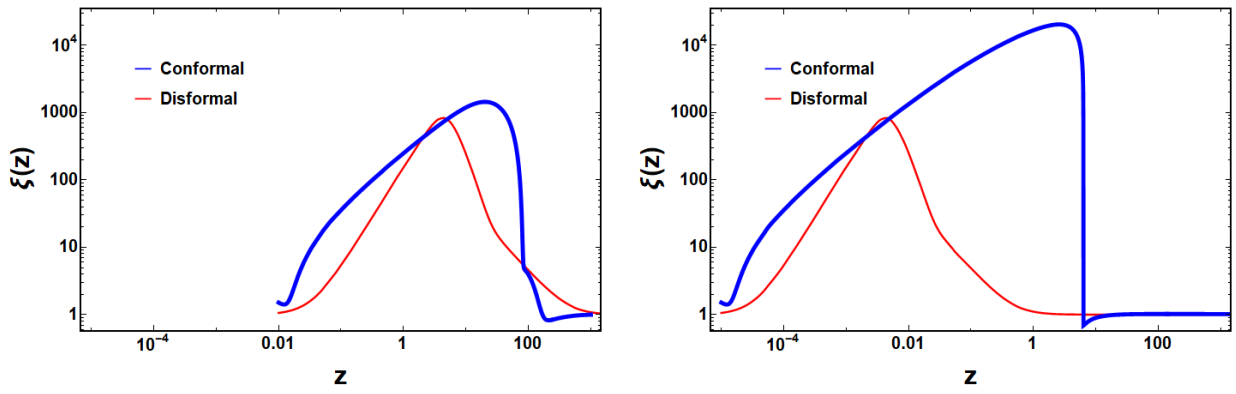

Figure 5.1: Two examples for the speedup factor $\xi(z)$ for conformal (thick blue lines) and disformal (thin red lines) scenarios, as a function of $z = 1\,\mathrm{TeV/T}$ with T the temperature. Left plot: $\xi(z)$ in a conformal scenario with initial conditions $(\varphi_i, \varphi_i') = (0.8, -1.83)$ and initial temperature 100 TeV, and in a disformal scenario with $(\varphi_i, \varphi_i') = (0.2, -2 \times 10^{-6})$ and a mass scale $M = 2.5\,\mathrm{TeV}$. Right plot: $\xi(z)$ in a conformal and disformal scenario with initial conditions as before, but initial temperature $T = 10^5$ TeV, and $M = 2500\,\mathrm{TeV}$ for the disformal case.

where $\langle\Gamma_N\rangle$ is the thermal averaged decay rate and $n_N^{\rm eq}$ the equilibrium density. We use the fiducial variable $z = M_N/T$ with T the temperature, and write the time derivative as:

$$\frac{d}{dt} = z\left(\frac{1}{z}\frac{dz}{dt}\right)\frac{d}{dz} = z\left(\frac{1}{a}\frac{da}{dt}\right)\frac{d}{dz} = z\tilde{H}\frac{d}{dz}\,. \tag{5.6}$$

The second step relies on entropy conservation $d(sa^3)/dt = 0$ with $s \propto T^3$ the entropy density which implies the usual temperature-scale factor relation $T \propto 1/a$, while $\tilde{H}$ is the physical Hubble parameter defined as the rate of change of the physical length scale. The rest is standard: denoting by $\gamma_N = n_N^{\rm eq}\langle\Gamma_N\rangle$ the density of the reaction, and normalizing the particle number densities to the entropic density as $Y_N = n_N/s$ we have:

$$\frac{dY_N}{dz} = \frac{1}{sz\tilde{H}}\left(1 - \frac{Y_N}{Y_N^{\rm eq}}\right)\gamma_N = \frac{1}{szH}\left(1 - \frac{Y_N}{Y_N^{\rm eq}}\right)\frac{\gamma_N}{\xi(z)}\,. \tag{5.7}$$

In the second equation we have rewritten $\tilde{H} = H\,\xi(z)$ with $H = H_{GR}$ and $\xi(z) > 1$ the T-dependent speedup factor, to put in evidence how in the BE its effect is equivalent to "slowing down" the decay and inverse decay reactions, favoring the enforcement of the out-of-equilibrium

condition.

In the next section, we will show how a simple (non-resonant) leptogenesis model, when embedded in a non-standard cosmology characterized by a boosted expansion rate allows getting around the constraint (5.4). It is interesting to remark that if a particle physics model can be experimentally established as responsible for the cosmological baryon asymmetry via (non-resonant) baryogenesis via decays of TeV scale particles, this would constitute a direct evidence of non-standard cosmology in a temperature range unreachable by all other cosmological probes (DM freeze-out, EW phase transition, etc.).

5.3 A simple test model

Besides the generic constraint in (5.4), the type-I (non-resonant) leptogenesis is subject to (5.1) from neutrino mass. In order to get around the latter, a simple way is to assume that the VEV responsible for the neutrino masses is much smaller than the full EW breaking VEV: $v_\nu \ll v \sim 174\,\text{GeV}$. By requiring a sufficient CP asymmetry $\epsilon_1 \gtrsim 10^{-7}$, the scale $M_1 \sim 1\,\text{TeV}$ can be reached for $v_\nu \lesssim 0.2\,\text{GeV}$. One has to introduce an *ad hoc* Higgs field with $\langle H_\nu \rangle = v_\nu$ coupled to RH neutrinos N_j as $\lambda_{j\alpha}\bar{N}_j L_\alpha H_\nu$, and forbid the couplings with the standard Higgs H via some $\mathbb{Z}_2$ or $U(1)$ symmetry (a $U(1)$ softly broken might be preferable to avoid domain wall problems with a spontaneously broken $\mathbb{Z}_2$). Such model exists, see for example [32], or [33] for various different possibilities (in the last paper, Model Type I with $m_{12}^2 > 0$ and $\lambda_5 = 0$ is probably the best option). Although the 'neutrinophilic' VEV model (we will denote it as v_ν-model) might not represent the most elegant possibility, its structure remains very similar to the standard type-I see-saw model, with the advantage that it minimizes the differences with respect to the standard leptogenesis case, rendering it suitable as a test model to illustrate the effects of non-standard cosmologies.[3] The usual seesaw formula still holds:

$$m_\nu \simeq \lambda^T \frac{v_\nu^2}{M} \lambda, \tag{5.8}$$

[3]Some $\Delta L = 1$ $2 \leftrightarrow 2$ washouts involving the top quark, like $Q_{3L} L \leftrightarrow N t_R$ and $Q_{3L} \bar{t}_R \leftrightarrow N \bar{L}$ will be absent, since H_ν does not couple to the top-quark. This has no major impact in determining the viable leptogenesis scale.

and so does the Casas Ibarra parametrization of the Yukawa couplings:

$$\lambda_{j\alpha} = \frac{1}{v_\nu}\sqrt{M_j}R_{j\beta}\sqrt{m_\beta}(U^\dagger)_{\beta\alpha}\,, \tag{5.9}$$

with M_j and m_β the heavy and light neutrino mass eigenvalues, U the neutrino mixing matrix, and R a generic complex orthogonal matrix ($RR^T = I$).

Let us consider (5.8). In the usual seesaw with the SM VEV $v \sim 174\,\text{GeV}$, to allow for a low value of M while still ensuring $m_\nu \lesssim 0.1\,\text{eV}$, one has to take tiny Yukawa couplings λ, which in turn imply tiny CP asymmetries.[4] In the v_ν-model instead, the couplings λ can be large since it is v_ν that is small, and thus the CP asymmetries can be also large. However, if the scale M_1 is low, leptogenesis will occur when the Universe expansion is slower, and then the $\Delta L = 2$ washouts $LH \leftrightarrow \bar{L}\bar{H}$ or $LL \leftrightarrow \bar{H}\bar{H}$ that are mediated by the same Yukawa couplings can attain thermal equilibrium, realizing the situation in which leptogenesis cannot be successful because of the constraint discussed in Section 5.1.

In order to illustrate these constraints in the GR, we show in Figure 5.2 the bounds on the lightest RH neutrino mass M_1 from leptogenesis in the v_ν-model as a function of *washout* parameter defined as

$$K_1 = \left.\frac{\Gamma_{N1}}{H}\right|_{T=M_1} \tag{5.10}$$

where $\Gamma_{N_1} = \frac{(\lambda\lambda^\dagger)_{11}M_1}{8\pi}$ is the total decay width of N_1. Outside these regions, one cannot generate sufficient baryon asymmetry. Notice that for $K_1 = 1$, the *effective* neutrino mass is

$$m_{\text{eff}} \equiv \frac{(\lambda\lambda^\dagger)_{11}v_\nu^2}{M_1} = 3.6\times 10^{-8}\sqrt{\frac{g_\star}{110.75}}\left(\frac{v_\nu}{1\,\text{GeV}}\right)^2\,\text{eV}. \tag{5.11}$$

This implies that even in the strong washout regime $K_1 \gg 1$, the lightest light neutrino remains essentially massless i.e. $m_1 \approx 0$.

[4] One could arrange for cancellations in the matrix multiplications to keep the coupling λ sizable [78, 79]. However, this requires exponential fine-tunings in the phases of the complex angles of the R matrix in (5.9) [80, 81] which, moreover, unless protected by some specific symmetry, are unstable under quantum corrections [82].

In Figure 5.2, the red/thick and blue/thin lines correspond respectively to values of $v_\nu = 1, 2$ GeV.[5] The solid lines are for the case of vanishing initial N_1 abundance $Y_{N_1}(0) = 0$ while dotted lines for thermal initial N_1 abundance $Y_{N_1}(0) = Y_{N_1}^{\rm eq}(0)$. The horizontal dashed lines refer to the absolute lower bounds obtained for the respective v_ν if leptogenesis proceeds with $Y_{N_1}(0) = Y_{N_1}^{\rm eq}(0)$ in the absence of washout (or in the weak washout regime $K_1 \ll 1$). The lower and upper bounds are respectively due to (5.1) and $\Delta L = 2$ washout scattering discussed in Section 5.1. Notice that one cannot lower the scale of M_1 indefinitely by lowing v_ν, at some point, the washout will be too strong to generate sufficient baryon asymmetry. This is the case for $v_\nu = 1$ GeV where no solution exists for the case of $Y_{N_1}(0) = 0$. In this case, one arrives at lower bound on M_1 of few times 10^5 GeV in agreement with the estimation in Section 5.1.[6]

5.4 Boltzmann equations in modified cosmology

In the following, we will describe a particle X in term of abundance $Y_X \equiv n_X/s$ defined as its number density n_X normalized over entropic density $s = \frac{2\pi^2}{45} g_\star T^3$. We will fix $g_\star = 110.75$ for the SM with an additional (neutrinophilic) Higgs doublet. Taking into account the modification due to speedup factor as discussed in (5.7), the BEs for Y_{N_1} and Y_{Δ_α} with $\Delta_\alpha \equiv \frac{B}{3} - L_\alpha$ can be written down as follows[7]

$$
\begin{aligned}
s\xi H z \frac{dY_{N_1}}{dz} &= -\gamma_{N_1}\left(\frac{Y_{N_1}}{Y_{N_1}^{\rm eq}} - 1\right), && (5.12)\\
s\xi H z \frac{dY_{\Delta_\alpha}}{dz} &= -\epsilon_{1\alpha}\gamma_{N_1}\left(\frac{Y_{N_1}}{Y_{N_1}^{\rm eq}} - 1\right) + \frac{1}{2}P_{1\alpha}\gamma_{N_1}\left(\frac{Y_{\Delta\ell_\alpha}}{Y_f} + \frac{Y_{\Delta H_\nu}}{Y_b}\right) \\
&\quad + \gamma_{22}^{\alpha\alpha}\left(\frac{Y_{\Delta\ell_\alpha}}{Y_f} + \frac{Y_{\Delta H_\nu}}{Y_b}\right) + \sum_{\beta\neq\alpha}\gamma_{22}^{\alpha\beta}\left(\frac{Y_{\Delta\ell_\alpha}}{2Y_f} + \frac{Y_{\Delta\ell_\beta}}{2Y_f} + \frac{Y_{\Delta H_\nu}}{Y_b}\right), && (5.13)
\end{aligned}
$$

where we have defined $z \equiv \frac{M_1}{T}$, $Y_f \equiv \frac{15}{8\pi^2 g_\star}$ and $Y_b \equiv \frac{15}{4\pi^2 g_\star}$. In the above, $Y_{\Delta\ell_\alpha}$ and $Y_{\Delta H_\nu}$ refer to abundances per gauge degrees of freedom. Explicitly, the total thermal averaged decay reaction

[5] The results are obtained from solving eqs. (5.12) and (5.18) by setting $\xi = 1$ and the heaviest neutrino mass $m_3 = 0.05$ eV. For further details, refer to Section 5.4.

[6] Our results for $Y_{N_1}(0) = Y_{N_1}^{\rm eq}(0)$ are also consistent with the estimation in refs. [32, 33].

[7] To avoid double counting in the BE for Y_{Δ_α}, we have subtracted off the CP-violating $\Delta L = 2$ scattering involving on-shell N_1 and ignored the off-shell contribution [83, 84].

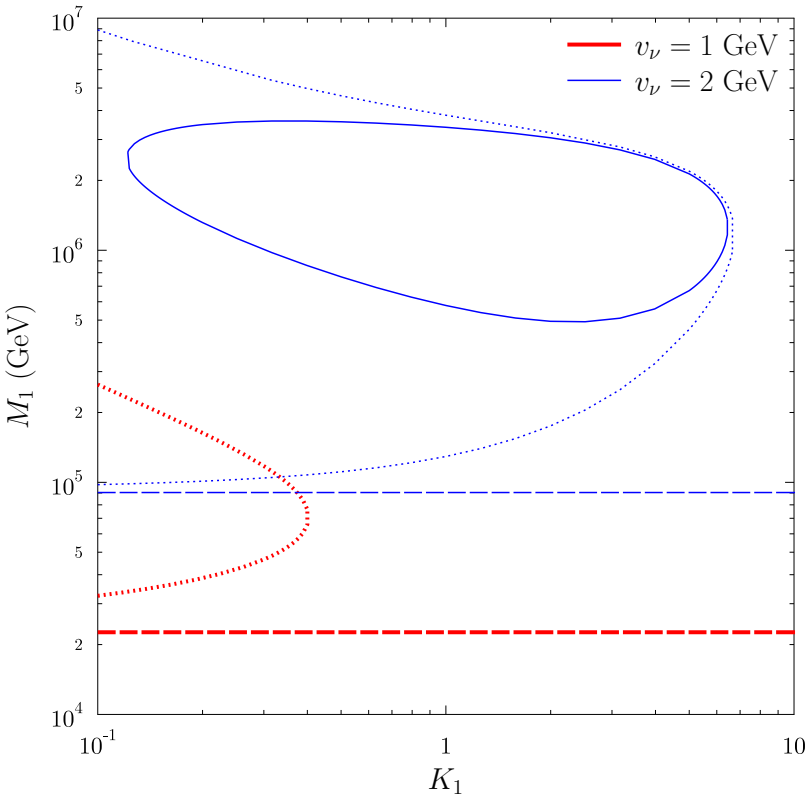

Figure 5.2: The bounds on M_1 for $v_\nu = 1, 2$ GeV (red/thick, blue/thin lines) as a function of K_1 defined in (5.10). Outside these closed regimes, one cannot obtain sufficient baryon asymmetry. The solid lines are for zero initial abundance of N_1 while dotted lines for thermal initial abundance of N_1. The horizontal dashed lines are the absolute lower bounds obtained for the respective v_ν which correspond to having thermal initial abundance of N_1 and no washout.

density γ_{N_1} is given by

$$\gamma_{N_1} = \sum_\alpha \gamma_{N_1 \to \ell_\alpha H_\nu} = n_{N_1}^{\rm eq} \Gamma_{N_1} \frac{\mathcal{K}_1(z)}{\mathcal{K}_2(z)}, \tag{5.14}$$

where $\mathcal{K}_n(z)$ refers to the modified Bessel function of second type of order n and the branching ratio for N_1 decay to lepton of flavor α as $P_{1\alpha} \equiv \frac{\gamma_{N_1 \to \ell_\alpha H_\nu}}{\gamma_{N_1}}$. The $\Delta L = 2$ washout mediated by

off-shell N_i is described by $\gamma_{22}^{\alpha\beta}$.[8] In order to minimize the complication from flavor effects and focus solely on the effect of ST cosmology, we choose the democratic flavor structure as follows

$$\begin{aligned}
\epsilon_{1e} &= \epsilon_{1\mu} = \epsilon_{1\tau} \equiv \frac{\epsilon_1}{3}, && (5.15)\\
P_{1e} &= P_{1\mu} = P_{1\tau} = \frac{1}{3}, && (5.16)\\
\gamma_{22}^{\alpha\beta} &\equiv \frac{1}{9}\gamma_{22}, && (5.17)
\end{aligned}$$

where $\epsilon_1 \equiv \sum_\alpha \epsilon_{1\alpha}$ and $\gamma_{22} \equiv \sum_{\alpha\beta} \gamma_{22}^{\alpha\beta}$. With the above assumptions, the BE for Y_{Δ_α} becomes

$$\begin{aligned}
s\xi Hz\frac{dY_{\Delta_\alpha}}{dz} &= -\frac{1}{3}\gamma_{N_1}\epsilon_1\left(\frac{Y_{N_1}}{Y_{N_1}^{\rm eq}}-1\right)+\frac{1}{6}\gamma_{N_1}\left(\frac{Y_{\Delta\ell_\alpha}}{Y_f}+\frac{Y_{\Delta H_\nu}}{Y_b}\right)\\
&\quad +\frac{1}{9}\gamma_{22}\left(\frac{Y_{\Delta\ell_\alpha}}{Y_f}+\frac{Y_{\Delta H_\nu}}{Y_b}\right)+\frac{1}{9}\gamma_{22}\left(\frac{Y_{\Delta\ell_\alpha}}{Y_f}+2\frac{Y_{\Delta H_\nu}}{Y_b}+\frac{1}{2}\sum_{\beta\neq\alpha}\frac{Y_{\Delta\ell_\beta}}{Y_f}\right). \quad (5.18)
\end{aligned}$$

For $M_{2,3} \gg M_1$, the total CP parameter is given by [87]

$$\epsilon_1 \simeq -\frac{3}{16\pi}\sum_{j>1}\frac{{\rm Im}\left[\left(\lambda\lambda^\dagger\right)_{1j}^2\right]}{\left(\lambda\lambda^\dagger\right)_{11}}\frac{M_1}{M_j}, \quad (5.19)$$

and using (5.9), one can derive the Davidson-Ibarra bound [31]

$$|\epsilon_1| \leq \frac{3}{16\pi}\frac{M_1}{v_\nu^2}\left(m_3-m_1\right) \equiv \epsilon_1^{\rm max}, \quad (5.20)$$

as introduced in (5.1) but with $v \to v_\nu$. We further parametrize the off-shell $\Delta L = 2$ washout mediated by N_i valid for $T < M_i$ as follows

$$\gamma_{22} \equiv \frac{n}{\pi^3}\frac{{\rm Tr}\left[m_\nu m_\nu^\dagger\right]}{v_\nu^4}T^3 = \frac{nM_1^3}{\pi^3 z^3}\frac{\sum_i m_i^2}{v_\nu^4}, \quad (5.21)$$

[8] The $\Delta L = 1$ scatterings involving gauge bosons are not considered since to consider them consistently, one also needs to consider CP violation in them which will result in a small net effect [85, 86]. As for flavor changing but $\Delta L = 0$ scatterings, their rates go as $\frac{T^5}{M_i^4}$ for $T < M_i$ which are less important than that of $\Delta L = 2$ reactions which go as $\frac{T^3}{M_i^2}$ for $T < M_i$. Furthermore, in the following, we will consider democratic flavor structure where they are either not relevant or in thermal equilibrium and can be dropped from the BEs.

where $n = \frac{2}{\pi^2} T^3$. As shown in (5.11), the lightest light neutrino mass m_1 can be neglected and we can rewrite the above in term of (5.20) as follows

$$\gamma_{22} \simeq \frac{256n}{9\pi} \frac{M_1}{z^3} \epsilon_1^{\max,2}. \tag{5.22}$$

From the above, we see that the $\Delta L = 2$ washout is indeed proportional to $\epsilon_1^{\max,2}$ as argued in (5.2), so that M_1 remains bounded from below by the general lower limit given in (5.4). As in the standard type-I seesaw, also in the present case an upper bound on M_1 exists, which follows from the requirement that $\Delta L = 2$ washout scatterings will not become too strong to erase the asymmetry. (5.21) shows that once the neutrino mass scale m_i is fixed, for each value of v_ν there is a limiting upper value of M_1 for which γ_{22} remains sufficiently out of equilibrium. However, while in the standard case this hints to a loose upper limit of order $\sim 10^{14}$ GeV, due to the large hierarchy $v_\nu/v \lesssim 10^{-2}$ and to the quartic dependence on the VEV values, in the neutrinophilic VEV model the corresponding constraint is much stronger.

For the spectator effects [88, 89], we consider the temperature regime $T \lesssim 10^5$ GeV where all Yukawa interactions are in chemical equilibrium. We further assume that H_ν does not carry a conserved charge[9] and we have

$$\begin{pmatrix} Y_{\Delta\ell_e} \\ Y_{\Delta\ell_\mu} \\ Y_{\Delta\ell_\tau} \end{pmatrix} = \frac{1}{207} \begin{pmatrix} -64 & 5 & 5 \\ 5 & -64 & 5 \\ 5 & 5 & -64 \end{pmatrix} \begin{pmatrix} Y_{\Delta_e} \\ Y_{\Delta_\mu} \\ Y_{\Delta_\tau} \end{pmatrix}, \tag{5.23}$$

$$Y_{\Delta H_\nu} = -\frac{2}{23} \left(Y_{\Delta_e} + Y_{\Delta_\mu} + Y_{\Delta_\tau} \right). \tag{5.24}$$

[9]This can be due to fast interactions induced by $\lambda_5 \left(H^\dagger H_\nu\right)^2$ in the scalar potential.

Substituting the result above into (5.18) and summing over α on both sides, the BE becomes

$$\begin{aligned} s\xi Hz\frac{dY_\Delta}{dz} &= -\gamma_{N_1}\epsilon_1\left(\frac{Y_{N_1}}{Y_{N_1}^{\rm eq}}-1\right)+\frac{1}{6}\gamma_{N_1}\left(-\frac{6}{23}\frac{Y_\Delta}{Y_f}-\frac{6}{23}\frac{Y_\Delta}{Y_b}\right) \\ &\quad +\frac{1}{9}\gamma_{22}\left(-\frac{6}{23}\frac{Y_\Delta}{Y_f}-\frac{6}{23}\frac{Y_\Delta}{Y_b}\right)+\frac{2}{9}\gamma_{22}\left(-\frac{6}{23}\frac{Y_\Delta}{Y_f}-\frac{6}{23}\frac{Y_\Delta}{Y_b}\right) \\ &= -\gamma_{N_1}\epsilon_1\left(\frac{Y_{N_1}}{Y_{N_1}^{\rm eq}}-1\right)-\frac{3}{23}\left(\gamma_{N_1}+2\gamma_{22}\right)\frac{Y_\Delta}{Y_f}, \end{aligned} \tag{5.25}$$

where we have defined $Y_\Delta \equiv Y_{\Delta_e}+Y_{\Delta_\mu}+Y_{\Delta_\tau}$. In [90], assuming the SM, it was obtained that the EW sphaleron processes freeze out at $T_{\rm EWSp}=132$ GeV after the EW symmetry breaking at $T_c=159$ GeV. Assuming the EW symmetry breaking also happens before $T_{\rm EWSp}$ in v_ν-model, we have [91, 92]

$$Y_{\Delta B} = \frac{30}{97}Y_\Delta, \tag{5.26}$$

excluding the contributions from heavy charged (neutrinophilic) Higgs and top quark.

5.5 Results

The asymmetry Y_Δ can be parametrized in term of *efficiency* factor $\eta=\eta(K_1,v_\nu,m_3,M_1)$ as follows

$$Y_\Delta = \epsilon_1 Y_{N_1}^{\rm eq,0}\eta, \tag{5.27}$$

where $Y_{N_1}^{\rm eq,0}\equiv Y_{N_1}^{\rm eq}(0)=\frac{45}{\pi^4 g_\star}$. The above parametrization is convenient because once we substitute it into (5.25), for temperature-independent ϵ_1, the BE becomes independent of ϵ_1. The final asymmetry is obtained by evaluating the final efficiency $\eta=\eta(z\to\infty)$. In the case with an initial thermal abundance of N_1, one saturates to the maximal efficiency $\eta=1$ in the limit of weak washout $K_1\ll 1$ and small $\Delta L=2$ washout. As we will see in more detail later, as M_1 gets close to the EW sphaleron freezeout temperature $T_{\rm EWSp}$, one might not be able to saturate the efficiency factor because the baryon asymmetry will be frozen before all N_1 can decay.

Using (5.20) and (5.26), the maximal asymmetry is given by

$$Y_{\Delta B}^{\max} = \frac{30}{97}\frac{3}{16\pi}\frac{M_1 m_3}{v_\nu^2} Y_{N_1}^{\mathrm{eq},0}\eta. \tag{5.28}$$

Setting $Y_{\Delta B}^{\max} = Y_{\Delta B}^{\mathrm{obs}} = 8.7\times 10^{-11}$, we can derive both upper and lower bounds on M_1. Starting from a very small M_1 while keeping the $\Delta L = 2$ washout under control, the CP parameter might be too small and we need to increase M_1 until $Y_{\Delta B}^{\max} = Y_{\Delta B}^{\mathrm{obs}}$, which gives us the lower bound on M_1. As we continue to increase M_1, eventually the $\Delta L = 2$ washout (5.21) will become too strong until which we are no longer able to obtain sufficient baryon asymmetry and this gives us an upper bound on M_1. As we explain below (5.22), this upper bound is specific to the model we have chosen due to neutrino mass constraint. In other words, from the following equation

$$M_1\eta\left(K_1, v_\nu, m_3, M_1\right) = \frac{97}{30}\frac{16\pi}{3}\frac{v_\nu^2}{m_3}\frac{Y_{\Delta B}^{\mathrm{obs}}}{Y_{N_1}^{\mathrm{eq},0}}, \tag{5.29}$$

for a given v_ν and m_3, we can have no solution, one solution, or two solutions for M_1. The two solutions will correspond to upper and lower bounds on M_1. Notice that as we go to smaller M_1, the EW sphaleron freezeout temperature becomes relevant and we fix this to be $T_{\mathrm{EWSp}} = 132$ GeV after which the value of baryon asymmetry will be frozen.

It is important to note the temperature where speedup happens is crucial for leptogenesis. As discussed in Section 5.2, while the regime of speedup for the conformal case depends on initial temperature and φ field configurations, the regime of speedup for the disformal case depends on a new mass scale M_D. Besides this point, the qualitative effect of the speedup for both scenarios on leptogenesis remains the same. Hence we will only illustrate the result for speedup factor for the conformal case as shown in the left plot of Figure 5.1. In this example where speedup happens in the range $10\,\mathrm{GeV} < T < 10^5\,\mathrm{GeV}$, it will affect leptogenesis with M_1 which falls in the relevant mass range.

Our main results are presented in Figure 5.3 in the $K_1 - M_1$ plane for a fixed $m_3 = 0.05$ eV and $v_\nu = 0.1, 1$ GeV (red/thick, blue/thin lines) where outside these closed regime, one cannot

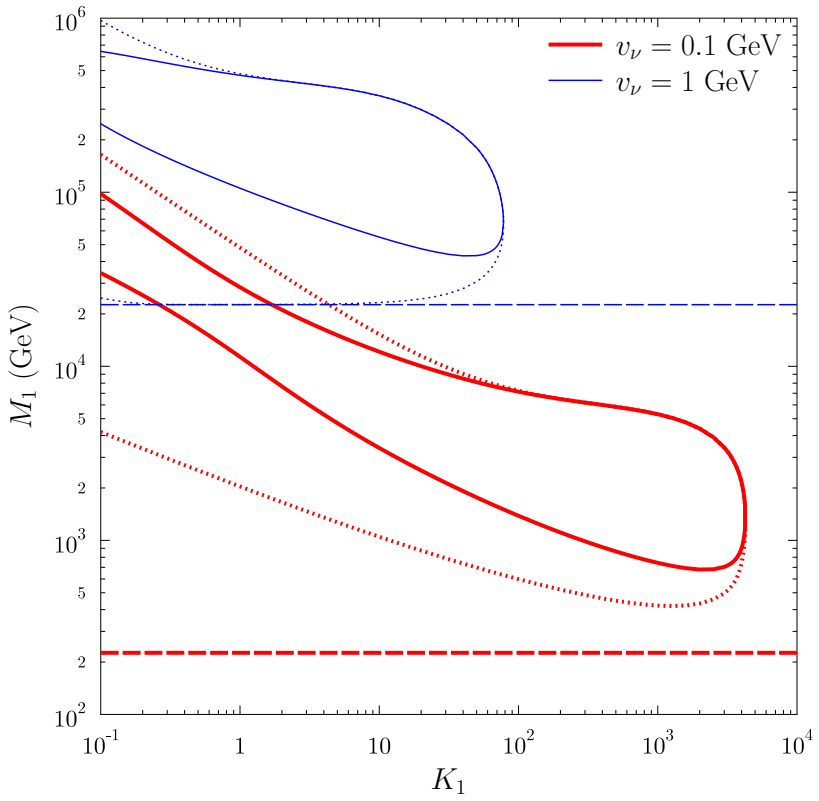

Figure 5.3: The bounds on M_1 for $v_\nu = 0.1, 1$ GeV (red/thick, blue/thin lines) as a function of K_1 defined in (5.10). Outside the closed regimes, one cannot obtain sufficient baryon asymmetry. The solid lines are for zero initial abundance of N_1 while dotted lines for thermal initial abundance. The horizontal dashed lines represent the absolute lower bounds on M_1 for the respective v_ν obtained with initial thermal abundance of N_1 and no washout.

obtain sufficient baryon asymmetry. The solid lines are for $Y_{N_1}(0) = 0$ while dotted lines for $Y_{N_1}(0) = Y_{N_1}^{\rm eq}(0)$. The horizontal dashed lines are the absolute lower bounds obtained for the respective v_ν which correspond to having $Y_{N_1}(0) = Y_{N_1}^{\rm eq}(0)$ and no washout. For $Y_{N_1}(0) = 0$ and small K_1, due to the speedup in the Hubble expansion, the inverse decay is not efficient in populating N_1. Less N_1 results in less asymmetry being produced and hence M_1 needs to increase correspondingly to enhance the CP violation. As one goes to larger K_1, N_1 is more efficiently

populated and one is allowed to have smaller M_1. Crucially, in all cases, $\Delta L = 2$ washout is suppressed sufficiently due to the speedup factor ξ as evidence from the fact that one is able to obtain successful leptogenesis for M_1 much below 10^5 GeV (Figure 5.2). In fact, a smaller speedup in the early times (see Figure 5.1) allows an efficient washout of an initial 'wrong' sign asymmetry (generated during the production of N_1) by $\Delta L = 2$ scattering and one ends up enhancing the final asymmetry. Instead of a curse, $\Delta L = 2$ becomes a blessing. Numerically, we found the lowest M_1 to be around 350 GeV which corresponds to $v_\nu \sim 0.03$ GeV and $K_1 \sim 3000$.

As a final remark, notice that the behaviors of M_1 lower bounds for $Y_{N_1}(0) = Y_{N_1}^{\rm eq}(0)$ for small K_1 are different for the case of $v_\nu = 0.1, 1$ GeV. In the small K_1 regime, we expect them to approach the absolute lower bounds (the horizontal dashed lines). While this happens for the case of $v_\nu = 1$ GeV, the lower bound actually moves away from the horizontal line for the case of $v_\nu = 0.1$ GeV. The reason is that for $M_1 \sim$ TeV and small K_1, the decays happen very late close to the EW sphaleron freezeout temperature $T_{\rm EWSp}$. When we reach this temperature, the baryon asymmetry will be frozen before all N_1 can decay, resulting in smaller final asymmetry.

5.6 Minimal Supersymmetric Standard Model and Right-handed Neutrinos

In section 3.4.3, we mentioned that the scale for the enhanced expansion rate can be moved around as a function of the new scale associated with $D(\varphi)$ term in the disformal D-brane coupling scenario. In the conformal case, an extension of the SM can change the enhancement scale. In this section, we discuss the scale for enhancement in the cases of MSSM and SM with 3 RH neutrinos.

In the left plot of Figure 5.1, we show the speedup factor, in the conformal scenario, for one set of values for φ and φ' at an initial temperature of 100 TeV considering only the SM particle spectrum. If we add three 10 TeV RH neutrinos, the speedup factor and its slope at around 1 TeV are the same as in the SM case, but ξ drops to 1 slightly earlier.

We now add the RH neutrinos to the spectrum of the SM and MSSM. In Figure 5.4, we show the enhancements for various values of φ' and initial temperatures. We add three RH neutrinos at $\sim$ 10 TeV in the particle spectrum along with the SM (solid lines). In the bottom panel of the figure, we show $\tilde{\omega}$ as a function of z (blue solid line) and we find a new small trough at around

10 TeV due to the new RH neutrinos. The other dips in $\tilde{\omega}$ are due to the SM particles. The expansion rate increases when φ' increases, however, if φ' is too large, the speedup factor does not get reduced to 1 before the BBN. As mentioned before, a sudden drop of the enhancement factor to the standard GR value occurs due to the troughs in $\tilde{\omega}$, which create an attractive effective potential when $\tilde{\omega} \neq 1/3$. For large initial values of φ', the scalar field overcomes this attractive potential and the enhancement factor never reduces to one.

In Figure 5.4, left plot, we consider an initial temperature of 100 TeV. The expansion rate can be enhanced by a factor of 100, or more, for temperatures between 100 GeV and 1 TeV. If, however, we increase the initial temperature to 10^5 TeV or higher, the enhancement scale moves to a higher temperature and enhancements bigger than 100 can occur for temperatures between 1 TeV and 10^4 TeV. At higher temperature, the Hubble friction slows down the scalar field faster, and since the attractive effective potential kicks in early, due to the trough in $\tilde{\omega}$ caused by the RH neutrinos (at around 10 TeV), the enhancement factor drops to one at a higher temperature.

Using dotted lines in Figure 5.4, we show the speedup factors due to the MSSM particles, where we keep the SUSY partners of the SM particles at around 1 TeV and, for illustration, three RH neutrinos (and their SUSY partners) at $\sim$ 10 TeV. In the panel below the figure, we show $\tilde{\omega}$ (red dotted line) for MSSM + 3 RH neutrinos and we find a new deep trough in $\tilde{\omega}$ at around 1 TeV due to the SUSY particles (we put all of them together). The other dips are due to the SM particles. Like before, we find that the enhancement and its slope does not change much compared to the SM case but the speedup factor reduces to one for higher temperature.

It is also important to mention, no matter what particle spectrum we consider, that the initial value of the scalar field does not play a relevant roll in the shape and slope of the speedup factor, as long as this value is positive and order one.

We find that an enhancement of the expansion rate with an initial temperature at 10^{2-3} TeV is most effective in producing a successful leptogenesis, with the enhancement scale around TeV, caused by the SM particle spectrum. Now, the initial temperature is set by the inflation scale. In the case of the MSSM, it is shown that the thermal leptogenesis constraint from the type I seesaw

is $T_R > 10^6$ TeV [93, 94]. This bound conflicts with the cosmological gravitino bound for unstable gravitinos. For a gravitino mass closer to a 100 GeV DM mass, BBN implies stringent upper bound on reheating temperature $\leq O(1) \times 10^2$ TeV [95]. Based on our analysis, this low reheating scale is very helpful to have the leptogenesis scale to be around 1 TeV.

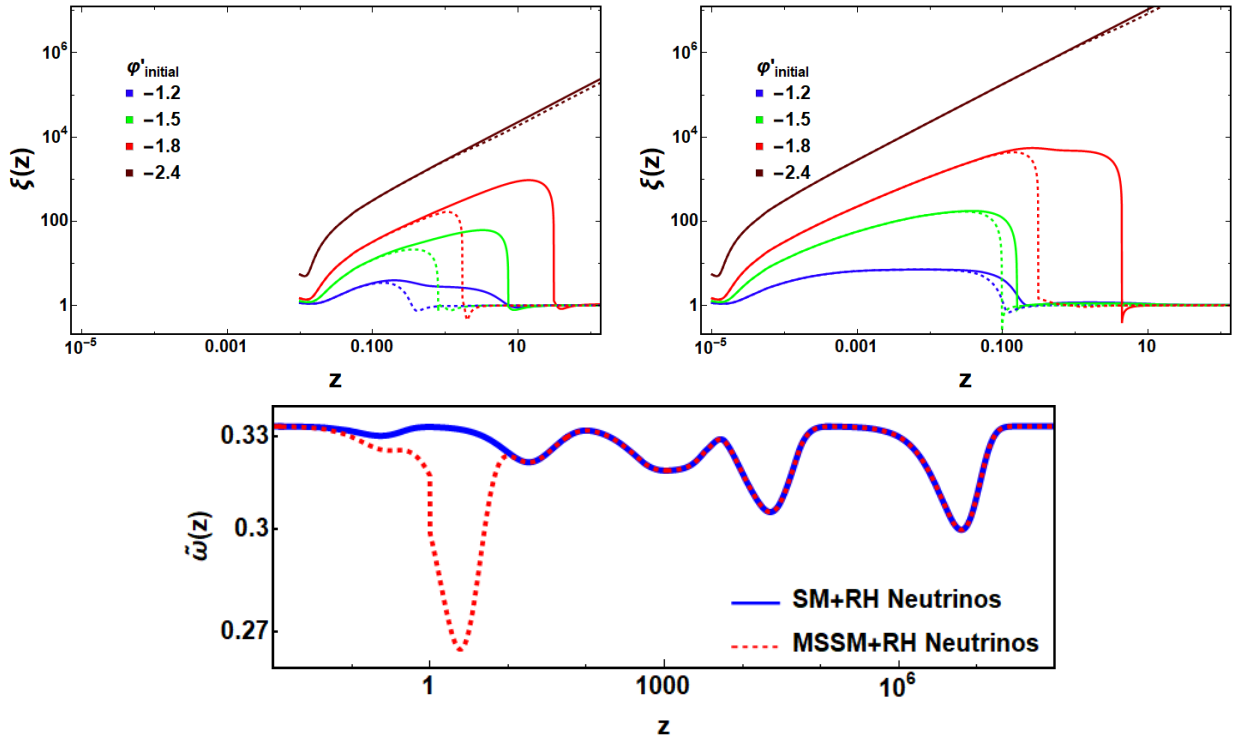

Figure 5.4: Speedup factor $\xi(z)$ as a function of $z = 1\,\mathrm{TeV}/\mathrm{T}$ for SM+3 RH neutrinos (solid lines) and MSSM+3 RH neutrinos (dotted lines) for various values of φ'. The RH neutrinos mass value is 10 TeV, and the initial temperatures are 10^5 GeV (left plot) and 10^8 GeV (right plot). The bottom figure shows the equation of state parameter $\tilde{\omega}$ for the two cases.

6. CONCLUSIONS

Since it is difficult to probe the universe between inflation and the onset of BBN, the evolution of the universe is mostly unconstrained during this period. Origins of DM, baryon abundances, etc, crucially depend on the evolution history around that time. During this epoch, the expansion rate can be different in ST theories compared to the standard cosmology even though the universe is still radiation dominated.

Scalar-tensor theories where the gravitational interaction is mediated by both the metric and scalar fields arise commonly in modifications of GR. The prototype example is the Brans-Dicke theory where the metric and a scalar field are related via the conformal coupling as $\tilde{g}_{\mu\nu} = C(\phi)g_{\mu\nu}$. However, the most general physically consistent relation between the two metrics includes a disformal (or derivative) coupling [13]: $\tilde{g}_{\mu\nu} = C(\phi)g_{\mu\nu} + D(\phi)\partial_\mu\phi\partial_\nu\phi$.

Both couplings C and D can give rise to a different expansion rate from the standard cosmological model in the early universe, and still be in agreement with current constraints from BBN and gravity. In particular, BBN imposes a strong constraint on the speed-up parameter, ξ, which needs to be very close to one before the onset of BBN.

In Chapter 2, we explored an ST theory coupled both conformally and disformally to matter. For the pure conformal case, we investigated a conformal factor of the type $C = (1 + b\, e^{-\beta\varphi})^2$. We found the modified expansion rate, $\tilde{H}$, during the radiation dominated. When comparing the expansion rate, $\tilde{H}$, to the standard expansion rate, H_{GR}, we found that the speed-up factor, $\xi = \frac{\tilde{H}}{H_{GR}}$, increases up to 200 and then become of order 1 prior to BBN (see Figure 2.3).

We also started to investigate the effects on the early evolution of a disformal factor in the metric (2.2). We noticed that in order to have a consistent solution, i.e. a real positive $\tilde{H}$, the conformal and disformal factors need to satisfy a very specific relation, (2.48). We studied the effect of a disformal factor by turning on a small disformal contribution to the conformal case, given by $D(\varphi) = -4.9 \times 10^{-14}\varphi^2$. We found, in Section 2.5, that when both, the conformal and disformal function, are turned on, $\tilde{H}$ has a very similar profile as for the pure conformal case, with

an enhancement and a notch compared to the standard expansion rate. However, the position of the notch changes. The disformal factor is moving the notch to higher temperatures.

In Chapter 3 we introduce the disformal D-brane coupling scenario. In this case, the functions C and D are closely related and are dictated by another theory, for example, type IIB string theory. Moreover, the scalar field has a geometrical origin in terms of the transverse fluctuations of the D-brane, while matter lives on the brane and it comes from the longitudinal fluctuations. In this chapter, we investigated the modification to the expansion rate due to the disformally coupled scalar, where $D = 1/M^4 C$ (Figures 3.2, 3.5 and 3.8).

We numerically solved the coupled equations for H and φ (see (3.44) and (3.45)) and used this to find the modified expansion rate. We noted that contrary to the purely conformal case, in the presence of the disformal term it is not possible to eliminate H from the system to solve a single master equation, as in Section 2.4. So we needed to carefully take into account both equations as well as the initial conditions for H. This introduced a cubic equation for H in terms of the other parameters $(\varphi, \tilde{\rho})$ and a lower bound for the scale M, given the initial conditions for $(\varphi_i, \tilde{\rho}_i)$ (see Section 3.4.2).

In section 3.4.3 we presented for the first time the purely disformal case corresponding to $C = \text{const.}$ where the modification to the expansion rate is fully driven by the derivative coupling through γ (see Eq. (3.55)). For the disformal D-brane coupling scenario, the expansion rate is always faster-than-usual (Figure 3.2). We found that the larger the value of the new scale M the earlier the enhancement in the expansion rate appears (Figure 3.5). Therefore, depending on the value of M, the modified expansion rate can occur at a different temperature in the early universe. We also found that the expansion rate can be up to ~ 1000 times bigger than the standard GR case.

Again, we studied the effect of M on the profiles of the expansion rates. We considered in detail for concreteness only the conformal function used in Chapter 2. For this function, the numerical analysis is relatively simple; however, there is in principle no obstruction to find similar effects for other functions. We looked at the function $C = (bx^2 + c)^2$ (for $b = 4, 8, 15$, $c = 1$), which can be a toy model for a smooth warp factor in a string theory setup. For this example, we found

a relatively small enhancement with $\xi \sim 4$. We expect that a wider search of parameters and conformal functions will give rise to a larger enhancement as well as a decrease in the modified expansion rate.

As we showed in Chapter 4, the enhanced expansion rate has important consequences on the evolution of the abundance of dark matter particles. So, we also investigated the effect on the abundance of dark matter particles. In the pure conformal ST scenario, we observed that for dark matter particles of large mass, the particles undergo a second annihilation process and then freeze-out once and for all in (see Figure 4.2). Moreover, we found that for large masses the annihilation cross-section has to be up to four times larger than that of standard cosmology models in order to satisfy the dark matter content of the universe of 27 %. On the other hand, for small masses, this re-annihilation process is not present, but we found that for masses around 130 GeV, the annihilation cross-section can be smaller than the annihilation cross-section for the standard cosmological model (see Figure 4.3).

For the disformal D-brane coupling scenario, the modified expansion rate is always enhanced with respect to the standard one (Figure 3.2), which implies an anticipated freeze-out and an enhancement of the cross section $\langle \sigma v \rangle$ (Figure 4.7). For the $C \neq$ const case (section 3.4.4) we saw that it is possible to have an enhancement as well as a reduction of the expansion rate with respect to the standard case, that is $\xi > 1$ and $\xi < 1$ (Fig. 3.8). This diminution gives the possibility of a reannihilation process, as in the conformal and disformal cases studied in Chapter 2. Thus the effect on the relic abundance and annihilation rate is analogous.

Finally, in Chapter 5 we study leptogenesis in a faster-than-usual cosmic expansion. The scale of leptogenesis in the case of a typical type I seesaw model is very high and is out of reach for the ongoing experimental facilities. However, many models with a much lower leptogenesis scale exist where the RH neutrino masses arise due to new physics around multi-TeV scale. In these models, it is found that (if no resonant enhancement of CP asymmetries is assumed), there exists a lower bound on the scale of leptogenesis which is ~ 10 TeV under the assumption of an initial thermal abundance for RH neutrinos along with no washout. The lower bound increases in the case

of zero initial abundance. This conclusion changes in ST theories with an enhanced expansion rate which helps the leptogenesis models to be probed in the ongoing experiments.

In the case of an enhanced expansion, the requirement of a larger washout scattering rate demands the scale of leptogenesis to be smaller since the scattering rate is inversely proportional to M^n where the exact value of n (≥ 0) depends on the details of the initial and final state particle properties. We used a toy model of leptogenesis to manifest the lowering of the leptogenesis scale due to an enhanced expansion rate. In this model, the RH neutrinos do not couple to the SM Higgs, instead, they couple to a new Higgs. We found that the scale of leptogenesis can be lowered down to $\sim$ TeV for both zero and thermal initial abundances for the RH neutrinos for a wide range of model parameter space which allows these models to be probed at the ongoing experimental facilities. In some parameter space of the model, we showed that an enhancement of the expansion rate can lower the leptogenesis scale down to ~ 400 GeV. The existence of an enhanced expansion rate between 100 GeV to a few TeV due to the SM particle spectrum (plus the RH neutrinos) in the case of a conformal modification of the metric is crucial to lowering the scale of leptogenesis. If an enhancement happens at a higher scale, the scale of leptogenesis is not lowered and an enhancement at a smaller scale is also not helpful in lowering the leptogenesis scale with the correct amount of asymmetry since the EW sphaleron freezeout occurs at around 130 GeV. All of our findings for this model should apply to any leptogenesis model.

REFERENCES

[1] R. H. Cyburt, B. D. Fields, K. A. Olive, and T.-H. Yeh, "Big Bang Nucleosynthesis: 2015," *Rev. Mod. Phys.* **88** (2016) 015004, arXiv:1505.01076 [astro-ph.CO].

[2] L. E. Ibanez and A. M. Uranga, *String theory and particle physics: An introduction to string phenomenology*. Cambridge University Press, 2012.

[3] T. Koivisto, D. Wills, and I. Zavala, "Dark D-brane Cosmology," *JCAP* **1406** (2014) 036, arXiv:1312.2597 [hep-th].

[4] T. Damour and K. Nordtvedt, "General relativity as a cosmological attractor of tensor scalar theories," *Phys. Rev. Lett.* **70** (1993) 2217–2219.

[5] T. Damour and K. Nordtvedt, "Tensor - scalar cosmological models and their relaxation toward general relativity," *Phys. Rev.* **D48** (1993) 3436–3450.

[6] J. D. Bekenstein, "The Relation between physical and gravitational geometry," *Phys. Rev.* **D48** (1993) 3641–3647, arXiv:gr-qc/9211017 [gr-qc].

[7] R. Catena, N. Fornengo, A. Masiero, M. Pietroni, and F. Rosati, "Dark matter relic abundance and scalar - tensor dark energy," *Phys. Rev.* **D70** (2004) 063519, arXiv:astro-ph/0403614 [astro-ph].

[8] R. Catena, N. Fornengo, M. Pato, L. Pieri, and A. Masiero, "Thermal Relics in Modified Cosmologies: Bounds on Evolution Histories of the Early Universe and Cosmological Boosts for PAMELA," *Phys. Rev.* **D81** (2010) 123522, arXiv:0912.4421 [astro-ph.CO].

[9] G. B. Gelmini, J.-H. Huh, and T. Rehagen, "Asymmetric dark matter annihilation as a test of non-standard cosmologies," *JCAP* **1308** (2013) 003, arXiv:1304.3679 [hep-ph].

[10] T. Rehagen and G. B. Gelmini, "Effects of kination and scalar-tensor cosmologies on sterile neutrinos," *JCAP* **1406** (2014) 044, arXiv:1402.0607 [hep-ph].

[11] S.-z. Wang, H. Iminniyaz, and M. Mamat, "Asymmetric dark matter and the scalar-tensor model," *Int. J. Mod. Phys.* **A31** (2016) no. 07, 1650021, arXiv:1503.06519 [hep-ph].

[12] M. T. Meehan and I. B. Whittingham, "Dark matter relic density in scalar-tensor gravity revisited," arXiv:1508.05174 [astro-ph.CO].

[13] J. D. Bekenstein, "The Relation between physical and gravitational geometry," *Phys.Rev.* **D48** (1993) 3641–3647, arXiv:gr-qc/9211017 [gr-qc].

[14] F. D'Eramo, N. Fernandez, and S. Profumo, "When the Universe Expands Too Fast: Relentless Dark Matter," *JCAP* **1705** (2017) no. 05, 012, arXiv:1703.04793 [hep-ph].

[15] **DES, Fermi-LAT** Collaboration, A. Albert et al., "Searching for Dark Matter Annihilation in Recently Discovered Milky Way Satellites with Fermi-LAT," arXiv:1611.03184 [astro-ph.HE].

[16] **Planck** Collaboration, P. A. R. Ade et al., "Planck 2015 results. XIII. Cosmological parameters," *Astron. Astrophys.* **594** (2016) A13, arXiv:1502.01589 [astro-ph.CO].

[17] **HAWC** Collaboration, A. U. Abeysekara et al., "Sensitivity of HAWC to high-mass dark matter annihilations," *Phys. Rev.* **D90** (2014) no. 12, 122002, arXiv:1405.1730 [astro-ph.HE].

[18] **CTA** Collaboration, J. Carr et al., "Prospects for Indirect Dark Matter Searches with the Cherenkov Telescope Array (CTA)," *PoS* **ICRC2015** (2016) 1203, arXiv:1508.06128 [astro-ph.HE].

[19] A. Lahanas, N. Mavromatos, and D. V. Nanopoulos, "Dilaton and off-shell (non-critical string) effects in Boltzmann equation for species abundances," *PMC Phys.* **A1** (2007) 2, arXiv:hep-ph/0608153 [hep-ph].

[20] C. Pallis, "Cold Dark Matter in non-Standard Cosmologies, PAMELA, ATIC and Fermi LAT," *Nucl. Phys.* **B831** (2010) 217–247, arXiv:0909.3026 [hep-ph].

[21] P. Salati, "Quintessence and the relic density of neutralinos," *Phys. Lett.* **B571** (2003) 121–131, arXiv:astro-ph/0207396 [astro-ph].

[22] A. Arbey and F. Mahmoudi, "SUSY constraints from relic density: High sensitivity to pre-BBN expansion rate," *Phys. Lett.* **B669** (2008) 46–51, arXiv:0803.0741 [hep-ph].

[23] H. Iminniyaz and X. Chen, "Relic Abundance of Asymmetric Dark Matter in Quintessence," *Astropart. Phys.* **54** (2014) 125–131, arXiv:1308.0353 [hep-ph].

[24] M. T. Meehan and I. B. Whittingham, "Asymmetric dark matter in braneworld cosmology," *JCAP* **1406** (2014) 018, arXiv:1403.6934 [astro-ph.CO].

[25] M. T. Meehan and I. B. Whittingham, "Dark matter relic density in Gauss-Bonnet braneworld cosmology," *JCAP* **1412** (2014) 034, arXiv:1404.4424 [astro-ph.CO].

[26] M. Fukugita and T. Yanagida, "Baryogenesis Without Grand Unification," *Phys. Lett.* **B174** (1986) 45–47.

[27] V. A. Kuzmin, V. A. Rubakov, and M. E. Shaposhnikov, "On the Anomalous Electroweak Baryon Number Nonconservation in the Early Universe," *Phys. Lett.* **B155** (1985) 36.

[28] V. A. Rubakov and M. E. Shaposhnikov, "Electroweak baryon number non-conservation in the early universe and in high-energy collisions," *Usp. Fiz. Nauk* **166** (1996) 493–537, arXiv:hep-ph/9603208.

[29] S. Davidson, E. Nardi, and Y. Nir, "Leptogenesis," *Phys. Rept.* **466** (2008) 105–177, arXiv:0802.2962 [hep-ph].

[30] C. S. Fong, E. Nardi, and A. Riotto, "Leptogenesis in the Universe," *Adv. High Energy Phys.* **2012** (2012) 158303, arXiv:1301.3062 [hep-ph].

[31] S. Davidson and A. Ibarra, "A lower bound on the right-handed neutrino mass from leptogenesis," *Phys. Lett.* **B535** (2002) 25, arXiv:hep-ph/0202239.

[32] N. Haba and O. Seto, "Low scale thermal leptogenesis in neutrinophilic Higgs doublet models," *Prog. Theor. Phys.* **125** (2011) 1155–1169, arXiv:1102.2889 [hep-ph].

[33] J. D. Clarke, R. Foot, and R. R. Volkas, "Natural leptogenesis and neutrino masses with two Higgs doublets," *Phys. Rev.* **D92** (2015) no. 3, 033006, arXiv:1505.05744 [hep-ph].

[34] Y.-K. E. Cheung, C. Li, and J. D. Vergados, "Big Bounce Genesis and Possible Experimental Tests - A Brief Review," arXiv:1611.04027 [astro-ph.CO].

[35] P. Creminelli, M. A. Luty, A. Nicolis, and L. Senatore, "Starting the Universe: Stable Violation of the Null Energy Condition and Non-standard Cosmologies," *JHEP* **12** (2006) 080, arXiv:hep-th/0606090 [hep-th].

[36] K. Nordtvedt, Jr., "PostNewtonian metric for a general class of scalar tensor gravitational theories and observational consequences," *Astrophys. J.* **161** (1970) 1059–1067.

[37] A. Coc, K. A. Olive, J.-P. Uzan, and E. Vangioni, "Big bang nucleosynthesis constraints on scalar-tensor theories of gravity," *Phys. Rev.* **D73** (2006) 083525, arXiv:astro-ph/0601299 [astro-ph].

[38] A. L. Erickcek, N. Barnaby, C. Burrage, and Z. Huang, "Chameleons in the Early Universe: Kicks, Rebounds, and Particle Production," *Phys. Rev.* **D89** (2014) no. 8, 084074, arXiv:1310.5149 [astro-ph.CO].

[39] G. Esposito-Farese and D. Polarski, "Scalar tensor gravity in an accelerating universe," *Phys. Rev.* **D63** (2001) 063504, arXiv:gr-qc/0009034 [gr-qc].

[40] C. M. Will, "The Confrontation between general relativity and experiment," *Living Rev. Rel.* **4** (2001) 4, arXiv:gr-qc/0103036 [gr-qc].

[41] J. G. Williams, X. X. Newhall, and J. O. Dickey, "Relativity parameters determined from lunar laser ranging," *Phys. Rev.* **D53** (1996) 6730–6739.

[42] S. S. Shapiro, J. L. Davis, D. E. Lebach, and J. S. Gregory, "Measurement of the Solar Gravitational Deflection of Radio Waves using Geodetic Very-Long-Baseline Interferometry Data, 1979-1999," *Phys. Rev. Lett.* **92** (2004) 121101.

[43] B. Bertotti, L. Iess, and P. Tortora, "A test of general relativity using radio links with the Cassini spacecraft," *Nature* **425** (2003) 374–376.

[44] R. Allahverdi, M. Cicoli, B. Dutta, and K. Sinha, "Nonthermal dark matter in string compactifications," *Phys. Rev.* **D88** (2013) no. 9, 095015, arXiv:1307.5086 [hep-ph].

[45] K. Dimopoulos, D. Wills, and I. Zavala, "Statistical Anisotropy from Vector Curvaton in D-brane Inflation," *Nucl. Phys.* **B868** (2013) 120–155, arXiv:1108.4424 [hep-th].

[46] H. Y. Ip, J. Sakstein, and F. Schmidt, "Solar System Constraints on Disformal Gravity Theories," *JCAP* **1510** (2015) 051, arXiv:1507.00568 [gr-qc].

[47] V. Balasubramanian, P. Berglund, J. P. Conlon, and F. Quevedo, "Systematics of moduli stabilisation in Calabi-Yau flux compactifications," *JHEP* **03** (2005) 007, arXiv:hep-th/0502058 [hep-th].

[48] J. P. Conlon, F. Quevedo, and K. Suruliz, "Large-volume flux compactifications: Moduli spectrum and D3/D7 soft supersymmetry breaking," *JHEP* **08** (2005) 007, arXiv:hep-th/0505076 [hep-th].

[49] D. Baumann and L. McAllister, *Inflation and String Theory*. Cambridge University Press, 2015. arXiv:1404.2601 [hep-th].

[50] P. Minkowski, "mu $\rightarrow$ e gamma at a rate of one out of 1-billion muon decays?," *Phys. Lett.* **B67** (1977) 421.

[51] M. Gell-Mann, P. Ramond, and R. Slansky, "Complex spinors and unified theories," (1979) . published in Supergravity, P. van Nieuwenhuizen and D.Z. Freedman (eds.), North Holland Publ. Co., 1979.

[52] T. Yanagida, "Horizontal gauge symmetry and masses of neutrinos," (1979) . In Proceedings of the Workshop on the Baryon Number of the Universe and Unified Theories, Tsukuba, Japan, 13-14 Feb 1979.

[53] R. N. Mohapatra and G. Senjanovic, "Neutrino Masses and Mixings in Gauge Models with Spontaneous Parity Violation," *Phys. Rev.* **D23** (1981) 165.

[54] A. D. Sakharov, "Violation of CP invariance, C asymmetry, and Baryon Asymmetry of the Universe," *Pisma Zh. Eksp. Teor. Fiz.* **5** (1967) 32–35.

[55] T. Hambye, M. Raidal, and A. Strumia, "Efficiency and maximal CP-asymmetry of scalar triplet leptogenesis," *Phys. Lett.* **B632** (2006) 667–674, arXiv:hep-ph/0510008 [hep-ph].

[56] G. Engelhard, Y. Grossman, E. Nardi, and Y. Nir, "The Importance of N2 leptogenesis," *Phys. Rev. Lett.* **99** (2007) 081802, arXiv:hep-ph/0612187 [hep-ph].

[57] A. Abada, S. Davidson, F.-X. Josse-Michaux, M. Losada, and A. Riotto, "Flavor issues in leptogenesis," *JCAP* **0604** (2006) 004, arXiv:hep-ph/0601083 [hep-ph].

[58] E. Nardi, Y. Nir, E. Roulet, and J. Racker, "The Importance of flavor in leptogenesis," *JHEP* **01** (2006) 164, arXiv:hep-ph/0601084 [hep-ph].

[59] A. Abada, S. Davidson, A. Ibarra, F. X. Josse-Michaux, M. Losada, and A. Riotto, "Flavour Matters in Leptogenesis," *JHEP* **09** (2006) 010, arXiv:hep-ph/0605281 [hep-ph].

[60] S. Blanchet and P. Di Bari, "Flavor effects on leptogenesis predictions," *JCAP* **0703** (2007) 018, arXiv:hep-ph/0607330 [hep-ph].

[61] J. Racker, M. Pena, and N. Rius, "Leptogenesis with small violation of B-L," *JCAP* **1207** (2012) 030, arXiv:1205.1948 [hep-ph].

[62] E. Ma, "Verifiable radiative seesaw mechanism of neutrino mass and dark matter," *Phys. Rev.* **D73** (2006) 077301, arXiv:hep-ph/0601225 [hep-ph].

[63] J. Racker, "Mass bounds for baryogenesis from particle decays and the inert doublet model," *JCAP* **1403** (2014) 025, arXiv:1308.1840 [hep-ph].

[64] D. Aristizabal Sierra, M. Dhen, and T. Hambye, "Scalar triplet flavored leptogenesis: a systematic approach," *JCAP* **1408** (2014) 003, arXiv:1401.4347 [hep-ph].

[65] D. Aristizabal Sierra, C. S. Fong, E. Nardi, and E. Peinado, "Cloistered Baryogenesis," *JCAP* **1402** (2014) 013, arXiv:1309.4770 [hep-ph].

[66] T. Hambye, "Leptogenesis: beyond the minimal type I seesaw scenario," *New J. Phys.* **14** (2012) 125014, arXiv:1212.2888 [hep-ph].

[67] D. Aristizabal Sierra, L. A. Munoz, and E. Nardi, "Purely Flavored Leptogenesis," *Phys. Rev.* **D80** (2009) 016007, arXiv:0904.3043 [hep-ph].

[68] M. C. Gonzalez-Garcia, J. Racker, and N. Rius, "Leptogenesis without violation of B-L," *JHEP* **11** (2009) 079, arXiv:0909.3518 [hep-ph].

[69] D. Aristizabal Sierra, M. Losada, and E. Nardi, "Variations on leptogenesis," *Phys. Lett.* **B659** (2008) 328–335, arXiv:0705.1489 [hep-ph].

[70] A. Pilaftsis and T. E. Underwood, "Resonant leptogenesis," *Nucl.Phys.* **B692** (2004) 303–345, arXiv:hep-ph/0309342 [hep-ph].

[71] A. Pilaftsis, "Resonant tau leptogenesis with observable lepton number violation," *Phys. Rev. Lett.* **95** (2005) 081602, arXiv:hep-ph/0408103.

[72] A. Pilaftsis and T. E. J. Underwood, "Electroweak-scale resonant leptogenesis," *Phys. Rev.* **D72** (2005) 113001, arXiv:hep-ph/0506107.

[73] B. Dev, M. Garny, J. Klaric, P. Millington, and D. Teresi, "Resonant enhancement in leptogenesis," *Int. J. Mod. Phys.* **A33** (2018) 1842003, arXiv:1711.02863 [hep-ph].

[74] E. J. Chun et al., "Probing Leptogenesis," arXiv:1711.02865 [hep-ph].

[75] P. Jordan, *Schwerkraft und Weltall: Grundlagen der theoretische Kosmologie*, vol. 107. Vieweg. (Braunschweig: und Sohns), 1955.

[76] M. Fierz, "On the physical interpretation of P.Jordan's extended theory of gravitation," *Helv. Phys. Acta* **29** (1956) 128–134.

[77] C. Brans and R. H. Dicke, "Mach's principle and a relativistic theory of gravitation," *Phys. Rev.* **124** (1961) 925–935.

[78] T. Hambye, Y. Lin, A. Notari, M. Papucci, and A. Strumia, "Constraints on neutrino masses from leptogenesis models," *Nucl. Phys.* **B695** (2004) 169–191, arXiv:hep-ph/0312203 [hep-ph].

[79] M. Raidal, A. Strumia, and K. Turzynski, "Low-scale standard supersymmetric leptogenesis," *Phys. Lett.* **B609** (2005) 351–359, arXiv:hep-ph/0408015 [hep-ph]. [Addendum: Phys. Lett.B632,752(2006)].

[80] A. Ibarra, E. Molinaro, and S. T. Petcov, "TeV Scale See-Saw Mechanisms of Neutrino Mass Generation, the Majorana Nature of the Heavy Singlet Neutrinos and $(\beta\beta)_{0\nu}$-Decay," *JHEP* **09** (2010) 108, arXiv:1007.2378 [hep-ph].

[81] B. Shuve and I. Yavin, "Baryogenesis through Neutrino Oscillations: A Unified Perspective," *Phys. Rev.* **D89** (2014) no. 7, 075014, arXiv:1401.2459 [hep-ph].

[82] D. Aristizabal Sierra and C. E. Yaguna, "On the importance of the 1-loop finite corrections to seesaw neutrino masses," *JHEP* **08** (2011) 013, arXiv:1106.3587 [hep-ph].

[83] E. W. Kolb and S. Wolfram, "Baryon Number Generation in the Early Universe," *Nucl. Phys.* **B172** (1980) 224. [Erratum: Nucl. Phys.B195,542(1982)].

[84] J. N. Fry, K. A. Olive, and M. S. Turner, "Evolution of Cosmological Baryon Asymmetries," *Phys. Rev.* **D22** (1980) 2953.

[85] E. Nardi, J. Racker, and E. Roulet, "CP violation in scatterings, three body processes and the Boltzmann equations for leptogenesis," *JHEP* **09** (2007) 090, arXiv:0707.0378 [hep-ph].

[86] C. S. Fong, M. C. Gonzalez-Garcia, and J. Racker, "CP Violation from Scatterings with Gauge Bosons in Leptogenesis," *Phys. Lett.* **B697** (2011) 463–470, arXiv:1010.2209 [hep-ph].

[87] E. Roulet, L. Covi, and F. Vissani, "On the CP asymmetries in Majorana neutrino decays," *Phys. Lett.* **B424** (1998) 101–105, arXiv:hep-ph/9712468.

[88] W. Buchmuller and M. Plumacher, "Spectator processes and baryogenesis," *Phys. Lett.* **B511** (2001) 74–76, arXiv:hep-ph/0104189 [hep-ph].

[89] E. Nardi, Y. Nir, J. Racker, and E. Roulet, "On Higgs and sphaleron effects during the leptogenesis era," *JHEP* **01** (2006) 068, arXiv:hep-ph/0512052 [hep-ph].

[90] M. D'Onofrio, K. Rummukainen, and A. Tranberg, "Sphaleron Rate in the Minimal Standard Model," *Phys. Rev. Lett.* **113** (2014) no. 14, 141602, arXiv:1404.3565 [hep-ph].

[91] J. A. Harvey and M. S. Turner, "Cosmological baryon and lepton number in the presence of electroweak fermion number violation," *Phys. Rev.* **D42** (1990) 3344–3349.

[92] T. Inui, T. Ichihara, Y. Mimura, and N. Sakai, "Cosmological baryon asymmetry in supersymmetric Standard Models and heavy particle effects," *Phys. Lett.* **B325** (1994) 392–400, arXiv:hep-ph/9310268 [hep-ph].

[93] W. Buchmuller, P. Di Bari, and M. Plumacher, "Leptogenesis for pedestrians," *Annals Phys.* **315** (2005) 305–351, arXiv:hep-ph/0401240 [hep-ph].

[94] G. F. Giudice, A. Notari, M. Raidal, A. Riotto, and A. Strumia, "Towards a complete theory of thermal leptogenesis in the SM and MSSM," *Nucl. Phys.* **B685** (2004) 89–149, arXiv:hep-ph/0310123 [hep-ph].

[95] M. Kawasaki, K. Kohri, T. Moroi, and A. Yotsuyanagi, "Big-Bang Nucleosynthesis and Gravitino," *Phys. Rev.* **D78** (2008) 065011, arXiv:0804.3745 [hep-ph].

APPENDIX A

GENERAL DISFORMAL SET-UP

The general scalar-tensor action coupled to matter, which can include a realisation in string theory compactifications is given by:

$$S = S_{EH} + S_{\phi} + S_m \,, \tag{A.1}$$

where:

$$S_{EH} = \frac{1}{2\kappa^2}\int d^4x\sqrt{-g}\, R, \tag{A.2}$$

$$S_{\phi} = -\int d^4x\sqrt{-g}\left[\frac{b}{2}(\partial\phi)^2 + M^4 \text{1}\!\text{1}^2(\phi)\sqrt{1+\frac{\text{1}\!\text{1}(\phi)}{\text{1}\!\text{1}(\phi)}(\partial\phi)^2} + V(\phi)\right], \tag{A.3}$$

$$S_m = -\int d^4x\sqrt{-\tilde{g}}\,\mathcal{L}_{DM}(\tilde{g}_{\mu\nu})\,, \tag{A.4}$$

and the disformally coupled metric is given by

$$\tilde{g}_{\mu\nu} = C_2(\phi)g_{\mu\nu} + D_2(\phi)\partial_\mu\phi\partial_\nu\phi\,. \tag{A.5}$$

b is a constant equal to 1 or 0, depending on the model one wants to consider; $C_i(\phi), D_i(\phi)$ are functions of ϕ, which can be identified as conformal and disformal couplings of the scalar to the metric, respectively. Finally, we have introduced the mass scale M to keep units right (remember that the conformal coupling is dimensionless, whereas the disformal has units of $Mass^{-4}$.)

The connection of the general action (A.1) to the different models in the literature can be obtained as follows: the case $C_1 = D_2$, $D_1 = D_2$, $b = 0$ arises when considering a D-brane moving along an extra dimension. This case was studied in [3] as a model of a coupled dark matter dark energy sector scenario, where scaling solutions arise naturally. Note that in this case, the kinetic

term for the scalar field, identified with dark energy for example, is automatically non-canonical and dictated by the DBI action (see [3]). On the other hand, phenomenological models considering a disformal coupling between matter and a scalar field, usually consider a canonical kinetic term, and therefore, in that case, $C_1 = D_1 = 0$ and $b = 1$ (C_1 can be taken to be non-zero and will be part of the scalar potential). Furthermore, the widely studied case of a conformal coupling is obtained for $b = 1, C_1 = D_1 = D_2 = 0$ or, as in the case of a D-brane for example[1], simply considering small velocities with $b = 0, C_1 = C_2$ and $D_1 = D_2$, and normalising canonically the scalar field (see Appendix B).

Finally, let us clarify further our nomenclature on frames. The action in (A.1) is written in the Einstein frame, which in string theory, is usually related to the frame in which the dilaton and the graviton degrees of freedom are decoupled. From this point of view, the dilaton field as well as all other moduli fields not relevant for the cosmological discussion are considered as stabilised, massive, and are therefore decoupled from the low energy effective theory. In the literature of scalar-tensor theories however (including conformal and disformal couplings), the Einstein and Jordan frames are identified with respect to the (usually single) scalar field to which gravity is coupled. In this paper, we follow this and call “Jordan" or “disformal frame" the frame in which dark matter is coupled only to the metric $\tilde{g}_{\mu\nu}$, rather than to the metric $g_{\mu\nu}$ and a scalar field ϕ.

The equations of motion obtained from (A.1) are (2.4):

$$R_{\mu\nu} - \frac{1}{2} g_{\mu\nu} R = \kappa^2 \left(T^{\phi}_{\mu\nu} + T^{DM}_{\mu\nu} \right) \,, \tag{A.6}$$

where in the frame relative to $g_{\mu\nu}$ the energy momentum tensors are defined in (2.5) and (2.6). The energy-momentum tensor for the scalar field in the general case is modified from (2.7) to:

$$T^{\phi}_{\mu\nu} = -g_{\mu\nu} \left[M^4 C_1^2 \gamma_1^{-1} + \frac{b}{2} (\partial\phi)^2 + V \right] + \left(M^4 C_1 D_1 \, \gamma_1 + b \right) \partial_\mu \phi \, \partial_\nu \phi \,, \tag{A.7}$$

[1]For the system corresponding to a D-brane moving in a typically warped compactification in string theory, the functions $C(\phi)$ and $D(\phi)$ are identified with powers of the so-called warp factor, usually denoted as $h(\phi)$. In this approach, the longitudinal and transverse fluctuations of the D-brane are identified with the dark matter and dark energy fluids respectively [3].

where now the energy density and pressure are given by:

$$\rho_\phi = -\frac{b}{2}(\partial\phi)^2 + M^4 C_1^2 \gamma_1 + V\,, \qquad P_\phi = -\frac{b}{2}(\partial\phi)^2 - M^4 C_1^2 \gamma_1^{-1} - V\,, \tag{A.8}$$

and the "Lorentz factor" γ_1 introduced above is defined by

$$\gamma_1 \equiv \left(1 + \frac{D_1}{C_1}\,(\partial\phi)^2\right)^{-1/2}\,. \tag{A.9}$$

We can rewrite (A.8) in a more succinct way, by defining $\mathcal{V} \equiv V + C_1^2 M^4$

$$\rho_\phi = -\left[\frac{b}{2} + \frac{M^4 C_1 D_1 \gamma_1}{\gamma + 1}\right](\partial\phi)^2 + \mathcal{V}\,, \qquad P_\phi = -\left[\frac{b}{2} + \frac{M^4 C_1 D_1 \gamma_1^{-1}}{\gamma + 1}\right](\partial\phi)^2 - \mathcal{V}\,. \tag{A.10}$$

The equation of motion for the scalar field becomes (compare with (2.9))

$$\begin{aligned} -\nabla_\mu\big[(M^4 D_1 C_1 \gamma_1 \; + b)\,\partial^\mu\phi\big] + \frac{\gamma_1^{-1} M^4 C_1^2}{2}\left[\frac{D_1'}{D_1} + 3\frac{C_1'}{C_1}\right] + \frac{\gamma_1\, M^4 C_1^2}{2}\left[\frac{C_1'}{C_1} - \frac{D_1'}{D_1}\right] + V' \\ -\frac{T^{\mu\nu}}{2}\left[\frac{C_2'}{C_2} g_{\mu\nu} + \frac{D_2'}{C_2}\partial_\mu\phi\partial_\nu\phi\right] + \nabla_\mu\left[\frac{D_2}{C_2} T^{\mu\nu}\partial_\nu\phi\right] = 0\,. \end{aligned} \tag{A.11}$$

Finally, the energy-momentum conservation equation gives rise to (2.11), where Q now is given in terms of C_2, D_2:

$$Q \equiv \nabla_\mu\left[\frac{D_2}{C_2}\, T^{\mu\lambda}\,\partial_\lambda\phi\right] - \frac{T^{\mu\nu}}{2}\left[\frac{C_2'}{C_2} g_{\mu\nu} + \frac{D_2'}{C_2}\,\partial_\mu\phi\,\partial_\nu\phi\right]\,. \tag{A.12}$$

General cosmological equations

The equations of motion for the general system in an FRW background become:

$$H^2 = \frac{\kappa^2}{3}\left[\rho_\phi + \rho\right] , \tag{A.13}$$

$$\dot{H} + H^2 = -\frac{\kappa^2}{6}\left[\rho_\phi + 3P_\phi + \rho + 3P\right] , \tag{A.14}$$

$$\begin{aligned}\ddot{\phi}\left[1 + \frac{b}{M^4 C_1 D_1 \gamma_1^3}\right] + 3H\dot{\phi}\,\gamma_1^{-2}\left[\frac{b}{M^4 C_1 D_1 \gamma_1} + 1\right] \\ + \frac{C_1}{2D_1}\left(\gamma_1^{-2}\left[\frac{5C_1'}{C_1} - \frac{D_1'}{D_1}\right] + \frac{D_1'}{D_1} - \frac{C_1'}{C_1} - 4\gamma_1^{-3}\frac{C'}{C}\right) + \frac{1}{M^4 C_1 D_1 \gamma_1^3}\left(\mathcal{V}' + Q_0\right) = 0 ,\end{aligned} \tag{A.15}$$

where, $H = \frac{\dot{a}}{a}$, dots are derivatives with respect to t, $' = d/d\phi$ and

$$\gamma_1 = (1 - D_1\,\dot{\phi}^2/C_1)^{-1/2}.$$

We also have the continuity equations for the scalar field and matter given by

$$\dot{\rho}_\phi + 3H(\rho_\phi + P_\phi) = -Q_0\dot{\phi} , \tag{A.16}$$

$$\dot{\rho} + 3H(\rho + P) = Q_0\,\dot{\phi} . \tag{A.17}$$

where Q_0 is given by

$$Q_0 = \rho\left[\frac{D_2}{C_2}\,\ddot{\phi} + \frac{D_2}{C_2}\,\dot{\phi}\left(3H + \frac{\dot{\rho}}{\rho}\right) + \left(\frac{D_2'}{2C_2} - \frac{D_2}{C_2}\frac{C_2'}{C_2}\right)\dot{\phi}^2 + \frac{C_2'}{2\,C_2}(1 - 3\,\omega)\right] . \tag{A.18}$$

Using (A.17) we can rewrite this in a more compact and useful form as

$$Q_0 = \rho\left(\frac{\dot{\gamma}_2}{\dot{\phi}\,\gamma_2} + \frac{C_2'}{2C_2}(1 - 3\,\omega\,\gamma_2^2) - 3H\omega\,\frac{(\gamma_2 - 1)}{\dot{\phi}}\right) , \tag{A.19}$$

where

$$\gamma_2 = (1 - D_2\,\dot{\phi}^2/C_2)^{-1/2}.$$

Plugging this into the (non-)conservation equation for dark matter (A.17), gives:

$$\dot{\rho} + 3H(\rho + P\,\gamma_2^2) = \rho\left[\frac{\dot{\gamma}_2}{\gamma_2} + \frac{C_2'}{2C_2}\,\dot{\phi}\,(1 - 3\,\omega\gamma_2^2)\right]. \tag{A.20}$$

The energy densities and pressures in the Einstein and Jordan frames are now related similarly to (2.19), replacing $\gamma \to \gamma_2$:

$$\tilde{\rho} = C_2^{-2}\gamma_2^{-1}\rho\,, \qquad \tilde{P} = C_2^{-2}\gamma_2\,P, \tag{A.21}$$

and therefore the equation of states in both frames are related by $\tilde{\omega} = \omega\gamma_2^2$. Similarly the physical proper time and the scale factors in the two frames are related via γ_2:

$$\tilde{a} = C_2^{1/2}a\,, \qquad d\tilde{\tau} = C_2^{1/2}\gamma_2^{-1}d\tau\,. \tag{A.22}$$

Defining the disformal frame Hubble parameter $\tilde{H} \equiv \frac{d\ln\tilde{a}}{d\tilde{\tau}}$, gives:

$$\tilde{H} = \frac{\gamma_2}{C_2^{1/2}}\left[H + \frac{C_2'}{2C_2}\dot{\phi}\right]. \tag{A.23}$$

To solve the equations of motion one now can proceed as in section 2.2 to write the equations in terms of derivatives w.r.t. the number of e-folds N and consider different cases by choosing appropriately the parameters b, C_i, D_i.

APPENDIX B

THE CONFORMAL CASE IN D-BRANE SCENARIOS

In this section we show how to recover the pure conformal case from the D-brane picture, that is, $b = 0$, $C_1 = C_2$, $D_1 = D_2$. We start by expanding the square root in the scalar part of the action (A.1). Doing this we get

$$\begin{aligned} S_\phi &= -\int d^4x\sqrt{-g}\left[M^4C_1^2\left(1+\frac{D_1}{2C_1}(\partial\phi)^2+\dots\right)+V(\phi)\right] \\ &= -\int d^4x\sqrt{-g}\left[\frac{M^4C_1D_1}{2}(\partial\phi)^2+M^4C_1^2(\phi)+V(\phi)+\dots\right] \\ &= -\int d^4x\sqrt{-g}\left[\frac{M^4C_1D_1}{2}(\partial\phi)^2+\mathcal{V}(\phi)+\dots\right]. \end{aligned} \tag{B.1}$$

On the other hand, the matter Lagrangean takes the form

$$\begin{aligned} S_{DM} &= -\int d^4x\sqrt{-\tilde{g}}\,\mathcal{L}_{DM}(\tilde{g}_{\mu\nu}) \\ &= -\int d^4x\sqrt{-g}\,C_1^2(\phi)\left(1+\frac{D_1}{2C_1}(\partial\phi)^2+\dots\right)\mathcal{L}_{DM}(\tilde{g}_{\mu\nu}) \\ &= -\int d^4x\sqrt{-g}\,C_1^2(\phi)\mathcal{L}_{DM}(\tilde{g}_{\mu\nu})+\dots = -\int d^4x\sqrt{-\tilde{g}}\,\mathcal{L}_{DM}(\tilde{g}_{\mu\nu})+\dots \end{aligned} \tag{B.2}$$

where now $\tilde{g}_{\mu\nu} = C_1(\phi)g_{\mu\nu}$ (and we have used that $\det\tilde{g}_{\mu\nu} = C_1^4(1 + D_1/C_1(\partial\phi)^2)$).

Finally, to compare the D-brane case with the pure conformal case, we need to canonically normalise ϕ. Calling φ the canonically normalised field, this is obtained from ϕ as

$$\varphi = \int M^2\sqrt{D_1C_1}\,d\phi\,. \tag{B.3}$$

It is clear that when $D_1 = 1/(M^4C_1)$, $\varphi = \phi$ and therefore the action for the scalar field (B.1) is already in the required form. We can now take the limit $\gamma \to 1$ into the equations of

motion (A.13)-(A.15) and make the identification $D_1 = 1/(M^4 C_1)$ to recover the conformal case equations of motion. Note that in this limit $Q_0 \to \rho C_1'/2C_1$, and is independent of D_1 (see (A.19) with $C_1 = C_2, D_1 = D_2$).